Research Square

Preprints are preliminary reports that have not undergone peer review.
They should not be considered conclusive, used to inform clinical practice,
or referenced by the media as validated information.

Cerebro-cerebellar dynamics during the acquisition of sensorimotor synchronisation: An exploratory Human electrophysiological investigation

Neil PM Todd

n.todd@unsw.edu.au

UNSW Clinical School

Sendhil Govender

UNSW Clinical School

Daniel Hochstrasser

Western Sydney University

Manuel Varlet

Western Sydney University

Peter E Keller

Aarhus University

James G Colebatch

UNSW Clinical School

Research Article

Keywords: cerebellum, conditioning, climbing fibre response, sensorimotor synchronisation

Posted Date: October 15th, 2026

DOI: https://doi.org/10.21203/rs.3.rs-11180747/v1

License: This work is licensed under a Creative Commons Attribution 4.0 International License.
Read Full License

Additional Declarations: No competing interests reported.

Cerebro-cerebellar dynamics during the acquisition of sensorimotor synchronisation: An exploratory Human electrophysiological investigation.

Neil PM Todd[a,b,], Sendhil Govender[b,c], Daniel Hochstrasser[d], Manuel Varlet[d,e], Peter E Keller[d,f] and James G Colebatch[b,c]

[a]Department of Psychology, University of Exeter, Exeter EX4 4QC, UK
[b]UNSW Clinical School, Randwick Campus, Sydney, NSW 2052, Australia.
[c]Neuroscience Research Australia, UNSW, Sydney, NSW 2052, Australia.
[d]MARCS Institute for Brain, Behaviour and Development, Western Sydney University, Penrith, NSW, 2751, Australia.
[e]School of Psychology, Western Sydney University, Penrith, NSW, 2751, Australia
[f]Center for Music in the Brain, Department of Clinical Medicine, Aarhus University, Aarhus 8000, Denmark

Corresponding author: Neil PM Todd. **Email:** n.todd@unsw.edu.au

Running head: Cerebro-cerebellar dynamics during sensorimotor synchronisation

Keywords: cerebellum, conditioning, climbing fibre response, sensorimotor synchronisation

Abstract

Understanding how subcortical and cortical systems interact to guide human motor timing remains a core question in systems neurophysiology. The cerebellum has long been implicated to have a major role in motor timing but due to a lack of high time-resolution techniques its physiology has remained poorly understood in humans. Here we report the results of an experiment to record non-invasively from the human cerebrum and cerebellum during synchronisation acquisition, proposed to be a form of conditioning, in response to a vestibular metronome, considered as a train of unconditional stimuli. Three randomly ordered tempi were used so that the tempo could not be determined until the second element. The inter-trial interval between presentations was also random, so that the first onset was likewise unpredictable. 10 human subjects were recruited and trained to carry out a foot tapping task while recording EEG and electro-cerebellogram (ECeG) with a 10% cerebellar extension montage, along with foot tap force and accelerometry. The behavioural results showed that the subjects were able to achieve synchrony within three to four taps. Analysis of potentials indicated that these parallel the behavioural data, reaching a steady state after three to four repetitions of the unconditional stimuli. Wavelet analysis of the high-frequency ECeG power confirmed the presence of unconditioned and conditioned ECeG pausing. Source analysis of the potentials also confirmed the likely presence of both unconditioned and conditioned short latency cerebellar evoked and predictive responses, consistent with the participation of conditioned climbing fibre response (C-CFR) activity, along with anticipatory SMA sources. Within the SMA source we also observed tempo-dependent post-N2 movement related down-ramp timed to make a zero-crossing about 100 ms prior to target irrespective of tempo. We argue that these data and exploratory analyses suggest the involvement of a cortico-basal ganglia-cerebellar-hippocampal adaptive learning network driven by a C-CRF/beta burst reward signal and a novel short interval time ramping mechanism.

List of Abbreviations

ACC – anterior cingulate cortex

ANOVA – analysis of variance

a-PFC / Fp-PFC – anterior / frontopolar prefrontal cortex

BESA – Brain Electrical Source Analysis

C-CFR – conditioned climbing fibre response

CEP – cerebellar evoked potential

CF – climbing fibre

CFR – climbing fibre response

CNV – contingent negative variation

CR – conditioned response

CS – conditional stimulus

CWT – continuous wavelet transform

DCN – deep cerebellar nuclei

dl-PFC – dorsolateral prefrontal cortex

ECeG – electro-cerebellogram

EEG – electroencephalogram

EMG – electromyogram

EOG – electrooculogram

GFP – global field power

GPe / GPi – globus pallidus external segment / internal segment

IPL – inferior parietal lobule

ITG / MTG / STG – inferior / middle / superior temporal gyrus

M1 / S1 – primary motor cortex / primary somatosensory cortex

MEG – magnetoencephalography

MF – mossy fibre

oVEMP – ocular vestibular evoked myogenic potential

PF – parallel fibre

PMC – premotor cortex

PMN – pre-movement negativity

PMP – post-motion positive

PPN – pedunculopontine nucleus

PPC – posterior parietal cortex

RAN – reafference negative

SMA – supplementary motor area

SMC – sensorimotor cortex

SMS – sensorimotor synchronisation

SNc / SNr – substantia nigra pars compacta / pars reticulata

SOL – soleus muscle

STN – subthalamic nucleus

TA – tibialis anterior muscle

UHF – ultra-high frequency

US – unconditional stimulus

VHF – very high frequency

VsCEP – vestibular cerebellar evoked potential

VTA – ventral tegmental area

1 Introduction

The cerebellum has long been implicated to have a major role in motor timing as cerebellar patients have deficits in both production and perception of time intervals (Ivry and Keele 1989). However, the cerebellum is also known to be part of a network of other brain areas also involved in timing, including the basal ganglia (Kung et al. 2013; Penhune et al. 1998), but these are described in different terms and in different combinations of brain areas by different theorists. Lewis & Miall (2003) refer to "automatically" and "cognitively" controlled systems, with the cerebellum largely associated with "automatic" motor timing. Grahn & Rowe (2012) associate the basal ganglia with beat based rhythms, and thus a "beat prediction" system, while they found that the cerebellum was more activated with irregular rhythms. Teki et al. (2011) similarly associate the basal ganglia with "beat-based" auditory timing, while the cerebellum is more associated with "duration-based" timing in their scheme. Todd and Lee (2015a, 2015b) in an alternative perspective on rhythm perception, described two systems for "externally" vs "internally" guided action involving respectively the cerebellum and basal ganglia.

One task in particular, that of classical eye-blink conditioning, has been well-studied for the role of the cerebellum in the acquisition of timed condition responses (CRs) to anticipate an unconditional stimulus (US), such as an eye-puff (Marr 1969; Albus 1971; Ito 2001; Gerwig et al. 2007). It is believed that cerebellar learning takes place from the conjunction of climbing fibre (CF) and mossy fibre (MF)/parallel fibre (PF) inputs which respectively signal the US and conditional stimuli (CS) (Marr 1969; Albus 1971). A climbing fibre response (CFR) recorded intracellularly is characterised by an initial field potential associated with a complex spike followed by pausing in the spontaneous simple spiking activity (Eccles et al. 1969; Latham and Paul 1971). A conditioned response is signalled in the cerebellum by pausing or suppression in the simple spike activity in anticipation of the US (Albus 1971; Jirenhead and Heslow 2016). However, eye-blink conditioning also gives rise to conditioned complex spikes following a CS, referred to as CS-complex spikes (Ohmae and Medina 2015; ten Brinke et al. 2019), which may signal novelty or that a US is to be expected, driving higher order acquisition. CS-complex spikes tend to occur as a pair within 100 ms following CS onset before CR onset, depending on the modality of the CS (ten Brinke et al. 2019). Thus following learning, two distinct conditioned changes may occur: (i) paired CS-complex spikes at a fixed time following CS onset and (ii) anticipatory conditioned pausing of simple-spike activity prior to US onset.

Recent developments in non-invasive electrophysiology have shown that, contrary to prior belief, the posterior lobe of the cerebellum at least is within the range of EEG and MEG sensors (Anderson et al 2020; Todd et al 2017, 2018a). In our prior work we have shown that it is possible to record both cerebellar evoked potentials (CEPs) and the spontaneous activity of the cerebellum, the electrocerebellogram (ECeG), the latter characteristically containing much higher frequency content than EEG (Todd et al. 2018b, 2019). Using these techniques we have been able to demonstrate the non-invasive recording of plasticity of cerebellar activity during classical eye-blink condition in which anticipatory conditioned pausing of simple-spike activity is manifest in a reduction of high frequency ECeG power (Todd et al 2021a, 2022). We were also able to generalise to voluntary eye-blink conditioning where an imperative stimulus or command is substituted for the unconditional stimulus (Todd et al. 2024b). In these experiments a climbing-fibre response (CFR) typically is observed in pause-bursting of the high-frequency ECeG, a manifestation of modulation of underlying simple-spike activity (Eccles et al 1967). These data also showed some evidence of paired CS-related CFRs (Todd et al 2022). In addition to eye-blink responses, CFRs and associated pause-bursting can also be readily evoked and recorded in humans to unconditional vestibular and postural perturbations which activate vestibular and axial muscle spindle receptors (Todd et al 2021b; Govender et al. 2024). Most recently we showed evidence of modulation of the ECeG associated with movement related potentials during self-paced spontaneous upper and lower limb movements (Todd et al 2023; Todd et al. 2024b). The vestibular CEP (VsCEP) and movement related changes in the ECeG have now been confirmed by other groups (e.g. Romero et al. 2025; Lattore et al. 2025).

The above results led us to hypothesise that we might be able to generalise further from voluntary (Ivanov-Smolensky) eye-blink conditioning to record non-invasively from the human cerebellum during Ivanov-Smolensky conditioning of somatic motor actions in a timing task. One such task is sensory-motor synchronisation (SMS). SMS entails the temporal coordination of actions with external rhythmic events. Laboratory tasks investigating SMS typically require an individual to align the timing of simple movements (e.g., finger taps) with repetitive events in pacing sequences presented in auditory, visual, or other sensory modalities (Repp, 2005; Todd, Keller, et al., 2024). A large body of research has addressed the mechanisms that enable individuals to maintain SMS (Keller et al., 2014; Repp, 2005; Repp & Su, 2013; Snyder et al., 2024) but the process of establishing it has received less attention. Previous work indicates that establishing synchrony at the start of a

trial, or re-establishing it after an unexpected tempo change, typically takes around three to four cycles (Fraisse & Repp, 2012; Novembre et al., 2017; Repp, 2005; Semjen et al., 1998). The rapid acquisition of synchrony may occur due to sharpening of temporal expectancies as uncertainty about phase and tempo decreases with the accumulation of information about event timing (Cannon, 2021).

We had previously theorised that SMS could be viewed as a form of Ivanov-Smolensky conditioning such that each successive element of a target metronome sequence could act as both as an US to the preceding and a CS to the following elements (Todd et al 2024b). Synchronisation would be achieved when the somatic response had become conditioned to anticipate each US in the sequence, analogous to classical eye-blink conditioning. Although the vestibular US is relatively weak for classical (Pavlovian) eye-blink conditioning, when employed as an imperative stimulus for Ivanov-Smolensky conditioning it is more consistently effective. In terms of expected changes in the spontaneous and evoked ECeG we would expect to see the two kinds of changes described in the animal work, i.e. CS-related CFRs following each US/CS, independent of any US-related CFRs, and conditioned pausing in the high-frequency ECeG prior to onset of each successive US. However, we also anticipate the observation of parallel effects within the cerebrum accompanying any cerebellar changes. In our prior work on recording from the cerebellum during classical conditioning we also observed the presence of a contingent negative variation (CNV) in central leads (Todd et al. 2023), thus implying that cerebellar changes may be necessary, but are not alone sufficient to account for the behaviour, consistent with the cerebellum as working in concert with a network of areas for timing behaviour. Of critical importance to interpretation, we should expect that CS-related CFRs (or C-CFRs), manifestations of CS-complex spikes, should not behave as signals of error correction, as CRFs are classically interpreted (Marr 1969; Albus 1971), but rather signals of prediction for the benefit of the whole network of areas engaged in timing behaviour (ten Brinke et al. 2019).

The present paper reports the result of an experiment to test the above theory of successive conditioning to explain the role of the cerebellum in SMS with pacing sequences presented in the vestibular modality. The vestibular system not only influences the perception of rhythms presented in other sensory modalities (Phillips-Silver & Trainor, 2005, 2008; Todd, 1999; Todd & Lee, 2015), but vestibular stimuli are themselves potent drivers of rhythmic responses (Todd et al., 2024a). Therefore, in order to maximise chances of observing the

hypothesised effects we chose a vestibular metronome in the form of head taps (Todd et al. 2008), rather than a more traditional auditory metronome, as head taps have been shown to give rise to robust CFRs and associated post-CFR pausing (Todd et al. 2018, 2019). Further, it is well-known that the vestibular VIII nerve projects to the cerebellum both as mossy and climbing fibres, directly as well as via the vestibular nuclei, thus well capable as acting as both a CS and US in the Marr/Albus/Ito framework. Also we have previously demonstrated at least weak classical conditioning with a vestibular US (Todd et al. 2021). From Todd et al. (2024b) it appeared that right-foot dorsi/plantar-flexion was the most effective manipulandum for observing movement-related changes in the ECeG, and the antagonist soleus and tibialis anterior muscles are easily accessible for robust EMG measurements. Thus in the experiment subjects were required to synchronise right foot tapping to a vestibular metronome. Although we would expect movement related signals associated with the active condition, we would still expect predictive and conditioned components in the passive condition.

To test the theory of successive conditioning, our analyses examine the transition from initial acquisition of synchronisation to the steady state of maintaining synchrony at behavioural and neural levels. The behavioural analyses decompose the physiology of foot tapping responses into different stages while neural analyses focus on differences in the profiles of initial brain responses versus steady state responses in terms of their topography and latency. We included active (foot tapping) and passive (no tapping) task conditions to separate stimulus-related and movement-related components, and the presentation rate of the pacing sequences was varied to dissociate early from late processes. In anticipation of cerebral effects accompanying any cerebellar changes, exploratory source analyses were used to suggest underlying brain networks. This enabled us to propose a circuit diagram that accounts for the role of cerebellar and related pathways in connectivity across cerebral and sub-cortical brain regions during SMS.

To summarise our position, we propose that the role of the cerebellum in the acquisition of SMS is as a substrate for a form of successive conditioning in which each successive element of a pacing sequence acts as both US and CS. From a Marr-Albus perspective this means that each element can simultaneously activate both CF and MF/PF inputs facilitating rapid predictive adaptation in the form of conditioned pausing of simple-spike activity prior to US onset and CS related or conditioned CFRs (C-CFRs). Both forms of predictive adaptation will be manifest non-invasively in the high-frequency ECeG as pre- and post-US conditioned

pausing. As C-CFRs tend to occur as doublets post-US conditioned pausing will manifest as a double burst-pause in the high-frequency ECeG. In contrast to the conventional Marr-Albus perspective, however, C-CFRs do not behave as signals of error, but rather as signals of reward prediction.

2 Methods

2.1 Subjects

On the basis of our prior conditioning studies (Todd et al. 2021b, 2023a, 2024b), a cohort of 10 healthy adult subjects (4 males, 6 female), with no known neurological or vestibular deficits, were recruited from staff and students at the Prince of Wales Hospital and the University of Western Sydney. Nine were right handed and one left handed (self-report). Five of the 10 had prior musical experience. Written informed consent was obtained from all subjects. The study was approved by the local ethics committees (South Eastern Sydney Local Health District Human Research Ethics Committee and Western Sydney University Human Research Ethics Committee).

2.2 Stimuli

The stimuli consisted of a train of seven impulsive accelerations (a 3rd order gamma waveform with a 4 ms rise time) generated using a laboratory interface (CED Power1401, Cambridge Electronic Design, Cambridge, UK), a custom power amplifier and customised software. These were delivered using a mini-shaker device (model 4810, Brüel & Kjær P/L, Denmark) with an attached cylindrical perspex rod (diameter: 2.5 cm, length 9.2 cm) applied to the right mastoid process. The stimulator was mounted on a 2:1 lever which could rotate freely in the horizontal plane and pivoted on an adjustable stand. A torque was applied at the opposite end of the lever by means of a 1 kg weight suspended by wire over a pulley below the fulcrum giving rise to a tonic applied force of approximately 3.5 N (Todd et al. 2008b). The drive voltage was fixed at 2 V peak corresponding to a peak head acceleration of about 0.1 g. The impulse train was arranged to have three alternative inter-pulse intervals of 500, 600 or 700 ms, represented in the Signal software as three alternative states.

2.3 Electrophysiological Recording

FIGURE 1 HERE

EEG was recorded using a 104 (96 cap + 8 external, EasyCap GmbH) channel custom 10% cerebellar extension montage, as illustrated in Figure 1 (Heine et al. 2020), with ActiveTwo amplifiers and ActiView software (BioSemi, Holland). 100 of the 104 channels were from cephalic electrode sites, including a pair of electrodes were placed infra-ocularly (IO). The last four of external electrodes were used to record EMG from the right tibialis anterior and soleus muscles. The sampling rate was 4096 Hz. For each of the three tempi, a unique digital code was assigned and recorded as a trigger code in the EEG file via the BioSemi trigger box at the start of each trial.

2.4 Accelerometry and Tap Force Recording.

In addition to the electrophysiological recording the foot tap force was recorded using a wide bar load cell (HTC-Sensor TAL201) connected to an Arduino Duemilanove board (Arduino) via an amplifier shield (Load Cell/Wheatstone Amplifier Shield, RobotShop) sampled at 10 kHz by the same CED 1401 used to drive the stimulator. Foot acceleration was also recorded by a BioSemi 2D accelerometer attached to the side of the right foot and sampled at 4096 kHz via the BioSemi Ergo input of the ActiveTwo AD Box. However, due a fault with the x-direction of the accelerometer the y-direction only was available, and scaled up approximately from the foot geoemetry in the figures, but not used subsequently in the analysis.

2.5 Procedure

FIGURE 2 HERE

Subjects were introduced to the experimental shielded booth where the recording was conducted and seated in front of a visual display unit (VDU) and instructions were read to them. They were informed that the experiment was to record their ability to synchronise with the rhythm of a head tap and shown the shaker set up. For each trial they would receive seven head taps and their task was to synchronise foot tapping to the rhythm starting on the 2nd tap. The recording would take place in eight blocks alternating between passive (Figure 2A) and active (Figure 2B) blocks. In the active blocks subjects were to tap their right foot on a force plate comfortably placed under their right foot with an ankle rest to avoid fatigue. In the

passive blocks subjects were to stay relaxed but mentally (silently) count the taps. At the start of an active block subjects were to tonically dorsiflex their right foot in readiness for a trial. Between blocks and in the passive blocks their right foot rested on the force plate. At the start of each block subjects were presented with a pictograph on the VDU to inform them whether the block was active or passive with reminder of instructions. Once the instructions were understood each subject was given one active block as a practise and any errors corrected. Following the practise block the EEG cap and electrodes were emplaced along with EMG electrodes to record from the right leg muscles and accelerometer.

Once the subject was ready to proceed and the stimulator located on the right mastoid, the subject initiated the start of the experimental blocks by pressing the space bar of a conveniently located keyboard. For each trial within a block the stimulus sequence was presented randomly alternating between the three rates with inter-pulse intervals of 500, 600 or 700 ms, corresponding to a fast, medium, and slow tempo, respectively. The inter-trial interval was randomized between 5 to 10 seconds so that the onset of first pulse of the train could not be predicted. Thus, the identity of the three alternatives could only be determined after the arrival of the second pulse. Once a block of 15 trials (5 per tempo) had completed subjects were told to rest while the responses were recorded and the next block initiated. After four blocks subjects were given a short break before the final four blocks were completed. Once practise trials were given, and recording apparatus set up, the actual recording time was about 20 minutes, with the total procedure about one hour duration.

2.6 Data analysis

Behavioural data consisted of the force/acceleration recordings in conjunction with the EMG from the TA and SOL muscles of the right foot. From the acceleration data it was also possible to estimate foot velocity and displacement. For each individual subject the mean tap force onset and peak (over an active block) could be measured by fitting a Gaussian curve to the tap initial profile, deriving three parameters, i.e. peak amplitude, centre (time) and sigma (standard deviation). The centre could then be used to determine the asynchrony from the target. Individual EMG measurements were also obtainable from the mean profile for each state. Due to cross-talk the SOL means were corrected by subtracting a proportion of the TA, the proportion of which was obtained by correlating the TA and SOL during tonic

dorsiflexion. For the resultant SOL bursts a Gaussian curve could also be fitted. For the TA cycle we measured the relaxation and contraction using a sigmoid curve fit.
Before detailed EEG analysis, EOG and ECG artefacts were removed by means of the algorithm provided by the Brain Electrical Source Analysis (BESA) software (version 7.1). A high-pass filter of 0.3 Hz was applied for epoching and averaging and a common average reference was employed. Following artefact removal, the EEG mean potentials across trials were obtained for each subject for each of the six conditions, active vs passive, and three rates, with inter-pulse intervals of 500, 600, 700 ms with an epoch of 500 ms before to 5000 ms after the onset of the first pulse. From these we obtained the grand means for the six conditions for the purpose of source analysis. We also extracted for each subject the EEG single trials for spectral power analysis.

2.7 Wavelet spectral power analysis of potentials

After recording EMG/EEG/ECeG and epoching, we performed spectral power analyses on all channels over the 5.5 s epoch using the continuous wavelet transform (CWT) as implemented in the MATLAB toolbox (R2019b, Mathworks, Natick, CA). To eliminate the effects of mains contamination, a narrow band-stop filter at 50 Hz and all harmonics to 650 Hz was applied prior to performance of the CWT. In the present analysis a Morlet wavelet was employed at a density of 24 voices per octave over 9 octaves. The CWTs were further transformed to scaleograms (time-frequency images) from the absolute value of the CWT and rescaled to be in dB per voice re 1 μV^2. Scaleograms were further split into eight frequency bands; delta (δ: 1.5 Hz – 3 Hz), theta (θ: 3 – 6 Hz), alpha (α: 6-12 Hz), beta (β: 13-30 Hz), gamma (γ: 30-80 Hz), ultra-gamma (u-γ: 80-160 Hz), very high frequency (VHF: 160-320 Hz) and ultra-high frequency (UHF: 320-640 Hz). The non-standard lower alpha boundary of 6 Hz was determined from the lobular structure of the Morlet wavelet spectral profile as implemented in MATLAB. These non-standard low frequency ranges are approximately an octave in band-width. The bands in turn were divided into 13 segments covering a smaller epoch for each beat to allow for ANOVA testing of changes in power. The beat related epochs were from – 300 ms to + 250 ms around the beat target.

2.8 Brain Electrical Source Analyses (BESA).

We adopt here a novel source analysis procedure involving multiple runs of an unconstrained genetic algorithm which we have previously pioneered (Todd et al., 2021a, 2024a, 2025). This has the advantage of bein assumption free (without areas of special interest) and provides a means to evaluate emergent source strength.

The standard four-shell ellipsoidal head model was employed with radial thicknesses of 85, 6, 7 and 1 mm for respectively the head, scalp, bone and CSF, with conductivities of 0.33, 0.33, 0.0042 and 1.0, respectively. Both cerebrum and cerebellum fall within the CSF volume conductor and are not discriminated by the BESA algorithm. The fitting was carried out using the BESA genetic algorithm with default parameter settings after remontaging to an average reference. A modelling strategy was to run a 15 dipole (maximum allowed by degrees of freedom) genetic algorithm fit 15 times to test its reproducibility. The resultant 225 locations for each modality were then subject to a hierarchical cluster analysis, using the between-groups linkage method with squared Euclidian distance measure, in order to eliminate the non-viable and very weak sources. A 5 mm^3 standard error was imposed on the cluster volumes and any isolated single dipole sources which resulted from that constraint were eliminated. In addition to the mean Talairach-Tournoux coordinates of the final surviving clusters, a weight was attributed to the clusters derived from the number of dipoles making up the cluster. For cerebellar coordinates the Schmahmann et al. (2000) atlas was used to determine the anatomical locations, while for other locations the Talairach Client application (version 2.4.3) was employed with a +/- 5mm cube search (see Todd et al., 2021a).

This procedure was repeated for six different epochs defined by the global field power for both active and passive cases for the initial and steady responses. Thus a total of 24 multiple runs. Each of these was then combined and a superordinate cluster analysis conducted from which a cluster weight could be defined. The top 11 current sources were then selected on the basis of weight and symmetry for a generic source model.

2.10 Wavelet spectral power of currents

After applying the source model to individual subjects we performed spectral power analyses on currents over the 5.5 s epoch using the CWT as for the potentials using the same segmentations for statistical analysis.

2.11 Statistics

For the behavioural results, repeated measures ANOVA were conducted with factors of BLOCK (1- 4), TEMPO (500, 600, 700 ms), and BEAT (1 – 7) on parameters of asynchrony, variability and foot tap force in the active condition. When comparing EMG and movement measures, we also added a STAGE (1 – 4) factor. For the analysis of spectral power of potentials, ANOVA were conducted with factors of TEMPO, BEAT and ACTIVITY, as above, then with a SEGMENT (1 – 13) factor after segmentation and with a BAND factor for spectral bands. When comparing multiple electrode sides a further ELECTRODE factor was introduced. For the analysis of spectral power of currents, the analysis was confined to the beta band as it was the most prominent and an ANOVA conducted using factors TEMPO, BEAT and SEGMENT. All above analyses were done using the SPSS statistical package.

3 Results

3.1 Behavioural

FIGURE 3 HERE

Figure 3 (left column) illustrates the grand mean of EMG (TA and SOL), aligned with the tap force and re-scaled y-acceleration for the three rates, i.e. Fig 3A 500 ms, Fig 3B 600 ms and Fig 3C 700 ms. For all three cases the initial tap appears very similar, occurring “late” for the 500 ms case and “early” for the 700 ms case. However, the subjects appear to have successfully achieved synchronisation within three to four taps where the tap force peak appears to occur very close to the target stimulus onset. In order to examine the details of a single cycle, for the 600 ms case a single cycle has been expanded in Fig 3 (right column). For the purpose of analysis the cycle can be described in five stages consisting of (1) TA relaxation, (2) SOL burst, (3) force peak, (4) TA contraction and (5) TA peak. This confirms the closeness of the tap force peak (stage 3; Figure 3E) to the target stimulus onset, while the SOL burst (stage 2; Figure 3D) peaks around 100 ms in advance. The TA relaxation and contraction profile appears to reciprocate the SOL burst as expected where the onset of the force decline occurs close to the cross-over of the two muscles.

FIGURE 4 HERE

In order to quantify the above observations we consider first the asynchrony, variability and amplitude of the foot tap force peak, as illustrated in Figure 4 which shows the ANOVA marginal means for effects of BLOCK (1 – 4), TEMPO (500, 600 and 700 ms) and BEAT (1-6). For the asynchrony (Figure 4A), there was a weak BLOCK effect ($F(3,27) = 2.9$, $p = 0.074$, $\eta^2 = 0.24$) where the peak force became less positively asynchronous with successive blocks, and main effects of TEMPO and BEAT (respectively $F(2,18) = 52$, $p < 0.001$, $\eta^2 = 0.85$ and $F(5,45) = 5.9$, $p < 0.05$, $\eta^2 = 0.39$), where asynchrony was reduced with successive beats. However, both these effects could be explained by the interaction of TEMPO and BEAT ($F(10,90) = 98$, $p < 0.001$, $\eta^2 = 0.92$) which indicated that subjects achieved a small and steady positive asynchrony of about 10 ms in peak force by the third or fourth beat, irrespective of tempo. As noted above, the initial asynchrony was tempo dependent such that for the faster tempo the initial response came late, while for the slower tempo it came early.

Considering the variability (Figure 4B), ANOVA also yielded main effects of BLOCK, TEMPO and BEAT (respectively $F(3,27) = 8.5$, $p < 0.01$, $\eta^2 = 0.49$, $F(2,18) = 14.4$, $p = 0.001$, $\eta^2 = 0.62$ and $F(5,45) = 19.1$, $p < 0.001$, $\eta^2 = 0.68$), indicating the tendency to becomes less variable with succeeding blocks and beats and for variability to increase with longer inter-tap intervals, respectively 37, 43 and 47 ms. Expressed as a percentage of the inter-tap intervals, these are respectively, 7.4, 7.2 and 6.7 %, thus roughly showing a Weber Law property. For the amplitude (Figure 4C), the ANOVA yielded a main effect of BEAT only, ($F(5,45) = 7.0$, $p < 0.005$, $\eta^2 = 0.44$), indicative that the tap force increased and/or became less variable with successive beats, but was independent of tempo.

FIGURE 5 HERE

When considering the asynchrony of the other stages compared with peak force (Figure 5, left column), as would be expected there is a main effect of STAGE ($F(3,24) = 86.8$, $p < 0.001$, $\eta^2 = 0.92$; Figure 5A), with the TA relaxation 50% point occurring about 200 ms prior to target, the SOL burst peak about 100 ms prior to target and the TA contraction 50% point occurring just after the target. Other than this main effect, each stage behaved very similarly in terms of the effect of TEMPO ($F(2,18) = 29.6$, $p < 0.001$, $\eta^2 = 0.77$; Figure 5B) and the interaction of TEMPO and BEAT ($F(10,80) = 125.7$, $p < 0.001$, $\eta^2 = 0.94$; Figure 5C), mirroring that of peak force. When combined, the other stages also show similar timing

variability effects to peak force (Figure 5, right column), with an overall main effect of BEAT and TEMPO (respectively $F(5,40) = 7.9$, $p = 0.001$, $F(2,16) = 19.0$, $\eta^2 = 0.50$, $p < 0.001$, $\eta^2 = 0.70$; Figure 5E,F), but with a main effect of STAGE ($F(3,24) = 26.5$, $p < 0.001$, $\eta^2 = 0.77$; Figure 5D), and a BEAT by STAGE interaction ($F(15,120) = 2.7$, $p < 0.05$, $\eta^2 = 0.25$; Figure 5G), indicating that the TA relaxation/contraction stages show overall lower variability than the SOL burst and peak force stages, along with an absence of a sharpening effect with beat, in contrast to the SOL burst and peak force.

3.2 Neural 1 – Potentials

FIGURE 6 HERE

Figure 6 shows the grand mean soleus EMG and midline EEG potentials for the 500 ms (Fig 6A), 600 ms (Fig 6B) and 700 ms (Fig 6C) tempi/rates, active versus passive. Within the cerebral leads, the initial response, prominent at FCz, is characterised by a large negative/positive deflection followed by a slower negativity which appears independent of tempo. Thereafter the successive responses adapt within two of three stimuli to a steady unchanging morphology, characterised by a complex N1, with rapid sub-components, followed by a steady P2, N2 waves. This pattern of initial, then steady morphology is reflected in all leads and occurs for both active and passive conditions. In cerebellar leads, the early rapid waves are more prominent, e.g. at Bz, comprising a N-P-N-P-N morphology. In relation to the movements, the SOL burst occurs after the peak in the N2 wave at FCz.

FIGURE 7 HERE

In order to appreciate the change in morphology from initial to steady response, we show in Figure 7 the grand mean global field power (GFP), IO2 and EEG channels across all tempi. The initial response (Figure 7A, left column) versus the grand mean of the steady response for the last four beats (Figure 7B, right column). In order to assist in classification, and for later source analysis, these have been divided into three epochs, and the responses contained therein referred to as short (SL, 10-50 ms), medium (ML, 50 – 80 ms) and long latency (LL, 80 – 500 ms). The LL have been further divided into LL1 and LL2 at the boundary between the P2 and later N2 related components. The SL components, following the stimulus artefact, remain largely invariant irrespective of condition, initial vs steady, or active vs passive, and

are dominated by vestibular sources, including the oVEMP in IO leads, and early VsCEPs, most easily recognised in PO9 (P20 and N26 peaks; late VsCEP) and PO10 (P12 and N17 peaks; early VsCEP), as has been reported (Govender et al., 2022). The ML and SL components, however, are radically different between the initial and steady responses. For the ML we see the appearance of the last components of the cerebellar N-P-N-P-N complex at Bz, along with associated rapid N1 components at FCz. For the LL the initial large N-P is strongly attenuated, especially around the N1 latency, both in the central and cerebellar leads.

FIGURE 8 HERE

Figure 8A separates the steady responses at FCz and Bz by condition (tempo and activity) and overlays the SOL EMG burst which occurs at a fixed position relative to target. Visual inspection would suggest that the latencies of the EEG components are generally independent of tempo, but the later components are affected by activity. Figure 8B shows the grand mean across tempi for active versus passive and also illustrates the difference potential obtained by subtracting the passive from the active from which we can recognise a number of features. Following the target we can identify what appear to be an initial reafference negative (RAN1) and post-motion positive (PMP1) associated with the down stroke (Praamstra et al 2001), followed by a second RAN/PMP associated with the up stroke of the foot tap. A broad pre-movement negativity (PMN) can be discerned prior to the TA relaxation/SOL burst, more clearly present at Cz.

TABLES 1 & 2 HERE

For the purpose of later analysis we label the components at FCz and Bz as in Figure 8. At FCz, prior to the LL N1-P2-N2, we can identify three early components, a P24, N40 and P60, and the N1 is generally split into two sub-components N1a and N1b. At Bz we identify a sequence of rapid potentials which co-occur with the early rapid potentials at FCz, i.e. N23, P40, N59, then P78, N94, P109, N123, followed by two slower waves N188 and P380. The mean latency and amplitude of these are provided in Tables 1 and 2.

3.3 Neural 2 – Power Spectra of Potentials

FIGURE 9 HERE

Figure 9 illustrates scaleograms produced by averaging the output of the continuous wavelet transform averaged across trials and subjects and then again across the last four beats and three tempi in the steady state at FCz and Iz for active (Figure 9A; left column), passive (Figure 9B; middle column) and subtracted conditions (Figure 9C; right column). The power at FCz is dominated by the low-frequency power over the θ, α and β bands. The higher frequency burst above 30 Hz close to the stimulus onset is caused by stimulus artefact. In contrast the power at Iz contains a prominent high-frequency band in u-γ, VHF and UHF bands. Following the stimulus is a prominent double burst-pause in both active and passive conditions.

FIGURE 10 HERE

Further details of the double burst-pause can be seen in Figure 10 which aligns the VHF/UHF power (Figure 10A,C) with the potentials at Bz, PO9/10, Iz and FCz (Figure 10B,D). We can see that the onset of the initial burst1 occurs close to the onset of initial positivity of the contra VsCEP at PO10, whilst the split peak of the initial burst1 aligns with the P12 and P20 of the contra and ipsi VsCEPs respectively. At Iz during the same period there is a mix of the P12 and P20, inverted at Bz with the N23. The subsequent VHF/UHF pause1 aligns approximately with the P40/N40 at Bz/FCz and the following burst 2 with the N60/P60 at Bz/FCz. The final pause2 is aligned with rising edge of the P78 wave and the N94 peak. From these alignments we can infer that the initial burst1 is associated with the sources contributing to the bilateral VsCEPs (climbing fibre responses or CFRs), while the subsequent pause1 is likely associated a post-CFR pause for both VsCEPs sources and with an additional third source contributing to the potential at Bz. The following burst2/pause2 is likely associated with the third source, a question explored more fully in the following section.

The time values for the boundaries demarking the double burst/pause were subsequently employed to define segments (SEGMENTS 7 – 10) for a statistical analysis of power. Due to the stimulus artefact, in order to avoid contamination the segment from -10 ms to + 12 ms following stimulus onset was not included in the analysis. The prior pre-stimulus interval was subdivided into six 50 ms segments (SEGMENTS 1 – 6) and post burst/pausing interval into three 50 ms segments (SEGMENTS 11 – 13). As outlined in the Introduction, we had

hypothesised that the role of the cerebellum could be considered analogous to voluntary conditioning whereby a conditioned response anticipating a US would be manifest as a conditioned pause on simple-spike activity, appearing in the ECeG as a reduction in high-frequency activity. In order to test this here we conducted an ANOVA on VHF/UHF power, initially with factors of TEMPO (500, 600 and 700 ms), BAND (u-gamma, VHF, UHF), BEAT (1-7) and SEGMENT (1-13).

TABLE 3 HERE

FIGURE 11 HERE

The outcomes of the ANOVAs, run separately for the passive and active conditions and then combined, are given in Table 3, and illustrated in Figure 11. Although there was a trend for the power to be overall higher for the active conditions, this did not reach statistical significance at the 5% level, nor were there any significant ACTIVITY interactions, possibly indicating that the conditioning effects were taking place irrespective of whether the subjects were tapping or not. Similarly there was no main effect of TEMPO nor any significant TEMPO interactions (Figure 11C). Although a main effect of BEAT effect at the 5% level for the passive condition was observed, indicating a small reduction in power with successive beats, this did not extend to the active and combo cases. Of particular interest, a main effect of SEGMENT was obtained for all three analyses (Figure 11A), but no significant interaction of SEGMENT by ACTIVITY. Pair-wise comparison showed a significant change from the initial segment for all three analyses with segments 8 and 9 (respectively p <.01 and <.05 in the combo analysis), corresponding to the post-stimulus pause1 and burst2. For the active and combo analyses, additionally significant pair-wise difference were obtained with pre-stimulus segments 4 and 5 (respectively p <.05 and <.05 in the combo analysis). In addition to the main effect, a SEGMENT by BEAT interaction was obtained for all three analyses (Figure 11B) indicating that the BEAT effect occurred only on specific pre- and post-stimulus segments, indicating a rapid adaptation with successive beat, even already after the 2nd US/CS head tap. The observation of these interactions is consistent with the hypothesised adaptation, and further illustrated in Figure 11C which shows the presence of both anticipatory pausing prior to US/CS onset, and the double burst/pause following US/CS onset, irrespective of tempo.

As the appearance of the double burst/pause even after the 2nd US/CS head tap is critical to the proposed account, we carried out a separate post-hoc analysis on segments 9 and 10

corresponding to burst2/pause2 (Figure 11D), which alone show a SEGMENT by BEAT interaction ($F(6,54) = 10.4$, $p < .01$, $\eta^2 = 0.53$), but no ACTIVITY interaction. If split again, main effects of BEAT are obtained independently for both segments 9 and 10 (Figure 11E and 11F) (respectively $F(6,54) = 8.3$, $p < 0.005$, $\eta^2 = 0.48$ and $= 7.3$, $p < 0.5$, $\eta^2 = 0.45$), with again no ACTIVITY interaction. A pair-wise comparison confirms that for segment 9 (burst 2), the adaptation is complete by beat 3, and for segment 10 (pause 2), by beat 2. Thus the conditioned double burst/pause appears rapidly within 2 to 3 beats, irrespective of whether there is an overt movement and irrespective of tempo.

3.4 Neural 3 – Currents

From the potential and power analyses, it is clear that there are multiple cerebral and cerebellar generators underlying the observed potentials. Within the cerebellum there are at least three, corresponding to the bilateral VsCEPs at PO9/10 and a source or sources corresponding to the potentials at Bz (Figures 5 and 8). The initial activity across electrode sites was relatively unchanged up to about 50 ms, irrespective of whether during the initial or steady responses. There then followed a series of rapid, then longer latency waves which were radically different for the initial vs steady responses. For this reason, for the purpose of a source analysis the epoch was divided into three sub-epochs, short (SL, 10 – 50 ms), medium (ML, 50 – 90 ms) and long (LL, 90 – 500 ms), and the BESA genetic algorithm run over six epoch combinations: SL, SL+ML, ML, ML + LL, LL and late LL (250 – 500 ms). These were applied for the four conditions: the active vs passive and the initial vs steady response. To improve signal to noise the active and passive cases were each averaged across the three tempi. Thus there was a total of 24 epoch/condition combinations. For each of the epoch/condition combinations the BESA genetic algorithm with 15 dipoles, repeated for 15 runs, resulting in 225 dipoles per epoch/condition combination and a cluster analysis applied to weed out the unreliable dipoles, with an exclusion criteria of a cluster SD of 5 mm.

TABLE 4 HERE

Table 4 shows an example of the outcome for the ML/passive/steady combination. The clusters were broadly categorised between cephalic and non-cephalic, of which included stimulus artefact clusters close to the point of stimulation. The cephalic clusters were subdivided between cerebral cortex and sub-cortex. Clusters were assigned a weight N,

depending on the number of dipoles they contained, and mean Talaraich and Tournoux X, Y, Z coordinate values (Talaraich and Tournoux 1988). For the cerebral cortical clusters they were further characterised by their lobular location, their Talairach sub-lobular mapping and Brodmann Area (BA) based on a +- 5 mm cube. The sub-cortical cerebellar clusters, were characterised by their Schmahmann Atlas (SA) location (Schmahmann et al. 1999). As can be seen from Table 5, the cerebral cortical clusters were widely distributed with a large number frontally, including in pre-frontal and pre-motor areas, as well as in temporal, parietal and occipital areas. Similarly, the cerebellar clusters were widely distributed. including in anterior and posterior lobes as well as in the hemispheres.

FIGURE 12 HERE

The combined outputs of the above process for each of the 24 epoch/condition combinations, 5376 input dipoles, resulted in a total of 657 dipole clusters which are illustrated in Figure 12A, B & C as a scatter plot in three planes. Collectively these form an approximately exponential distribution (Figure 12D), with parameters N = 950 and $\lambda = 0.238$, which implies that a total of 293 size one clusters (about 12 per epoch/condition combination) were excluded. Integration of the distribution give a sum of 3620 dipoles, meaning that of the original input dipoles, 1756 were either unreliable or non-cephalic, which would include stimulus artefact, ocular and EMG sources.

FIGURE 13 HERE

Of the final cephalic clusters, 467 (71%) were within the cerebrum and 190 (29%) sub-cortical. Within the cerebral sources (Figure 13A), 89 were located in the frontopolar (anterior) PFC (area 10), 70 in the temporal lobe, 51 in medial area 6, 50 in the occipital lobe, 42 in PPC or temporal/parietal cortex and 38 DL-PFC. Only a small number, 13, were directly located within SMC. Only 8 were located in the basal ganglia and none within the thalamus. Within the cerebellar sources (Figure 13B), the vast majority, 154, were located within the posterior cerebellar cortex, with 31 within the brainstem, but only 11 in anterior cerebellum, and 4 deep cerebellar nuclei. Comparing the source distribution for the initial versus the steady response, there was no significant difference for the cerebral sources overall ($\chi^2 = 17.6$, df = 15, $p = .28$, V = .19) but there was for the cerebellar sources ($\chi^2 = 19.7$, df =

4, p = .001, V = .32), consistent with the cerebellum being more active for the steady response. Comparing the source distribution for the active versus passive conditions (Supp. Figure 4C, D), for the SMC clusters, it was 9 versus 4 clusters for active versus passive, but neither the cerebral nor the cerebellar sources showed a significant difference overall.

TABLE 5 HERE

In order to further appreciate the organisation of the cephalic clusters, a second tier of cluster analysis was conducted, with the same exclusion criteria applied, and the result of 28 cephalic superordinate clusters displayed in Table 5. A large number of the superordinate clusters are located frontally, with a combined weight of 176 sub-clusters for PFC (predominantly area 10), 73 for medial PMC (area 6), 31 lateral PMC (area 6) and 18 for anterior cingulate cortex (ACC). Temporal lobe superordinate clusters make a combined weight of 67, widely distributed in superior (STG), middle (MTG) and inferior (ITG) lobes. Parietal superordinate clusters, with a combined weight of 79, are primarily located within the insula/inferior parital lobule (IPL), and to a lesser extent posterior cingulate (PCC)/superior parietal lobule (SPL). Occipital superordinate clusters, with a combined weight of 40 sub-clusters, are located predominantly within the cuneus (areas 18/19). For the subcortical superordinate clusters, the bulk are located in the posterior cerebellum, with a combined weight of 146 clusters, with a smaller number within the hemispheres (Crus I) and brainstem.

FIGURE 14 HERE

For the purpose of a generic dipole model for current analysis, the top superordinate 11 cephalic custers were selected, determined by weight, marked in bold in Table 5 and plotted separately as a scatter plot in Figure 14. For the cerebral sources, these are bilateral Fp-PFC (Sc. 1 & 2), rostral and caudal medial PMC (Sc. 3 & 4), which we label pre-SMA (Sc. 3) and SMA (Sc. 4) respectively, bilateral IPL (Sc. 5 & 6) and cuneus (Sc. 11). For the sub-cortical sources, these are the brainstem (Sc. 7), bilateral H VIIIA (Sc. 8 & 9) and right H VIIIB (Sc. 10). Four additional non-cephalic clusters were included, two right sided artefact sources (Sc. 12 & 13) and a symmetrical pair of ocular regional sources (Sc. 14 & 15). The artefact sources were determined by running the full model over the very initial artefact period (10 ms), and thereafter fixed in location and orientation. The ocular pair were located by running the full model after the artefact on the whole epoch of the grand mean, and

thereafter fixed. The orientations of the cephalic dipoles were obtained by running the full model over whole epoch separately for the grand means of the initial and steady conditions.

FIGURE 15 HERE

Figure 15 shows the currents measured separately for the first 10 sources for active vs passive conditions and initial (Figure 15A, left column) versus steady responses (Figure 15B, right column). The polarities are chosen to approximately match the long latency P2/N2 potentials, with a negative current (a sink) up. Within the initial or steady currents the dipole orientations are fixed from the grand mean of active and passive. As would be expected from the potentials (Figure 7), the currents, apart from during the initial SL epoch, are dramatically different between the intial and the steady responses, both in magnitude and morphology for all sources except the bilateral vestibular H VIIIA (Sc. 8 & 9).

FIGURE 16 HERE

In order to see how the currents align with potentials and high-frequency power we illustrate in Figure 16 seven of currents (Figure 16B; three cerebral, four sub-cortical) with five midline potentials (Figure 16A; Fpz, FCz, PO9/10 and Bz) and UHF power (Figure 16C). The peaks and troughs of the UHF double burst-pause are used to determine the alignment lines (and segments for the statistical analysis). The double initial burst (B1a/b at 15.2 and 23.1 ms) aligns within 2 ms with the initial positivities P14/P22 of the PO9/10 potentials and closely with the initial positive currents in the bilateral H VIIIA sources (Sc. 8 & 9). This suggests that these correspond to previously described VsCEP sources, observable at PO9 & PO10. Both brainstem (Sc. 7) and R VIIIB (Sc. 10) initial negative-positive deflections are also closely aligned (within 1 ms) with the initial double burst and the initial N23 of the Bz potential and P24 of the FCz potential with the 2nd of the initial double burst. The following double pause (P1a/b at 31.6 and 41.4 ms) is aligned (within 2 ms) with the second negative-positive deflections the R VIIIB (Sc. 10) and brainstem (Sc. 7) sources. The P1b also aligns within 2 ms with P40/N40 of the Bz/FCz potentials. For the second UHF burst-pause, there is a close alignment with both the R VIIIB source (Sc. 10) third –ve/+ve deflection and the Bz N60/P78 potential, along with the SMA source (Sc. 4) –ve/+ve deflection at the same (within 1 ms) latency.

FIGURE 17 HERE

In order to examine the properties of the source current in relation to the effects of tempo, we show in Figure 17 four key cerebral sources R a-PFC (Sc.2), pre-SMA (Sc.3), SMA (Sc.4) and R IPL (Sc 6) aligned with the R VIIIB source (Sc. 10) for an epoch averaged over the last four cycles for an epoch of -300 to + 500 ms. Several features are apparent. For the SMA source in particular, following the synchronous rapid deflections aligned with the 2nd UHF burst-pause, there are for the active conditions systematic movement-related negative deflections consisting of rising and falling slope components centred around the latency of the N2 potential. The falling slope components, starting at the N2 latency, are marked in red (Fig 17A), green (Fig 17B) and blue (Fig 17C) respectively for the three tempi with a linear approximation. In each case there are two examples, either side of the target. When superimposed, as shown in Figure 17D (top) for the active cases, we can see that the three movement-related falling slopes, as well as all starting around the latency of the N2, also appear to all reach their zero-crossing around 100 ms before target. Thus each of the post-N2 falling current slopes increased in length by 100 ms to achieve this (approximately 100, 200 and 300 ms respectively for the three tempi). After extraction, for each of the three pairs pre and post target we obtained linear slopes of -109.7 and -107.2 nA/s for the 500 ms case (respectively $R^2 = .87$, $p < .001$ and $R^2 = .85$, $p < .001$), -56.4 and -41.5 nA/s for 600 ms (respectively $R^2 = .83$, $p < .001$ and $R^2 = .74$, $p < .001$), and -19.2 and -26.5 nA/s for 700 ms (respectively $R^2 = .52$, $p < .001$ and $R^2 = .63$, $p < .001$), which are all highly significantly different when compared between tempi (respectively for 500 and 600 ms, $R^2 = .45$, $p < .001$, and for 600 and 700 ms, $R^2 = .46$, $p < .001$, Figure 17D, middle and bottom).

The currents in Figure 17 also appears to show tempo related changes in the current wave amplitudes for the different sources but in different ways. The PFC, pre-SMA and IPL source waves appear to increase with ISI, respectively for the R aPFC source (Sc.2) 34.4, 38.8 and 41.7 nA, for the pre-SMA source (Sc.3) 24.6, 31.9 and 37.4 nA. In contrast, the SMA source (Sc.4) appears to decrease or not change, respectively 27.4, 27.1 and 19.7 nA. The R VIIIB source shows a mixed pattern of change with tempo, an increase with ISI for the initial deflection associated with the initial burst, respectively 71.1, 75.3 and 85.3 nA, but a decrease for the deflection associated with the 2nd burst, respectively 67.4, 58 and 56.6 nA, corresponding to a difference of 3.7, 17.3 and 28.7 nA.

3.5 Neural 4 – Power Spectra of Currents

FIGURE 18 HERE

In order to test these apparent tempo related changes statistically, the source model was applied to each individual subject and the source currents extracted. A wavelet spectral power analysis of the currents was then conducted. Examples of these are shown in Figure 18 for pre-SMA (18A; top row), SMA (18B; middle row) and R VIIIB (18C; bottom row) sources. It is apparent that they all exhibit beta/gamma bursting and a variety of delta/theta effects during the following slow activity associated with the P2/N2 after the burst. In order to quantify these effects, we conducted an ANOVA on the same time segments as for the potentials. The ANOVA was, however, confined to segments in the beta band during the Iz UHF double burst/pause, as the early rapid current activity is primarily in the beta/gamma frequency range. For the beta band analysis, the first three sources L/R PFC and pre-SMA show main effects of TEMPO, BEAT and SEGMENT (respectively: $F(2,18) = 4.0$, $p < .05$, $\eta^2 = .31$; $F(6,54) = 12.6$, $p = .001$, $\eta^2 = .58$; $F(4,36) = 7.7$, $p < .05$, $\eta^2 = .46$), along with a BEAT by SEGMENT interaction ($F(24,216) = 3.9$, $p < .05$, $\eta^2 = .30$), but no main effect of SOURCE ($F(2,18) = 0.7$, ns , $\eta^2 = .07$). This suggests that the fast early beta activity does increase in amplitude with ISI, but drops off with successive beats and segments. In contrast, the SMA and R VIIIB sources do not show main effects of TEMPO ($F(2,18) = 0.62$, ns , $\eta^2 = .06$), but do show main effects of SOURCE and SEGMENT (respectively: $F(1,9) = 13.3$, $p = .005$, $\eta^2 = .60$; $F(4,36) = 19.6$, $p < .001$, $\eta^2 = .69$), indicative that these do not change with tempo and are sustained over the beat sequence but the early beta activity is greater in the cerebellar source compared to the cerebral source. If confined to the R VIIIB source, a trend interaction of TEMPO by SEGMENT is obtained ($F(8,72) = 2.0$, $p = .14$, $\eta^2 = .18$), consistent with differential tempo response between the early and later deflections associated with initial and second Iz UHF bursts.

4 Discussion

4.1 Summary of Results

In our study subjects were required to synchronise a foot tap to a vestibular metronome in the form of a mini-shaker mastoid impulse sequence with three alternative tempi randomly

presented. The onset of the metronome as well as the inter onset interval were random, so that the tempo was only clear from the onset of the second event. In response to this task our subjects were able to successfully achieve synchrony rapidly within three to four taps, manifest in a tap force peak with a small +ve asynchrony of about 10 ms. The subjects as a whole adopted a common strategy of making an initial stereotyped response of about 630 ms, close to the average tempo (ISI 600 ms), so that for the 500 ms ISI it arrived late and for the 700 ms early. They then rapidly adapted over the second and third response to achieve a steady state synchrony for the remainder of the sequence.

When breaking down the physiology of the foot tap performance we observed reciprocal activity of the soleus (SOL) and tibialis anterior (TA) muscles such that from a tonic dorsiflextion starting point there was an alternation of the SOL and TA EMG activity during the tap cycle. A steady cycle could be described as the following: (1) the initiation of TA relaxation and SOL contraction (measured as the X50 of the TA relaxation), (2) the TA maximum relaxation and SOL burst peak at about 100 ms prior to the target, (3) the force peak, (4) contraction of TA (measured as the X50 of the TA contraction) and SOL relaxation and (5) plateau of TA contraction. Measurements of four of the stages show that they all exhibit the same timing pattern occurring in a fixed sequence of asynchrony relative to target, largely invariant of tempo, except for the re-contraction TA and SOL relaxation (associated with the up stroke) which occurs slightly later for the longer ISI. In terms of variability, there is a trend for the force to sharpen over block and with beat and to increase with ISI, consistent with prior literature (e.g., Cos et al., 2015; Hove et al., 2014; Madison, 2014; Madison et al., 2013; Sternad & Newell, 2000). The pattern of force variability is also reflected in the SOL burst variability, but not the TA relaxation/contraction, which does not sharpen with beat. In terms of force amplitude, this also tends to increase with successive beat across tempi.

The grand means for the three tempi indicate that the neural responses reflect the behavioural: an initial response gives way to a steady response after three to four cycles. Given the stereotyped nature of the initial response and the tempo independent timing of the steady state down-stroke relative to target, we were able to make a grand mean of averaged EEG across the three tempi for the initial response and the average of the last four cycles. These show that in the SL epoch, the responses are very similar for both initial and steady responses, irrespective of whether active or passive. These include oVEMPs at IO leads and associated

VsCEPs at PO9/10, consistent with the vestibular stimulus. Thereafter we see a dramatic change. For the initial response a large negative-positive excursion is present, most clearly observed at FCz with latencies of about 110 and 200 ms, which dominates the GFP, followed by 2nd slow negative excursion, most notably in the active condition, prior to the expected forthcoming 2nd stimulus of yet unknown latency. This is accompanied by changes of similar latency at other sites, including a positive-negative deflection at Bz. In the steady state response the large negative-positive excursion at FCz is replaced a regular N1ab/P2/N2 ERP preceded by a series rapid changes during the ML epoch which co-occur with a series of rapid changes at other sites, but most notably at Bz. Comparing the active and passive conditions it is apparent that the active condition contains a mix of stimulus and movement related components (Praamstra et al 2001). Subtraction of the passive from the active conditions at FCz and Cz suggest a pre-movement negative (PMN) about 200 to 100 ms prior to target, close to the onset of the SOL burst, followed by what appears to be a double RAN/PMP, likely linked to the down and up phases of the tap cycle.

Of particular importance to the main hypotheses proposed, a spectral power analysis showed for the steady state response, the presence of a double burst pause in high-frequency ECeG at Iz which aligns with the evoked responses over the cerebellum. The initial burst-pause aligns with the VsCEPs at PO9/10 as previously identified, and is likely a CFR and associated post-CFR pause. The second burst-pause aligns with the rapid potentials at Bz and is thus likely manifestation of a conditioned CFR which only appears in the context of a forthcoming predicted event. Further, the ANOVA of high-frequency ECeG power following time segmentation showed consistent SEGMENT by BEAT interaction for both passive and active cases. Post-hoc analyses further indicated these changes occurred in key post-stimulus segments corresponding to the double burst and pre-stimulus segments associated with the period around the SOL burst. These results thus provide evidence of both conditioned predictive pausing in the ECeG prior to the expected US, analogous to that obtained with classical conditioning, and the emergence of a CS-related double CFR following repeated pairing. These conditioning effects occurred for both active and passive conditions, consistent with the notion that cerebellar conditioning occurs automatically and rapidly, irrespective of whether it results in an overt movement. This aspect of cerebellar conditioning parallels our prior observation in the case of classical conditioning (Todd et al. 2023a), i.e. that there must an additional cerebral mechanism which controls movement selection and preprogramming.

Finally, we conducted a source analysis of the grand mean initial (unconditioned) response and steady state (conditioned) response. These indicated “main player” sources in areas that have been strongly implicated in imaging studies (e.g., Bijsterbosch et al., 2011; Harry et al., 2023; Kasdan et al., 2022; Nozaradan et al., 2016; Snyder et al., 2024; Witt et al., 2008; Xu et al., 2006), including bilateral prefrontal cortex, pre-SMA, SMA and bilateral IPL, along with bilateral lobule VIIIA vestibular sources, brainstem and critically, a right lobule VIIIB source corresponding to the rapid Bz potential and associated conditioned CFR manifest in high-frequency ECeG. A further analysis of the spectral power of the currents, confirms that the rapid early potentials and associated conditioned CFR are predominantly the beta-gamma frequency range with later theta activity associated with the slow potentials. ANOVA of the beta current bursting along with changes in current amplitude with TEMPO showed high beta source coherence and a dissociation in the behaviour of sources. The bilateral PFC and pre-SMA group show an increase with ISI while the SMA and R VIIIB cerebellar source do not increase with ISI and may even decrease with ISI. The R VIIIB cerebellar source also showed evidence that the early and later components of the beta burst associated with the conditioned CFR may diverge in their tempo dependency. Of particular interest, the SMA source showed a very clear and highly significant tempo dependent change in the post N2 movement-related falling slopes which anticipate the SOL burst.

4.2 A cortico-basal ganglia-cerebellar-hippocampal network for SMS.

FIGURE 19 HERE

In order to interpret these results we articulate what is known about the connectivity of the cerebral and cerebellar sources obtained, and their inputs and outputs in relation to the vestibular and the somatic motor systems, illustrated in Figure 19. Several models of timing behaviour account for cerebellar connectivity with other subcortical as well as cerebral regions (e.g., Andersen & Dalal, 2024; Gibbon et al., 1997; Petter et al., 2016; Schwartze & Kotz, 2013; Teki et al., 2012) but the precise cerebellar pathways have remained unresolved. Our theoretical framework and empirical findings are informative about these specific pathways in relation to broader established patterns of connectivity.

Our stimulus clearly was effective in activating the vestibular system as we observed oVEMPs and bilateral VsCEPs and sources close to those obtained previously (Todd et al.

2021a). The vestibular receptors are known to project to the cerebellum directly and via the vestibular nuclei both as climbing fibres via the inferior olive and as mossy fibres via the pons (Buttner-Enever 1999). The vestibular system also projects widely to the cerebral cortex via multiple areas of the thalamus (Wijesinghe et al. 2015), allowing wide convergence with other sensory systems and with the basal ganglia. As we hypothesised, this means that vestibular stimuli are capable of acting both as a US and CS with conjunctive inputs of CFs and PFs on Purkinje cells (PCs) in the cerebellar cortex to facilitate motor learning within the Marr/Albus framework (Marr 1969; Albus 1971). Our observation of evidence of conditioned pausing in the high-frequency ECeG prior to the target supports this interpretation.

The output of the cerebellum is via the deep cerebellar nuclei which project widely to the brainstem, reticular formation and thalamus (Eccles et al. 1969). It had been traditionally thought that the deep cerebellar nuclei (DCN) project via the VL thalamus for sensorimotor function (Eccles et al. 1969), and specifically VL pars caudalis (VLc) (Passingham 1994), but it is now accepted that they are more widely distributed, including VPL and CM (Haines 2008), and beyond including VM, MD, CL nuclei to support the broader involvement in cognitive and affective function (Heck et al 2023). Our observation of the double burst-pause and associated beta current burst in the R VIIIB source following the target stimulus is consistent with the presence of a CS-complex spike, which tend to occur as a pair within 100 ms following CS onset before CR onset (Ohmae and Medina 2015; ten Brinke et al. 2019). The wide distribution through multiple thalamic nuclei, therefore, means that this signal would be available to drive higher order acquisition/learning in multiple regions within the cerebrum (ten Brinke et al. 2019).

Of the dominant cerebral cortical sources, bilateral aPFC (area 10), pre-SMA (area 6), SMA (area 6) and bilateral IPL (area 40) have long been associated with sensorimotor processing (Petter et al 2016). However, the implication of BA 10 specifically suggests the involvement of a prospective memory mechanism for future action (Cona et al. 2015). BA 10 is known to be involved in the encoding, maintenance and retrieval of intention (Cona et al. 2015). Although our task involved the rapid adaptation to the metronome, it also involved the memorisation of the three alternative timed responses (with intervals of 500, 600 and 700 ms) during training, cued retrieval of one of the three on detection during the start of a trial, then execution of the intention during the synchronisation phase. aPFC (area 10) and IPL are implicated in all three of these phases (Cona et al. 2015). dl-PFC/IPL are said to make up the

"central executive network" implicated in attention and memory (Mulders et al 2015). Although dl-PFC was not one of the sources in the generic model, it was one of the clusters in the complete analysis.

Pre-SMA (area 6) and SMA (area 6), along with M1/S1 are also implicated in the execution of intentional actions (Cona et al. 2015). Medial premotor cortex (BA 6) has long been central to the account to temporal processing (Schwartze et al 2012), but it is generally considered that pre-SMA and SMA are dissociated in their function, between sensory and sensorimotor aspects (Schwartze et al 2012). Anatomically they are also distinct (Rahimpour et al. 2022). Pre-SMA and SMA both share extensive connections with the cerebellum, the basal ganglia, other regions of the frontal cortex and posterior parietal areas. However, they do not have direct cortico-cortical connections, but rather interact via their common connections, including the basal ganglia, although these are separate circuits (Rahimpour et al. 2022). Pre-SMA is strongly connected to PFC but with little input to M1 and is thought to be associated with cognitive processes. In contrast, SMA is strongly connected to M1 and thought to be directly involved with motor planning (Rahimpour et al. 2022).

For our current sources too, the pre-SMA and SMA are distinct. Whereas the pre-SMA current amplitudes increase in amplitude with ISI, the SMA source does not show the same trend but has a direct movement related tempo dependent feature. This is in the form of post N2 movement-related falling slopes which anticipate the SOL burst, an index of movement planning. The pre-SMA source shows a strong BEAT effect, consistent with it being primarily responsive at the initial external cue detection stage. The SMA source does not show a BEAT effect and remains relatively constant throughout the sequence. This difference may also reflect another recognised contrast of pre-SMA and SMA, between externally vs internally guided action (Nachev et al. 2007). As the sequence progresses the balance between external and internal guidance shifts from one to the other.

Given the extensive connectivity of the PFC, pre-SMA and SMA to the basal ganglia, we have included the basal ganglia in the circuit. We did not strongly detect either basal ganglia or thalamic activity with our method, and this is one of its limitations. However, the fact of SMA involvement indicates that the basal ganglia were participating in the task (Rahimpour et al. 2022). The basal ganglia have been strongly indicated in rhythm perception, production, and sensorimotor synchronization (Cannon & Patel, 2021; Levitin et al., 2018; Schwartze et

al 2011; Snyder et al., 2024). In the circuit we have indicated the indirect pathway via striatum, GPe and STN, the direct pathway via striatum to GPi/SNr and hyperdirect which cuts out the striatum. The loop is completed with the output of GPi/SNr to the thalamus to VL or VA, depending on whether it is the PFC, pre-SMA or SMA loop. SNc provides dopaminergic input to both direct and indirect pathways, but with differential receptors, D1 v D2 (Gerfen & Surmeier, 2011). We also indicate the limbic loop within the ventral striatum (nucleus accumbens NA) and dopaminergic input via the VTA.

Of particular relevance to the case is the fact that increasingly it has become clear that the basal ganglia and cerebellum should not be seen as functionally distinct, but rather nodes in a common network with the cerebral cortex (Andersen & Dalal, 2024; Bostan and Strick 2018; Criscuolo et al., 2025; Kasdan et al., 2022). Of critical importance to this debate, is the realisation that the cerebellum and basal ganglia are directly connected sub-cortically (Milardi et al., 2019) and these connections are indicated in the diagram. The basal ganglia output reaches the pons via the STN, thus allowing it to provide context in cerebellar learning. In the other direction, the cerebellum can provide input to the striatum via the CM nucleus of the thalamus (Bostan and Strick 2018), and more generally via the parafascicular (Pf) nucleus which forms a complex with the CM nucleus (Gonzalo-Martin et al. 2024). More recently, it has been shown that the cerebellum also projects more directly to the output stations GPe and SNr (Milardi et al. 2019; Washburn et al 2024) and to dopaminergic neurons including the VTA and SNc, either directly or via the Pf-CM complex (Carta et al 2019; Yoshida et al 2022; Baek et al. 2022; Gonzalo-Martin et al. 2024). There is also evidence of direct vestibular inputs via the same Pf-CM complex (Smith 2018), or via the parabrachial nuclei (Balaban 2004; Balaban and Yates 2004). Thus the cerebellum is well placed to drive reward based learning in the basal ganglia, including for learning a timed output to drive the synchronised motor response via SMA/M1.

Any such outputs, either directly from the STN or via descending cortico-fugal influences from SMA/M1 will be available as convergent inputs to the pons (Passingham 1994), along with with any reafferent spinocerebellar influences to reinforce cerebellar learning (Eccles et al 1969; Haines 2008). The spinocerebellar influences also include spino-olivary projections (Eccles et al 1969; Haines 2008), so that these may play a role in error correction. Ascending spino-thalamo-cortical reafference, via the dorsal column- medial lemniscus system and VPL nucleus of the thalamus (Haines 2008), also fascilitates sensori-motor coordination at a

cortical level (Davis et al. 2022). Our data suggests that there were two major ascending reafference volleys associated with the down and up strokes as we observed a double RAP/PMN (Praamstra et al 2003). Reafference information would also be available to posterior parietal cortex for higher level planning and sequencing, including memory retrieval and attention for sensory-guided action via cortico-cortical connectivity and via a loop through the cerebellum via the pons (Stein 1986; Stein and Glickstein 1992).

The above described network is, however, incomplete without the inclusion of a third subcortical structure involved in timing, namely the hippocampus, if for no other reason that trace conditioning, in which the CS and US are separated by an inter-stimulus interval, requires an intact hippocampus (Bangasser et al. 2006; Petter et al. 2016). We did not directly detect hippocampal sources, but there were a very large number of temporal lobe sources (second only to prefrontal sources), including from ITG and MTG, as well as STG. Among these also there were sources that were in area 37, which can be regarded as parahippocampal, and sources in both anterior and posterior cingulate areas which are strongly connected to hippocampus. It is now also realised that the cerebellum and hippocampus are strongly inter-connected (Watson et al. 2019; Froula et al. 2023; Bernard 2025), and that this connectivity may be direct from the DCN (Arrigo et al. 2014), including a direct return to the pontine nuclei (Newman and Reza 1979; Cragg and Hamlyn 1959). As well as cerebellar direct inputs, the vestibular system is also known to have very strong connections to the hippocampus for orientation, spatial processing and navigation (Hitier et al. et al. 2014; Stackman et al. 2002; Zwergal et al. 2024).

In addition to the hippocampal-cerebellar interaction, the hippocampus also has a direct interaction with the basal ganglia (Sabatino et al. 1986; Du et al. 2021; Wylie et al. 2023). This interaction plays an important role in learning, memory and motor control (Penhune and Steele 2012), including in sensorimotor integration (Hallworth and Bland 2004). From the hippocampus, there are multiple direct and indirect projections to ventral (nucleus accumbems) and dorsal striatum (Du et al. 2021). In turn the basal gangla may influence the hippocampus via palladial outputs to the penduculopontine nucleus (PPN) and septal nucleus (SeN) (Sabatino et al. 1986). Further, the hippocampus is involved in a loop with the VTA (Lisman et al 2005), thought to play a role in controlling long-term episodic memory, along with prefrontal cortex (Eichenbaum 2017), including for prospective memory (Rolls 2023). Both vestibular system and cerebellum have strong influence on the PPN, which along with

direct cerebellar influence on the VTA provide the basis the cerebellum to drive reward based espisodic learning and memory formation in the hippocampal-prefrontal system, as well as the basal ganglia.

4.3 A cortico-basal ganglia-cerebellar-hippocampal timing mechanism.

We aimed in this study to show evidence of cerebellar involvement in the acquisition of SMS in a manner consistent with it being analogous to a form of conditioning. We anticipated two distinct possible sources of evidence for this: (1) conditioned anticipatory pausing in the high-frequency ECeG indicative of pausing of underlying simple spike activity prior to US onset (Albus 1971; Jirenhead and Heslow 2016); and (2) conditioned CF activity and an associated double burst pause following CS onset when a US was expected (Ohmae and Medina 2015; ten Brinke et al. 2019). We found evidence of both mechanisms, which provide evidence to support the view that the cerebellum was indeed playing such a role, although the magnitude of the anticipatory pausing was not large. The C-CRFs and associated double burst pause, appear rapidly, already after the 2nd CS/US, and are thus rapidly available for signalling to the rest of the network of brain areas involved in timing for the rapid acquisition of synchronisation. In addition to the double burst-pause in the high frequency ECeG, the C-CFRs were also associated with beta-gamma burst in our source R VIIIB which was highly coherent with the PFC, SMA and IPL sources, key hubs in the timing network. Thus the beta-gamma bursting is likely the mechanism by which the network achieves synchrony.

Previous research has examined modulations in cerebral beta power and coherence (Fujioka et al., 2012, 2015; Gulberti et al., 2024), beta band cortico-muscular coherence (Nijhuis et al., 2021; Varlet et al., 2020), and gamma amplitude (Harding et al., 2025; Snyder & Large, 2005; Zanto et al., 2006) in active and passive rhythmic tasks, but cerebellar involvement in such modulations has been not previously been studied in the context of SMS. However, cerebro-cerebellar coherence in the beta band has been widely observed during both active and passive expectancy (Courtemanche and Lammarre 2005), and during precision gripping (Soteropoulos and Baker 2006). It is thought to be one of the main mechanisms by which the cerebro-cereballar system maintains functional connectivity (Watson and Apps 2022), but may however play different roles (Nougaret et al. 2024). Low beta power has also been

implicated in models of timing (Tanaka et al. 2024), and beta/gamma bursting has been observed in the striatum during synchronisation/continuation (Bartolo et al. 2014).

Of the key cerebral hubs in the acquisition of SMS, the strong participation of aPFC (area 10) is indicative that subjects were employing a prospective memory system for the three alternative timed responses (Cona et al 2015; Underwood et al. 2015; Burgess et al 2022), involving the encoding of prospective memory for intention during the learning trials which were retrieved at the start of each trial the when the temporal cue was detected. The strong participation of the SMA system in the form of tempo dependent post N2 pre-movement negative slopes was also indicative of participation of underlying basal ganglia involvement, as it has been demonstrated that pre-movement negativities, both the BP and CNV involve the basal ganglia (Purzer et al. 2007). The account must also include a role for the hippocampus (Petter et al, 2016). The SMA and basal ganglia are central to many models and theories of both interval and beat based timing (Cannon & Patel, 2021; Merchant et al. 2024; Rueda-Orozco et al 2024; Schwartze and Kotz 2024). However, hippocampus is also implicated in timing tasks beyond trace classical conditioning (Lusk et al. 2016), especially for encoding and retrieval of sequential timed movements in conjunction with PFC (Wise and Murray 1999; Eichenbaum 2017; Rolls 2023; Dolfen et al. 2024; Yewbrey and Kornysheva 2024).

Thus we may see the participation of three learning mechanisms as suggested by Bostan and Strick (2018), a cerebral cortical unsupervised learning mechanism, a basal ganglia reinforcement/reward based learning mechanism and a cerebellar supervised/error based learning mechanism. However, in the present case, the strict division between error and reward cannot hold as the C-CFRs do not behave as an error correction mechanism, but rather more as a predictive reward signal. As noted by Ohmae and Medina (2015), these C-CFRs are “markedly similar to the responses of dopamine neurons during reinforcement learning”. This view has received substantive support subsequently (Heffley et al. 2018, 2019; Dimitar et al. 2019; Javier 2019; Mario e al. 2024; Shuyang and Hull, 2025; Rin et al. 2025). Thus, C-CFRs and their downstream basal ganglia targets, in the SNc and VTA, hence the nigro-striatal, mesolimbic and mesocortical dopamenergic projections, are powerfully placed to drive both basal ganglia and cerebral cortical learning of anticipated reward from the vestibular US (Heffley and Hull 2019; Soares et al 2016), along with hippocampal-prefrontal episodic memory formation (Lisman et al. 2005).

Of particular interest, the SMA and basal ganglia are widely acknowledged as critical to maintenance of motor timing once the interval has been acquired, but their exact function is not agreed. Several hypotheses have been proposed. One common proposed mechanism is a ramping accumulator behaviour instantiated in the SMA/basal ganglia system (Casini and Vidal 2011; Merchant and Lafuent 2024; Merchant et al. 2024). The pace-maker accumulator approach is one such model which accumulates an oscillatory input and a decision is made when the ramp achieves a threshold (Balci and Simen 2024). In an alternative implementation, the "striatal beat frequency model" (Buhusi and Meck 2005), it is envisaged that "neural oscillators" in prefrontal cortex provide a clock, which combined with a striatal working memory and dopaminergic reinforcement provide the basis for a timed output to SMA (Oprisan and Buhisi 2014). Ramping behaviour in predictive CNVs during implicit timing has also been observed, suggesting basal ganglia involvement (Praamstra et al. 2006; Casini and Vidal 2011), and also in cued temporal prediction (Breska and Ivry 2020). Examples of ramping behaviour have been observed in VL thalamic and DCN neurones in prepatory activity for self-paced saccades (Tanaka et al 2024), and striatal and DCN neurones to triggered saccades (Kameda et al. 2023).

None of these behaviours, such as CNV-like ramping, match the data we observed in the present study, however. This is consistent with the tendency of the CNV to diminish over the course of an experiment (Petter et al 2016), and a CNV may only be present for single response timing (Breska and Ivry 2020), or at the start of a trial with multiple rhythmic responses. We did observe a down-ramping behaviour in the SMA source, but its initial up-slope (with –ve up) and amplitude were relatively fixed at the start of the post-N2 period and its down-slope was tempo-dependent so that for all three tempi the zero-crossing was reached at about the same time before the target. Rather than being a variable accumulator CNV-like up-ramp system (with –ve up), it behaves more like an "hourglass" timer with a fixed initial quantity of sand particles but with a variable aperture to control the rate of flow, or from an electrical point of view, a discharge with a fixed initial charge and a variable resistance. This suggests that although the SMA/basal ganglia are producing a variably timed output, they are being pre-programmed and triggered elsewhere, in this case by the cerebellum. The C-CFR and associated beta burst provides a trigger to start the timer and may also provide information about the expected interval. As noted in the results (Figure 17), the initial and 2nd burst/pause and associated current burst (R VIIIB source) show evidence of tempo

dependent changes. The cerebellar conditioned pausing activity, and associated theta desynchronisation (Todd et al. 2025), prior to the target may also be available as a timing guide for the SMA/basal ganglia system.

The proposal of a neural "hourglass" mechanism in the form of time ramping cells for short interval timing at the millisecond scale would, however, appear to be a novel one. In fact, "hourglass"-like time ramping behaviour has been observed in the entorhinal cortex of the hippocampus (Rolls and Mills 2019; Rolls 2023), though these are typically over 10s to 100s of seconds. It is proposed that these combine in multiple competing populations for the generation and representation of episodic memory. It would also need to be coordinated with striato-cortical activity to translate into a motor output, e.g. via PFC-striatal route.

It is accepted that the cerebellum is essential for the acquisition of synchronisation at low millisecond timescales (Lusk et al 2016; Iversen and Balasubramaniam 2016). Whether the above observations would still be apparent during a continuation phase, where it is believed the role of cerebellum is less paramount (Chauvigne et al 2015; Iversen and Balasubramaniam 2016), and the SMA/basal ganglia system predominant can only be answered by further experimentation. However, once synchrony has been achieved, in principle continuation by means of the cortico-basal ganglia-cerebellar timing mechanism is still feasible where both descending and ascending reafference could provide both CF and MF inputs without vestibular reinforcement. It has been suggested, based on a meta analysis of 43 imaging studies (Chauvigne et al 2015), that the spino-cerebellum does not participate at all in continuation. However, the Chauvigne et al (2015) study did not report any activity from lobules VII, VIII, IX, X or Crus I/II or brainstem from any of the studies in either synchronisation (externally paced) or continuation (self-paced), suggesting that most of the imaging studies did not fully cover the cerebellum or brainstem in field of view or did not report from the cerebellum or brainstem. The under representation of the cerebellum remains a common problem with imaging in general, which perhaps contributes to a basal ganglia centric bias (Wang et al. 2025).

Our dominant cerebellar sources in the present study were in fact all from the inferior/posterior cerebellum. Our previous study of self-paced voluntary movement showed extensive activation of the cerebellum in both the anterior and posterior cerebellum, from vermis and hemispheres for hand and foot movements (Todd et al 2023). This was consistent

with the implication of lesion studies for a role of the cerebellum in generation of the Bereitshaftpotential, as well as SMA/basal ganglia, (Sasaki et al. 1979; Shibasaki et al. 1986; Ikeda et al 1994; Wessel et al. 1994). Furthermore, studies with cerebellar patients have shown deficits in both synchronisation and continuation phases in a synchronisation/continuation task (Breska and Ivry 2016), especially in variability compared PD patients and healthy controls, even at intervals greater than 1 second (Classen et al. 2012). The greater timing variability with cerebellar patients extends to spontaneous self-paced tapping (Schwartze et al. 2016), and is specific in the case of unilateral lesions to the impaired limb (Ivry et al 2006). As it happens, our source R VIIIB (Sc. 10) corresponding to the CCFR and associated beta burst was on the right side, ipsilateral to the right foot.
It does seem likely, however, that a short interval neural "hourglass" mechansism involving a cortico-basal ganglia-cerebellar network could only operate up to a limit and likely gives way for intervals longer than about 1 second to an alternative, perhaps cortico-striatal CNV-like ramping mechanism, (Buhusi and Meck 2005; Petter et al. 2016; Lusk et al 2016). Even in this case, the cerebellum is likely still to make a contribution, e.g. by means of slow theta desynchronization (Todd et al. 2025), or perhaps by other novel mechanisms (Garcia-Garcia et al. 2024).

4.4 Conclusion

In the present study we recorded from cerebrum and cerebellum during the acquisition of synchronised foot tapping to three alternative randomly presented tempi. Following an initial stereotyped response, the subjects were able to acquire synchrony rapidly within three to four foot taps whereby the asynchronies of the stages within the tap cycle were invariant with tempo. These characteristics were reflected in the neural data which enabled averaging across tempi. In the steady state, potentials were characterised by a series of rapid short latency waves followed by slower N1/P2/N2 ERPs. Spectral power analysis of the potentials at Iz and a surrounding grid confirmed the presence of two distinct hypothesised conditioned changes, a conditioned climbing fibre response (CCFR) within 100 ms following the target onset and conditioned pausing in the high frequency ECeG in anticipation of the target onset. Thus these data support our proposal that SMS can be viewed as a form of successive conditioning.

However, as anticipated, source analysis revealed the involvement of widespread cerebral areas in bilateral PFC, pre-SMA, SMA, bilateral IPL as well as cerebellar areas in bilateral vestibular H VIIIA/VIIB sources along with a right H VIIIB source and a brainstem source. The right H VIIIB source was aligned with the CCRF and a potential at Bz. These confirmed that the CCRF was associated with beta/gamma bursting which was highly coherent across sources. Within the SMA source we also observed tempo-dependent post-N2 movement related down-ramp timed to make a zero-crossing about 100 ms prior to target irrespective of tempo. Collectively these data suggest the involvement of a cortico-basal ganglia-cerebellar-hippocampal adaptive learning network driven by a CCRF/beta burst reward signal and a novel cortico-striatal-hippocampal short interval time ramping mechanism. This conception of a cortico-basal ganglia-cerebellar timing network is not dissimilar to other proposals (e.g. Lewis & Miall 2003; Teki at al 2012; Petter et al. 2016; Schwartze and Kotz 2024), but with an essential difference. The strict separation of cerebellar and basal ganglia learning as being driven by error versus reward no longer holds, where the DCN have direct access to reward signalling in VTA and SNc, and the cerebellar classically conditioned interval timer may continue to contribute to the initiation and maintenance of sequential synchrony over the range of common tempi. As we note above, a hippocampal component is also required (Lusk et al. 2016).

Finally, given the exploratory nature of the present analyses, it will be interesting in future studies to confirm and explore the limits of this proposed mechanism in both synchronisation and continuation tapping, where it may break down with longer intervals, and in response to sudden perturbation of period or phase (Repp 2005; Repp and Su 2013).

Conflict of Interest Statement: The authors declare that the research was conducted in the absence of any commercial or financial relationships that could be construed as a potential conflict of interest.

Consent to Participate Declaration: Written informed consent was obtained from all subjects.

Ethics Statement: The study was approved by the local ethics committees (South Eastern Sydney Local Health District Human Research Ethics Committee and Western Sydney University Human Research Ethics Committee).

Author Contributions (CRediT). NPMT: Conceptualization, Methodology, Software, Data curation, Investigation, Validation, Formal analysis, Supervision, Funding acquisition, Visualization, Writing - original draft, Writing - review & editing. **SG:** Investigation, Visualization, Writing - review & editing. **DH:** Investigation, Visualization, Writing - review & editing, Data curation, Formal analysis. **MV:** Conceptualization, Project administration, Investigation, Writing - review & editing, Supervision. **PEK:** Conceptualization, Methodology, Writing - review & editing, Project administration, Supervision, Funding acquisition, Validation. **JGC:** Conceptualization, Methodology, Supervision, Resources, Project administration, Writing - review & editing, Funding acquisition, Validation.

Funding Statement: Research supported by a grant from the Australian Research Council DP210100552**.**

Data Availability Statement: Data available on request.

References

Albus JS. (1971) A theory of cerebellar function. *Math Biosci.*; 10: 25-61.

Andersen LM, Jerbi K, Dalal SS. (2020) Can EEG and MEG detect signals from the human cerebellum? *Neuroimage.* 215:116817.

Andersen LM, Dalal SS. (2024). The role of the cerebellum in timing. *Current Opinion in Behavioral Sciences*, *59*, 101427.https://doi.org/https://doi.org/10.1016/j.cobeha.2024.101427

Apps R, Watson TC (2022) Cerebro-cerebellar connections. In D. Manto, DL Gruol. JD Schmahmann, N Koibuchi, F Rossi (Eds) *Handbook of the Cerebellum and Cerebellar Disorders.* Springer, pp 1131-1153.

Arrigo A, Mormina E, Anastasi GP, Gaeta M, Calamuneri A, Quartarone A, et al. (2014) Constrained spherical deconvolution analysis of the limbic network in human, with emphasis on a direct cerebello-limbic pathway. *Front Hum Neurosci.* 8.

Baek SJ, Park JS, Kim J, Yamamoto Y, Tanaka-Yamamoto K (2022) VTA-projecting cerebellar neurons mediate stress-dependent depression-like behaviours. *Elife* 11, e72981.

Balaban CD (2004) Projections from the parabrachial nucleus to the vestibular nuclei: potential substrates for autonomic and limbic influences on vestibular responses. *Brain Res* 996, 126-137.

Balaban CD and Yates BJ (2004) Vestibuloautonomic interactions: A teleological perspective. In SM Highstein, RR Fay and AN Popper (Eds) *Anatomy and Physiology of the Central and Peripheral Vestibular System.* Springer-Verlag, Heidelberg, pp 286-342.

Balcı F, Simen P. (2024). Neurocomputational Models of Interval Timing: Seeing the Forest for the Trees. In: Merchant, H., de Lafuente, V. (eds) *Neurobiology of Interval Timing. Advances in Experimental Medicine and Biology, v*ol 1455. Springer, Cham. https://doi.org/10.1007/978-3-031-60183-5_4

Bangasser DA, Waxler DE, Santollo J, Shors TJ. (2006) Trace conditioning and the hippocampus: the importance of contiguity. *Journal of Neuroscience* 26, 8702-8706. doi: 10.1523/JNEUROSCI.1742-06.

Bartolo R, Prado L, Merchant H.(2014) Information processing in the primate basal ganglia during sensory-guided and internally driven rhythmic tapping. *Journal of Neuroscience* 11, 3910 - 3923. DOI: 10.1523/JNEUROSCI.2679-13.

Bernard JA. (2024) Cerebello-hippocampal interactions in the human brain: A New Pathway for Insights Into Aging. *Cerebellum* **23**, 2130–2141. https://doi.org/10.1007/s12311-024-01670-5

Bijsterbosch JD, Lee KH, Hunter MD, Tsoi DT, Lankappa S, Wilkinson ID, Barker AT, Woodruff PWR. (2011). The role of the cerebellum in sub- and supraliminal error correction during sensorimotor synchronization: evidence from fMRI and TMS. *Journal of Cognitive Neuroscience*, *23*, 1100-1112. https://doi.org/10.1162/jocn.2010.21506

Bostan AC, Strick PL. (2018). The basal ganglia and the cerebellum: nodes in an integrated network. *Nature Reviews Neuroscience, 19*(6), 338-350. https://doi.org/10.1038/s41583-018-0002-7

Breska A, Ivry RB. (2016). Taxonomies of timing: where does the cerebellum fit in? *Curr. Opin. Behav. Sci.,* 8. 282-288

Breska A, Ivry RB. (2020). Context specific control of the neural dynamics of temporal attention by the human cerebellum. *Science Advances* **6,** eabb1141.

Buhusi C, Meck W. (2005). What makes us tick? Functional and neural mechanisms of interval timing. *Nat Rev Neurosci* **6**, 755–765 https://doi.org/10.1038/nrn1764

Burgess P W, Crum J, Pinti P, Aichelburg C, Oliver D, Lind F, et al. (2022). Prefrontal cortical activation associated with prospective memory while walking around a real-world street environment. *NeuroImage, 258*, 119392.

Buttner-Enever JA (1999) A review of otolith pathways to brainstem and cerebellum. *Ann N Y Acad. Sci* 871, 51-64.

Cannon J. (2021). Expectancy-based rhythmic entrainment as continuous Bayesian inference. *PLOS Computational Biology*, *17*(6), e1009025. https://doi.org/10.1371/journal.pcbi.1009025

Carta I, Chen CH, Scott A, Dorizan S, Khodakhah K (2019). Cerebellar modulation of the reward circuitry and social behaviour. *Science* 363(6424).

Casini L, Vidal F (2011) The SMAs: Neural substrate of the temporal accumulator?. *Frontiers in Integrative Neuroscience* 5, 35. https://doi.org/10.3389/fnint.2011.00035.

Chauvigne LAS, Gitau KM, Brown S. (2014) The neural basis of audiomotor entrainment: an ALE meta-analysis. *Frontiers in Human Neuroscience* 8, 776.

Claassen DO, Jones CR, Yu M, Dirnberger G, Malone T, Parkinson M, Giunti P, Kubovy M, Jahanshahi M. (2013). Deciphering the impact of cerebellar and basal ganglia dysfunction in accuracy and variability of motor timing. *Neuropsychologia* 51, 267-74. doi: 10.1016/j.neuropsychologia.2012.09.018.

Cona G, Scarpazza C, Sartori G, Moscovitch M, Bisiacchi PS. (2015) Neural bases of prospective memory: A meta-analysis and the "Attention to Delayed Intention" (AtoDI) model. *Neuroscience and Biobehavioural Reviews* 52, 21-37.

Cos I, Girard B, Guigon E. (2015). Balancing out dwelling and moving: optimal sensorimotor synchronization. *Journal of Neurophysiology*, *114*(1), 146-158. https://doi.org/10.1152/jn.00175.2015

Courtemanche R, Lammarre Y. (2005) Local field potential oscillations in primate cerebellar cortex: synchronisation with cerebral cortex during active and passive expectancy. J *Neurophysiology* 93, 2039-2052.

Cragg BG, Hamlyn LH. (1959) Histologic connections and electrical and autonomic responses evoked by stimulation of the dorsal fornix in the rabbit. *Experimental Neurology* 1, 187-213. doi.org/10.1016/0014-4886(59)90001-9.

Criscuolo A, Schwartze M, Nozaradan S, Kotz SA. (2025). Basal ganglia and cerebellar lesions causally impact the neural encoding of temporal regularities. *Imaging Neuroscience*, *3*. https://doi.org/10.1162/imag_a_00492

Davis M, Wang Y, Bao S, Buchanan JJ, Wright DL, Lei Y (2022) The interactions between primary somatosensory and motor cortex during human grasping behaviours. *Neuroscience* 485, 1-11.

Dimitar K, Beau M, Blanco-Pozo M, Häusser M. (2019) Predictive and Reactive Reward Signals Conveyed by Climbing Fiber Inputs to Cerebellar Purkinje Cells. *Nature Neuroscience* 22 (6): 950-62. https://doi.org/10.1038/s41593-019-0381-8.

Dolfen N, Reverberi S, Op de Beek H, King BR, Albouy G (2024) The hippocampus represents information about movements in their temporal position in a learned motor sequence. *J Neuroscience* 44, e0584242024.

Du WR, Li E, Guo J, Chen Y, Oh SJ, Samuel A, Li Y, Oyibo HK, Xu W. (2021) Hippocampus-striatum wiring diagram revealed by directed stepwise polysynaptic tracing. bioRxiv doi.org/10.1101/2021.10.12.464132

Eccles JC, Ito M, Szentagothai J. (1967). *The Cerebellum as a Neuronal Machine.* Springer,Berlin.

Eichenbaum H. (2017). Prefrontal–hippocampal interactions in episodic memory. *Nat Rev Neurosci* 18, 547–558. https://doi.org/10.1038/nrn.2017.74

Fraisse P, Repp BH. (2012). Anticipation of rhythmic stimuli: Speed of establishment and precision of synchronization (1966). *Psychomusicology: Music, Mind, and Brain*, *22*, 84-93. https://doi.org/10.1037/a0028758

Froula JM, Hastings SD, Krook-Magnuson E. (2023) The little brain and the seahorse: *Cerebellar-hippocampal interactions Front. Syst. Neurosci.*17 1158492. doi.10.3389/fnsys.2023.1158492

Fujioka T, Trainor LJ, Large EW, Ross B. (2012). Internalized timing of isochronous sounds is represented in neuromagnetic beta oscillations. *The Journal of Neuroscience*, *32*, 1791-1802. https://doi.org/10.1523/JNEUROSCI.4107-11.2012

Fujioka T, Ross B, Trainor LJ. (2015). Beta-band oscillations represent auditory beat and its metrical hierarchy in perception and imagery. *Journal of Neuroscience*, *35*(45), 15187-15198. https://doi.org/10.1523/JNEUROSCI.2397-15.2015

Gerfen CR, Surmeier DJ. (2011). Modulation of striatal projec tion systems by dopamine. *Annual Review of Neuroscience,* 34, 441– 466. https://doi.org/10.1146/annur ev- neuro - 06101 0- 113641

Gerwig M, Kolb FB, Timman D (2007) The involvement of the human cerebellum in eye blink conditioning. *JNNP* 46(9), 844-847.

Gibbon J, Malapani C, Dale CL, Gallistel C. (1997). Toward a neurobiology of temporal cognition: Advances and challenges. *Current Opinion in Neurobiology*, *7*(2), 170-184. https://doi.org/10.1016/s0959-4388(97)80005-0

Gonzalo-Martin E, Alonso-Martinez C, Sepulveda LP, Clasca F (2024) Micropopulation mapping of the mouse parafascicular nucleus connections reveals diverse input-output motifs. *Frontiers in Neuroanatomy* 17, 1305500.

Govender S, Todd NPM, Colebatch JG (2022). Effects of posture on cerebellar evoked potentials (CEPs) following brief impulsive stimuli at the mastoid and trunk. *Exp Brain Res* 240:1371-1385.

Govender S, Hochstrasser D, Todd NPM, Keller PE, Colebatch JG (2024) Reponses to brief perturbations of stance: EMG, midline cortical and subcortical changes. *J Neurophysiol.* 132, 1014-1024.

Grahn JA, Rowe JB. (2012). Finding and feeling the musical beat: Striatal dissociations between detection and prediction of regularity. *Cerebral Cortex*, *23*(4), 913-921. https://doi.org/10.1093/cercor/bhs083

Gulberti A, Schneider TR, Galindo-Leon EE, Heise M, Pino A, Westphal M, Hamel W, Buhmann C, Zittel S, Gerloff C, Pötter-Nerger M, Engel AK, Moll CKE. (2024). Premotor cortical beta synchronization and the network neuromodulation of externally paced finger tapping in Parkinson's disease. *Neurobiology of Disease*, *197*, 106529. https://doi.org/https://doi.org/10.1016/j.nbd.2024.106529

Haines DE (2008) *Neuroanatomy: An Atlas of Structures, Sections and Systems.* 7th Edition. Wolters Kluwer.

Hallworth NE, Bland BH. (2004) Basal ganglia–hippocampal interactions support the role of the hippocampal formation in sensorimotor integration, *Experimental Neurology* 188, 430-443. doi.org/10.1016/j.expneurol.2004.04.014.

Harding EE, Kim JC, Demos AP, Roman IR, Tichko P, Palmer C, Large EW. (2025). Musical neurodynamics. *Nature Reviews Neuroscience*, *26*(5), 293-307. https://doi.org/10.1038/s41583-025-00915-4

Harry BB, Margulies DS, Falkiewicz M, Keller PE. (2023). Brain networks for temporal adaptation, anticipation, and sensory-motor integration in rhythmic human behavior. *Neuropsychologia*, *183*, 108524. https://doi.org/10.1016/j.neuropsychologia.2023.108524

Heine W, Dobrota MA, Schomer D, Wigton R, Herman S. (2020). High-density adaptive ten ten: proposal for electrode nomenclature for high-density EEG. *Journal of Clinical Neurophysiology*, 37(3), 263–270. https://doi.org/10.1097/wnp.0000000000000632.

Heffley W, Hull C. (2019) Classical conditioning drives learned reward prediction signals in climbing fibers across the lateral cerebellum. *Elife.* 2019 Sep 11;8:e46764. doi: 10.7554/eLife.46764.

Heffley W, Song EY, Xu Z, Taylor BN, Hughes MA, McKinney A, Joshua M, Hull C. (2018) Coordinated cerebellar climbing fiber activity signals learned sensorimotor predictions. *Nat Neurosci.* 21(10): 1431-1441. doi: 10.1038/s41593-018-0228-8.

Hitier M, Besnard S, Smith PF. (2014) Vestibular pathways involved in cognition. *Front Integr Neurosci*. 8, 1–16.

Hove MJ, Balasubramaniam R, Keller PE. (2014). The time course of phase correction: a kinematic investigation of motor adjustment to timing perturbations during sensorimotor synchronization. *Journal of Experimental Psychology: Human Perception and Performance*, *40*(6), 2243-2251. https://doi.org/10.1037/a0037826

Ikeda A, Shibasaki H, Nagamine T, Terada K, Kaji R, Fukuyama H, Kimura J. (1994). Dissociation between contingent negative variation and Bereitschaftspotential in a patient with cerebellar efferent lesion. *Clin Neurophysiol* 90, 359-364

Iversen J, Balasubramaniam R. (2016). Synchronization and temporal processing. *Current Opinion in Behavioral Science*, 8. 175-180. DOI: 10.1016/j.cobeha.2016.02.027

Ivry RB, Keele SW. (1989). Timing functions of the cerebellum. *Journal of Cognitive Neuroscience*, *1*(2), 136-152. https://doi.org/10.1162/jocn.1989.1.2.136

Javier M. (2019) Teaching the Cerebellum about Reward. *Nature Neuroscience* 22 (6): 846-48.

Jirenhead DA, Heslow G (2016) Are Purkinje cell pauses drivers of classically conditioned blink responses? *Cerebellum* 15(4), 526-534.

Kasdan AV, Burgess AN, Pizzagalli F, Scartozzi A, Chern A, Kotz SA, WilsonSM, Gordon RL. (2022). Identifying a brain network for musical rhythm: A functional neuroimaging meta-analysis and systematic review. *Neuroscience and Biobehavioral Reviews*, *136*, 104588. https://doi.org/https://doi.org/10.1016/j.neubiorev.2022.104588

Keller PE, Novembre G, Hove MJ. (2014). Rhythm in joint action: Psychological and neurophysiological mechanisms for real-time interpersonal coordination. *Philosophical Transactions of the Royal Society of London. Series B: Biological Sciences*, *369*(1658), 20130394. https://doi.org/10.1098/rstb.2013.0394

Kung, S-J, Chen, JL, Zatorre, RJ, Penhune, VB. (2013). Interacting cortical and basal ganglia networks underlying finding and tapping to the musical beat. *Journal of Cognitive Neuroscience*, *25*(3), 401-420. https://doi.org/10.1162/jocn_a_00325 %M 23163420

Latham A, Paul DA (1970) Climbing fibre responses of cerebellar Purkinje cells. *J Physiol.* 207 (2), 56P-57P.

Latorre A, Humiaidan K, Sanna M, Lavena ML, Pittalis S, Raimondi C, Casula EP, Rocchi L (2025) Surface EEG evidence for cerebellar control of distal upper limbs in humans. *Brain Sciences* **15,** 440.

Levitin DJ, Grahn JA, London J. (2018). The psychology of music: rhythm and movement. *Annual Review of Psychology*, *69*(1), 51-75. https://doi.org/10.1146/annurev-psych-122216-011740

Lewis PA, Miall RC. (2003). Distinct systems for automatic and cognitively controlled time measurement: Evidence from neuroimaging. *Current Opinion in Neurobiology*, *13*(2), 250-255. https://doi.org/10.1016/s0959-4388(03)00036-9

Lewis PA, Wing AM, Pope PA, Praamstra P, Miall RC. (2004). Brain activity correlates differentially with increasing temporal complexity of rhythms during initialization, synchronization, and continuation phases of paced finger tapping. *Neuropsychologia*, *42*, 1301-1312.

Lisman JE, Grace AA. (2005) The Hippocampal-VTA Loop: Controlling the entry of information into long-term memory. *Neuron* 46, 703-713. doi.org/10.1016/j.neuron.2005.05.002.

Lusk NA, Petter EA, Macdonald CJ, Meck WH. (2016). Cerebellar, hippocampal, and striatal time cells. *Curr. Opin. Behav. Sci.* 8, 186–192. doi: 10.1016/j.cobeha.2016.02.020

Madison G. (2014). Sensori-motor synchronisation variability decreases as the number of metrical levels in the stimulus signal increases. *Acta Psychologica*, *147*, 10-16. https://doi.org/https://doi.org/10.1016/j.actpsy.2013.10.002

Madison G, Karampela O, Ullén F, Holm L. (2013). Effects of practice on variability in an isochronous serial interval production task: Asymptotical levels of tapping variability after training are similar to those of musicians. *Acta Psychologica*, *143*(1), 119-128. https://doi.org/https://doi.org/10.1016/j.actpsy.2013.02.010

Merchant H, de Lafuente V. (2024). A Second Introduction to the Neurobiology of Interval Timing. In: Merchant, H., de Lafuente, V. (eds) *Neurobiology of Interval Timing. Advances in Experimental Medicine and Biology,* vol 1455. Springer, Cham. doi.org/10.1007/978-3-031-60183-5_1

Merchant H, Mendoza G, Pérez O, Betancourt A, García-Saldivar P, Prado L. (2024). Diverse Time Encoding Strategies Within the Medial Premotor Areas of the Primate. In: Merchant, H., de Lafuente, V. (eds) *Neurobiology of Interval Timing. Advances in Experimental Medicine and Biology,* vol 1455. Springer, Cham. doi.org/10.1007/978-3-031-60183-5_7

Mario M, Adamaszek M, Apps R, et al. Consensus paper: Cerebellum and reward. (2024) The Cerebellum 23 (5): 2169-92. https://doi.org/10.1007/s12311-024-01702-0.

Marr D (1969) A theory of cerebellar cortex. *J Physiol.* 202 437-470.

Middleton FA, Strick PL. (2001). Cerebellar projections to the prefrontal cortex of the primate. *The Journal of Neuroscience*, *21*(2), 700-712. doi.org/10.1523/jneurosci.21-02-00700.2001

Milardi D, Quartarone A, Bramanti A, Anastasi G, Bertino S, Basile GA, Buonsera P, Pilone G, Celeste G, Rizzo G, Bruschetta D, Cacciola A (2019) The cortico-basal ganglia-cerebellar network: Past, present and future. *Frontiers in Neuroscience* 13, 61.

Mulders PC, van Eijndhoven PF, Schene AH, Beckmann CF, Tendolka I (2015) Resting-state functional connectivity in major depressive disorder: A review. *Neuroscience and Biobehavioural Reviews* 56, 330-344.

Nachev P, Wydell H, O'Neill K, Husain M, Kennard C (2007) The role of the pre-supplementary motor area in the control of action. *Neuroimage* 36, Supplement 2, T155-T163.

Newman PP, Reza H. Functional relationships between the hippocampus and the cerebellum: an electrophysiological study of the cat. (1979) *J Physiol.* 287, 405-426. doi: 10.1113/jphysiol.1979.sp012667.

Nijhuis P, Keller PE, Nozaradan S, Varlet M. (2021). Dynamic modulation of cortico-muscular coupling during real and imagined sensorimotor synchronisation. *Neuroimage*, *238*, 118209. https://doi.org/https://doi.org/10.1016/j.neuroimage.2021.118209

Nougaret S, López-Galdo L, Caytan E, Poitreau J, Barthélemy FV, Kilavik BE (2024) Low and high beta rhythms have different motor cortical sources and distinct roles in movement control and spatiotemporal attention. *PLoS Biol* 22(6):e3002670. https://doi.org/10.1371/journal.pbio.3002670

Novembre G, Knoblich G, Dunne L, Keller PE. (2017). Interpersonal synchrony enhanced through 20 Hz phase-coupled dual brain stimulation. *Soc Cogn Affect Neurosci*. https://doi.org/10.1093/scan/nsw172

Nozaradan S, Schönwiesner M, Caron-Desrochers L, Lehmann A. (2016). Enhanced brainstem and cortical encoding of sound during synchronized movement. *Neuroimage*, *142*, 231-240. https://doi.org/10.1016/j.neuroimage.2016.07.015

Ohmae S, Medina JF (2015) Climbing fibres encode a temporal prediction error during cerebellar learning in mice. *Nat. Neurosci* 18, 1798-1803.

Oprisan SA, Buhusi CV. What is all the noise about in interval timing? *Philos Trans R Soc Lond B Biol Sci.* 2014 Jan 20;369(1637):20120459. doi: 10.1098/rstb.2012.0459.

Passingham R (1994) *The Frontal Lobes and Voluntary Action.* Oxford Science Publications.

Penhune, VB, Steele, CJ. (2012). Parallel contributions of cerebellar, striatal and M1 mechanisms to motor sequence learning. *Behavioural Brain Research*, *226*(2), 579-591. https://doi.org/https://doi.org/10.1016/j.bbr.2011.09.044

Penhune, VB, Zattore, RJ, Evans, AC. (1998). Cerebellar contributions to motor timing: a PET study of auditory and visual rhythm reproduction. *Journal of Cognitive Neuroscience*, *10*(6), 752-765. https://doi.org/10.1162/089892998563149

Petter EA, Lusk NA, Hesslow G, Meck WH. (2016) Interactive roles of the cerebellum and striatum in sub-second and supra-second timing: Support for an initiation, continuation, adjustment, and termination (ICAT) model of temporal processing. *Neuroscience & Biobehavioral Reviews* 71,739-755. https://doi.org/10.1016/j.neubiorev.2016.10.015.

Praamstra P, Turgeon M, Hesse CW, Wing AM, Perryer L (2003). Neurophysiological correlates of error correction in sensorimotor-synchronization. *Neuroimage* 20, 1283-1297.

Praamstra P, Kourtis D, Kwok HF, Oostenveld R (2006) Neurophysiology of implicit timing in serial choice reaction-time performance. *The Journal of Neuroscience* 26, 5448 –5455

Purzner J, Paradiso GO, Cunic D, Saint-Cyr JA, Hoque T, Lozano AM, Lang AE, Moro E, Hodaie M, Mazzella F, Chen R. (2007) Involvement of the basal ganglia and cerebellar motor pathways in the preparation of self-initiated and externally triggered movements in humans. *J Neurosci.* 27,6029-6036. doi: 10.1523/JNEUROSCI.5441-06.2007.

Rahimpour S, Rajkumar S, Hallet M (2022) The supplementary motor complex in Parkinson's Disease. *Journal of Movement Disorders* 15, 21-32.

Repp BH. (2005). Sensorimotor synchronization: A review of the tapping literature. *Psychonomic Bulletin & Review*, *12*, 969-992.

Repp BH, Su YH. (2013). Sensorimotor synchronization: a review of recent research (2006-2012). *Psychonomic Bulletin & Review*, *20*, 403-452. https://doi.org/10.3758/s13423-012-0371-2

Rin K, Yoshimura H, Yamazaki T. (2025) A theory of cerebellar learning as spike-based reinforcement learning in continuous time and space. *PNAS Nexus* 4 (10): pgaf302. https://doi.org/10.1093/pnasnexus/pgaf302.

Roerdink M, Bank PJ, Peper CL, Beek PJ. (2011). Walking to the beat of different drums: practical implications for the use of acoustic rhythms in gait rehabilitation. *Gait and Posture*, *33*(4), 690-694. https://doi.org/10.1016/j.gaitpost.2011.03.001

Rolls ET (2023) *Brain Computations and Connectivity*. OUP, Oxford.

Rolls ET, Mills P. (2019). The generation of time in the hippocampal memory system, *Cell Rep* 28, 1649–1658 e6.

Romero DJ, Roberts RA, Clay D, Picou E, Feller JJ, Englund J, Jacobson GP (2025) Recordability of the vestibular cerebellar evoked potential. *International Journal of Audiology* 64, 1 – 9.

Rueda-Orozco PE, Hidalgo-Balbuena AE, González-Pereyra P, Martinez-Montalvo MG, Báez-Cordero AS. (2024). The Interactions of Temporal and Sensory Representations in the Basal Ganglia. In: Merchant, H., de Lafuente, V. (eds) *Neurobiology of Interval Timing. Advances in Experimental Medicine and Biology*, vol 1455. Springer, Cham. https://doi.org/10.1007/978-3-031-60183-5_8

Sabatino M, La Grutta V, Ferraro G, La Grutta G. (1986) Relations between basal ganglia and hippocampus: Action of substantia nigra and pallidum. *Revue d'Electroencéphalographie et de Neurophysiologie Clinique* 16, 179-190. doi.org/10.1016/S0370-4475(86)80010-7.

Sasaki K, Gemba H, Hashimoto S Mizuno N. (1979). Influences of cerebellar hemispherectomy on slow potentials in the motor cortex preceding self-paced hand movement in the monkeys. *Neurosci. Lett.,* , 15: 23-28.

Schmahmann JD, Doyon J, McDonald D, Holmes C, Lavoie K, Hurwitz AS, Kabani N, Toga A, Evans A, Petrides M. (1999). Three-dimensional MRI atlas of the human cerebellum in proportional stereotaxic space. *Neuroimage* 10, 233–260. https://doi.org/10.1006/nimg.1999.0459.

Schwartze M, Keller PE, Patel AD, Kotz S. (2011) The impact of basal ganglia lesions on sensorimotor synchronization, spontaneous motor tempo, and the detection of tempo changes. *Behavioural and Brain Research* 216, 685-691.

Schwartze M, Keller PE, Kotz S. (2016). Spontaneous, synchronized, and corrective timing behavior in cerebellar lesion patients. *Behavioural Brain Research* 312, 285-293. https://doi.org/10.1016/j.bbr.2016.06.040

Schwartze M, Kotz SA. (2013). A dual-pathway neural architecture for specific temporal prediction. *Neuroscience and Biobehavioral Reviews*, *37*, 2587-2596. https://doi.org/10.1016/j.neubiorev.2013.08.005

Schwartze M, Kotz SA. (2024). Timing Patterns in the Extended Basal Ganglia System. In: Merchant, H., de Lafuente, V. (eds) Neurobiology of Interval Timing. Advances in Experimental Medicine and Biology, vol 1455. Springer, Cham. https://doi.org/10.1007/978-3-031-60183-5_15

Schwartze M, Rothermich K, Kotz S (2012). Functional dissociation of pre-SMA and SMA-proper in temporal processing. *Neuroimage* 60, 290-298.

Semjen A, Vorberg D, Schulze H-H. (1998). Getting synchronized with the metronome: Comparisons between phase and period correction. *Psychological Research*, *61*(1), 44-55. https://doi.org/10.1007/s004260050012

Shibasaki H, Barrett G, Neshige R, Hirata I, Tomoda H. (1986). Volitional movement is not preceded by cortical slow negativity in cerebellar dentate lesion in man. *Brain Res,* 368, 361-365

Shuyang J, Hull C. (2025) Reward-driven cerebellar climbing fiber activity influences both neural and behavioral learning. *Current Biology* 35 (18): 4383-4393.e4. https://doi.org/10.1016/j.cub.2025.07.064.

Smith PF (2018) Vestibular functions and Parkinson's Disaease. *Frontiers of Neurology* 9, 1085.

Snyder JS, Gordon RL, Hannon EE. (2024). Theoretical and empirical advances in understanding musical rhythm, beat and metre. *Nature Reviews Psychology*. https://doi.org/10.1038/s44159-024-00315-y

Snyder JS, Large EW. (2005). Gamma-band activity reflects the metric structure of rhythmic tone sequences. *Cognitive Brain Research*, *24*(1), 117-126. https://doi.org/https://doi.org/10.1016/j.cogbrainres.2004.12.014

Soares S, Atallah BV, Paton JJ. (2016) Midbrain dopamine neurons control judgment of time. *Science* 354, 1273-1277. doi: 10.1126/science.aah5234.

Soteropoulos DS, Baker SN. (2006) Cortico-cerebellar coherence during a precision grip task in the monkey. *Journal of Neurophysiology* 95, 1194–1206. doi: 10.1152
Stein JF (1986) Role of the cerebellum in the visual guidance of movement. *Nature* 323, 217-221.

Stackman RW, Clark AS, Taube JS. (2002) Hippocampal spatial representations require vestibular input. *Hippocampus* 12, 291-303. doi: 10.1002/hipo.1112.

Stein JF, Glickstein M (1992) Role of the cerebellum in the visual guidance of movement. *Physiological Reviews* 72, 967-2017.

Sternad DJDW, Newell KM. (2000). Force and timing variability in rhythmic unimanual tapping. *Journal of Motor Behavior*, *32*(3), 249-267. https://doi.org/10.1080/00222890009601376

Talairach J, Tournoux P. (1988). *Co-planar Stereotaxic Atlas of the Human Brain: 3-Dimensional Proportional System - an Approach to Cerebral Imaging*, Thieme Medical Publishers, New York, NY.

Tanaka M, Kameda M, Okada K. (2024). Temporal Information Processing in the Cerebellum and Basal Ganglia. In: Merchant, H., de Lafuente, V. (eds) *Neurobiology of Interval Timing. Advances in Experimental Medicine and Biology*, vol 1455. Springer, Cham. https://doi.org/10.1007/978-3-031-60183-5_6

ten Brinke MM, Boele HJ, De Zeeuw CI (2019). Conditioned climbing fibre responses in cerebellar cortex and nuclei. *Neurosci. Letts* 688, 26-36.

Teki S, Grube M, Kumar S, Griffiths TD. (2011). Distinct neural substrates of duration-based and beat-based auditory timing. *Journal of Neuroscience*, *31*(10), 3805-3812. https://doi.org/10.1523/jneurosci.5561-10.2011

Teki S, Grube M, Griffiths TD. (2012). A unified model of time perception accounts for duration-based and beat-based timing mechanisms. *Front. Integr. Neurosci.* 5:90. doi: 10.3389/fnint.2011.00090

Todd NPM, Rosengren SM, Colebatch JG (2008a) OVEMPs produced by impulsive head acceleration. *Clin. Neurophysiol.* 119, 1638-1651.

Todd NPM, Rosengren SM, Colebatch JG (2008b) Tuning and sensitivity of the human vestibular system to low-frequency vibration. *Neuroscience Letters* 444 (1), 36-41.

Todd, N.P.M., & Lee, C. S. (2015a). The sensory-motor theory of rhythm and beat induction 20 years on: A new synthesis and future perspectives. *Frontiers in Human Neuroscience*, *9*. https://doi.org/10.3389/fnhum.2015.00444

Todd, N.P.M., & Lee, C. S. (2015b). Source analysis of electrophysiological correlates of beat induction as sensory-guided action. *Frontiers in Psychology*, *6*.

Todd NPM, Govender S, Colebatch JG (2017) The inion response revisited: evidence for a possible cerebellar contribution to vestibular-evoked potentials produced by air-conducted sound stimulation, *J. Neurophysiol.* 117, 1000–1013.

Todd NPM, Govender S, Colebatch JG (2018a) The human electrocerebellogram (ECeG) recorded non-invasively using scalp electrodes. *Neurosci Lett.* 682, 124-131.

Todd NPM, Govender S, Colebatch JG (2018b) Vestibular cerebellar evoked potentials (VsCEPs) in humans and their modulation during optokinetic stimulation. *J Neurophysiol.* 6, 3099-3109.

Todd NPM, Govender S, Colebatch JG (2019) Modulation of the human electro-cerebellogram (ECeG) during vestibular and optokinetic stimulation *Neurosci Lett* 712, 134497.

Todd NPM, Govender S, Colebatch JG (2021a) Source analysis of axial and vestibular evoked potentials associated with brainstem-spinal reflexes. *Neurosci Lett* 757, 135960.

Todd NPM, Govender S, Colebatch JG (2021b) Non-invasive recording from the human cerebellum during a classical conditioning paradigm using the otolith-evoked blink reflex. *Neurosci Lett* 765, 136270.

Todd NPM, Govender S, Keller PE, Colebatch JG. (2023a). Electrophysiological activity from over the cerebellum and cerebrum during eye blink conditioning in human subjects. *Physiological Reports*, *11*, e15642. https://doi.org/10.14814/phy2.15642

Todd NPM, Govender S, Keller PE, Colebatch JG. (2024a). Electrophysiological activity associated with a cross-modal anapaest rhythm: Evidence for the vestibular syncopation hypothesis. *Timing & Time Perception*, 1-54. https://doi.org/https://doi.org/10.1163/22134468-bja10108

Todd NPM, Govender S, Keller PE, Colebatch JG (2024b) Electrophysiological activity from the eye muscles, cerebellum and cerebrum during reflexive (Pavlovian) versus voluntary (Ivanov-Smolensky) eye-blink conditioning. *Cerebellum* 23(3), 957-972.

Todd NPM, Govender S, Hochstrasser D, Keller PE, Colebatch JG (2025) Distinct movement related changes in EEG and ECeG power during finger and foot movement. *Neuroscience Letters* 853, 138207. https://doi.org/10.1016/j.neulet.2025.138207.

Varlet M, Nozaradan S, Trainor L, Keller PE. (2020). Dynamic modulation of beta band cortico-muscular coupling induced by audio–visual rhythms. *Cerebral Cortex Communications*, *1*(1). https://doi.org/10.1093/texcom/tgaa043

Washburn S, Oñate M, Yoshida J, Vera J, Bhuvanasundaram R, Khatami L, Nadim F, Khodakhah K. (2024) The cerebellum directly modulates the substantia nigra dopaminergic activity. *Nat Neurosci*. 27, 497-513. doi: 10.1038/s41593-023-01560-9.

Underwood AG, Guynn MJ, Cohen A-L (2015) The future orientation of past memory: the role of BA 10 in prospective and retrospective retrieval modes. *Front Hum Neurosci* 9, 668. doi:10.3389/fnhum.2015.00668 pmid:26733844

Wang B, LeBel A, D'Mello AM (2025) Ignoring the cerebellum is hindering progress in neuroscience. *Trends in Cognitive Neuroscience* 29, 318-330.

Watson TC, Obiang P, Torres-Herraez A, Watilliaux A, Coulon P, Rochefort C, Rondi-Reig L. (2019) Anatomical and physiological foundations of cerebello-hippocampal interaction eLife 8:e41896.https://doi.org/10.7554/eLife.41896

Wessell K, Verleger R, Nazarenus D, Vieregge P, Kömpf D (1994). Movement-related cortical potentials preceding sequential and goal-directed finger and arm movements in patients with cerebellar atrophy. *Electroenceph Clin Neurophysiol* 92:331-341 doi 10.1016/0168-5597(94)90101-5

Wijesinghe R, Protti DA, Camp AJ (2015) Vestibular interactions in the thalamus. *Frontiers in Neural Circuits* 9, 79.

Wise SP, Murray EA (1999) Role of the hippocampal system in conditional motor learning: Mapping antecedents to action. *Hippocampus* 9, 101-117.

Witt ST, Laird AR, Meyerand ME. (2008). Functional neuroimaging correlates of finger-tapping task variations: an ALE meta-analysis. *Neuroimage*, *42*, 343-356. https://doi.org/10.1016/j.neuroimage.2008.04.025

Wylie KP, Kluger BM, Medina LD, Holden SK, Kronberg E, Tregellas JR, Buard I. (2023) Hippocampal, basal ganglia and olfactory connectivity contribute to cognitive impairments in Parkinson's disease. *Eur J Neurosci.* 57, 511-526. doi: 10.1111/ejn.15899.

Xu D, Liu T, Ashe J, Bushara KO. (2006). Role of the olivo-cerebellar system in timing. *Journal of Neuroscience*, *26*(22), 5990-5995. https://doi.org/10.1523/jneurosci.0038-06.2006

Yewbrey R, Kornysheva K (2024) The hippocampus preorders movements for skilled action sequences. *J Neuroscince* 44, e0832242024.

Yoshida J, Onata M, Khatami L, Vera J, Nadim F, Khodakhar K (2022) Cerebellar contributions to the basal ganglia influence motor coordination, reward processing, and movement vigor. *Journal of Neuroscience* 42, 8406-8415.

Zanto TP, Snyder JS, Large EW. (2006). Neural correlates of rhythmic expectancy. *Advances in cognitive psychology*, *2*, 221-231.

Zwergal A, Grabova D, Schöberl F. Vestibular contribution to spatial orientation and navigation. (2024) *Current Opinion in Neurology* 37, 52-58. DOI: 10.1097/WCO.0000000000001230

Figure captions.

Fig 1: The electrode map is comprised of a standard BioSemi 64-channel 10-10 montage, with an extra 32 channels making up three additional 10% circumferences. The first completes the Iz circumference (outer circle) with two 10% circumferences below Iz, at SIz and Bz. Additional electrodes were positioned beneath the eyes (IO1, IO2), frontally (F11, F12), on the ear lobes (A1, A2) and bilaterally over the SCM muslces giving a total of 104 recording channels.

Fig 2: Illustration of the procedure carried out during passive and active recording blocks. Seven head taps were delivered in each recording block. For passive blocks (A), subjects rested their right foot and mentally counted the head taps. For active blocks (B), subjects tried to synchronise with the rhythm by tapping along with their right foot. Counting and tapping started on the 2nd head tap.

Fig 3: Behavioural grand mean data (n = 10) from the active blocks showing EMG (TA/SOL, black/grey) and tap force/acceleration (black/grey) for the 500 (A), 600 (B) and 700 ms (C) rates. Vertical lines indicate the onset of the 1st head tap with subsequent dashed vertical lines showing the onset of the 2nd to 7th head taps. The area shaded in grey is expanded in the right column and shows EMG (D; TA/SOL, black/grey) and (E) tap force/acceleration (black/grey) grand means for a single cycle at the 600 ms rate. Five stages are shown; (1) TA relaxation, (2) SOL burst, (3) peak force, (4) TA contraction and (5) TA peak. The dashed vertical line in the right column indicates the onset of the 6th head tap. TA = tibialis anterior, SOL = soleus

Fig 4: ANOVA effects for the asynchrony (A), variability (B) and amplitude (C) of the foot tap force. Main effects of BLOCK (first row), TEMPO (second row) and BEAT (third row) are shown as well as the BEAT by TEMPO interactions for all three measures (bottom row). * $p < 0.05$, ** $p \leq 0.01$, *** $p \leq 0.001$, ns = not significant. Error bars give standard error.

Fig 5: Main effects of STAGE (A), TEMPO (B) and interaction effect of BEAT by TEMPO (C) for asynchrony (left column) and main effects of STAGE (D), TEMPO (E), BEAT (F) and interaction effect of BEAT by STAGE (G) for variability (right column). * $p < 0.05$, ***

$p \leq 0.001$. Stages: (1) = TA relaxation, (2) = SOL burst, (3) = force peak and (4) = TA contraction.

Fig 6: Average of potentials (n = 10) from the Fpz, FCz and Bz electrode locations during the passive (grey) and active (black) recording blocks for the 500 (A), 600 (B) and 700 ms (C) rates. EMG from soleus (SOL; black traces) are shown above neural potentials for the three rates of stimuli. Vertical lines indicate the onset of the 1st head tap with subsequent dashed vertical lines showing the onset of the 2nd to 7th head taps.

Fig 7: Potentials averaged across all rates (n = 10) showing the initial response (A; left column) and steady response for the last four beats (B; right column). Active (black) and passive (grey) traces are overlaid across all potentials. GFP = global field power. Epochs: SL = short latency, ML = medium latency, LL = long latency.

Fig 8: (A) Grand mean steady responses from the FCz (left) and Bz (right) electrodes for all three rates during active (black traces) and passive (dark grey) blocks. For active block recordings, grand mean EMG from soleus (SOL; light grey) is overlaid for comparison with neural potentials. Thick vertical dashed lines show the alignment of the N2 potential across the three rates with the potential occurring earlier during the passive block. (B) Grand mean (black) and individual subject (grey) steady responses averaged across tempi from FCz (top row) and Bz (bottom row) during active (left column) and passive blocks (B; middle column). Waveforms obtained after subtracting active and passive recordings are also shown for the FCz and Bz electrodes (right column). RAN = initial reafferance negative, PMP = post-motion positive, PMN = pre-movement negative.

Fig 9: Scaleograms of the steady response during active (A), passive (B) and subtracted (C) conditions for the FCz and Iz electrodes. The VHF ECeG power shows a double burst-pause consistent with a conditioned climbing fibre response (C-CFR).

Fig 10: Alignment of high frequency power (A & C; UHF/VHF) at Iz with neural potentials (B & D) for the initial (left column) and steady response (right column). Dashed vertical lines (grey) illustrate the double burst-pause period and segments 7 to 10 in the ANOVA.

Fig 11: (A) Main effect of segment and (B) Segment × beat interaction, with modulation localized to segments 9–10 (grey shaded area; see D–F). (C) Segment × tempo × beat interaction, illustrated for beats 1 (left column) and 5 (right column) show little effect of tempo but marked differences across segments. Beat × segment interaction (D) and main effect of beat for segments 9 (E) and 10 (F) show divergent changes for the initial beats. * $p < 0.05$, ** $p \leq 0.01$, ns = not significant.

Fig 12: Scatter plots illustrating the spatial distribution of dipole clusters in the Y-X (A), Z-X (B) and Z-Y (C) planes. Overall, these form an exponential distribution (D). CB = cerebellum, BG = basal ganglia, DCN = deep cerebellar nuclei, DL-PFC = dorsolateral prefontral cortex, FP-PFC = frontopolar prefontral cortex, ACC = anterior cingulate cortex, PMC = premotor cortex, PPC = posterior parietal cortex, PCC = posterior cingulate cortex, SMC = supplementary motor complex, TP = temporal parietal junction, VL-PFC = ventrolateral prefrontal cortex, VM-PFC = ventromedial prefrontal cortex.

Fig 13: Cerebrum (A & C) and sub-cortical (B & D) sources for cephalic clusters comparing the initial and steady response (left column) and active and passive conditions (right column). FP-PFC = frontopolar prefontral cortex, PMC = premotor cortex, DL-PFC = dorsolateral prefontral cortex, PPC = posterior parietal cortex, PCC = posterior cingulate cortex, SMC = supplementary motor complex, ACC = anterior cingulate cortex, TP = temporal pole, VL-PFC = ventrolateral prefrontal cortex, BG = basal ganglia, VM-PFC = ventromedial prefrontal cortex, CB = cerebellum, DCN = deep cerebellar nuclei.

Fig 14: Scatter plots illustrating the spatial distribution of 11 cephalic clusters marked in bold in Table 6 in the Y-X (A), Z-X (B) and Z-Y (C) planes. For simplicity only the dominant cluster areas are shown. FP-PFC = frontopolar prefontral cortex, CB = cerebellum, PMC = premotor cortex, PCC = posterior cingulate cortex.

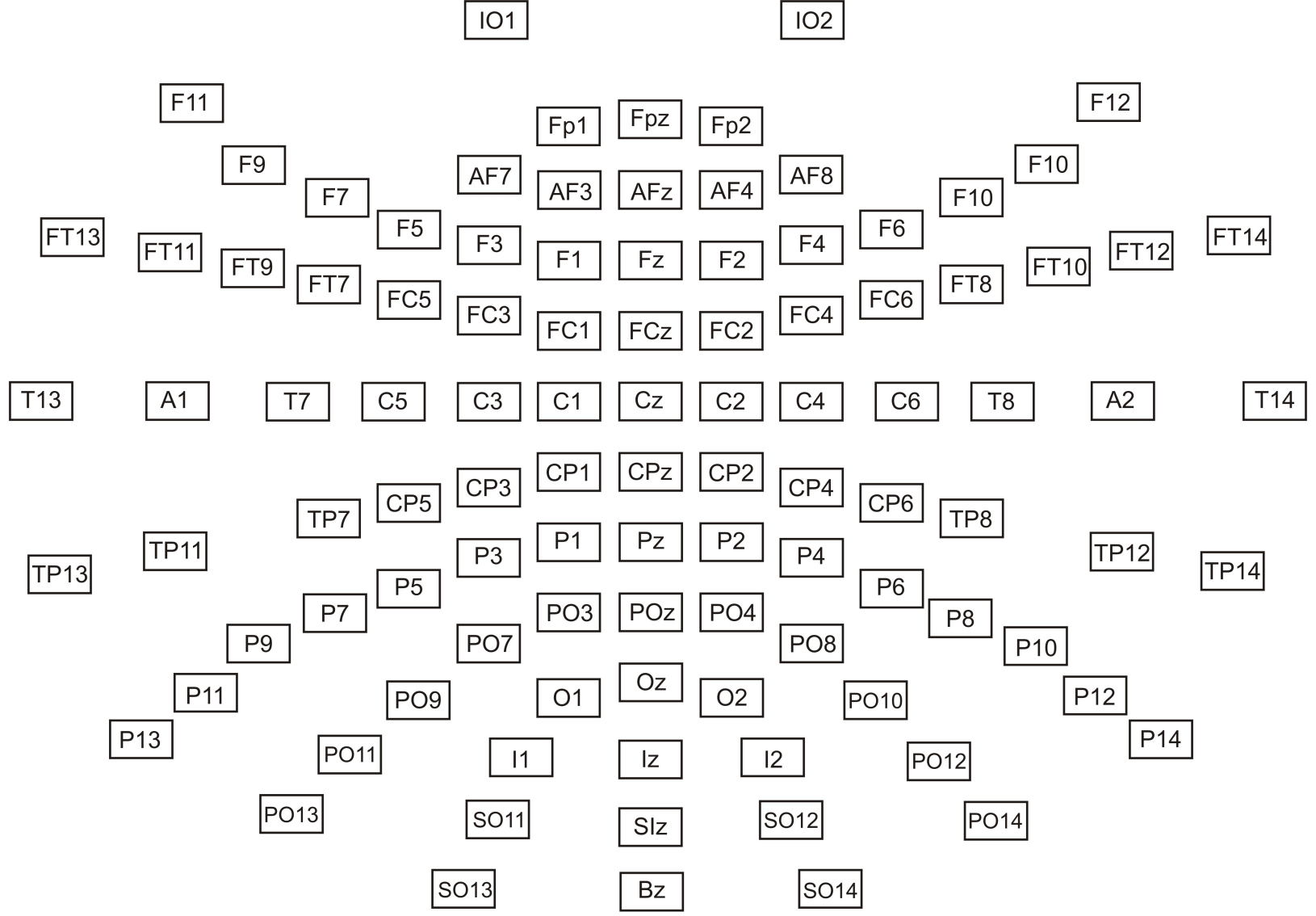
Fig 15: Grand mean source currents comparing active (black) and passive (grey) traces for the initial (A) and steady response (B). R = right, L = left, a-PFC = anterior prefontral cortex, SMA = supplementary motor area, IPL = inferior parietal lobe, R H = right hemisphere, L H = left hemisphere of the cerebellum.

Fig 16: Alignment of grand mean neural potentials (A), source currents (B) and high frequency power (UHF) at Iz for the active condition. R = right, L = left, PFC = prefontral cortex, SMA = supplementary motor area, R H = right hemisphere, L H = left hemisphere of the cerebellum.

Fig 17: Effects of tempo (A; 500 ms, B; 600 ms, C: 700 ms) on cerebral and cerebellar source currents. SMA source currents exhibit post-N2 tempo-dependent slopes which vary significantly between the 500 ms (red), 600 ms (green) and 700 ms (blue) rates. Movement-related post-N2 slopes in the SMA sources converge about 100 ms prior to target (D).

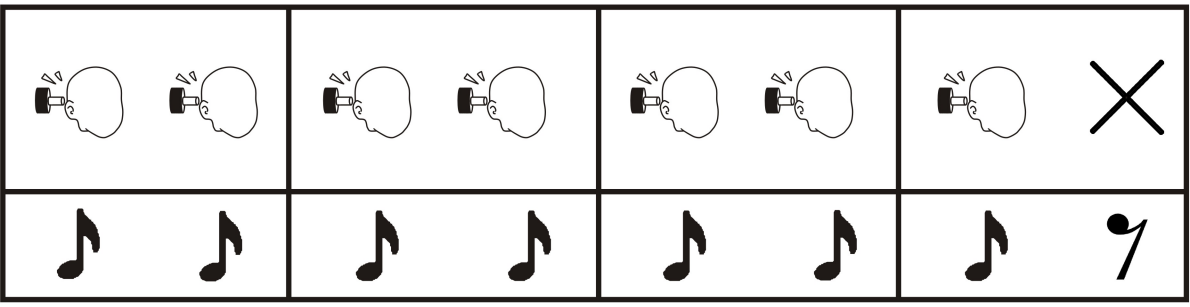
Fig 18: Grand mean scaleograms of source currents for the three tempi; (A) 500 ms, (B) 600 ms and (C) 700 ms. The three sources are shown; pre-SMA (1st row), SMA (2nd row) and R H VIIIB (3rd row).

Fig 19: Circuit diagram summarising the connectivity of cerebral and cerebellar sources with their inputs and outputs. AN = anterior nucleus of the thalamus, aPFC = anterior prefrontal cortex, BA = Brodmann area, CFs = Climbing fibers, D1 = type 1 dopamine receptor, D2 = type 2 dopamine receptor, DCN = deep cerebellar nuclei, GCs = granule cells, GN = lateral geniculate nucleus, GPe = globus pallidus externus, GPi = globus pallidus internus, IL = intralaminar nuclei, IO = inferior olive, IPL = inferior parietal lobule, M1 = primary motor cortex, MF = mossy fibers, NA = nucleus accumbens, PC = purkinje cells, Pf-CM = parafascicular-centromedian complex, PFs = parallel fibers, PPN = pedunculopontine nucleus, Pre-SMA = pre supplementary motor area, S1 = primary somatosensory cortex, SCT = spino-cerebellar tract, SeN = septal nucleus, SMA = supplementary motor area, SNc = substantia nigra pars compacta, SNr = substantia nigra pars reticulate, SOL = soleus, SOT = spino-olivary tract, STN = subthalamic nucleus, TA = tibialis anterior, Utr = utricle, VCT = vestibule-cerebellar tract, VI = ventral intermediate nucleus of the thalamus, VL-VA = ventral lateral-ventral anterior nucleus of the thalamus, VN = vestibular nucleus, VOT = vestibulo-olivary tract, VPL = ventral posterolateral nucleus, VTA = ventral tegmental area.

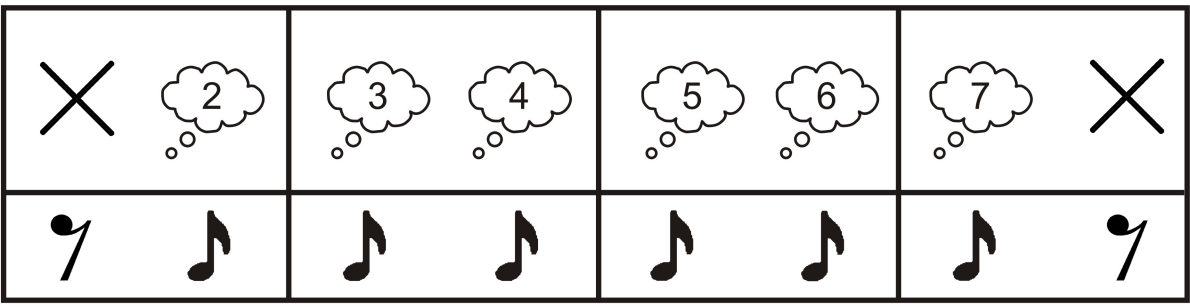

IO1
IO2
F11
F12
Fp1
Fpz
Fp2
F9
F10
AF7
AF8
F7
AF3
AFz
AF4
F10
FT13
FT11
F5
F3
F6
FT14
FT9
F1
Fz
F2
F4
FT12
FT7
FT10
FC5
FC6
FT8
FC3
FC4
FC1
FCz
FC2
T13
A1
T7
C5
C3
C1
Cz
C2
C4
C6
T8
A2
T14
CP1
CPz
CP2
CP3
CP4
CP5
CP6
TP7
TP8
TP11
P1
Pz
P2
TP12
TP13
P3
P4
TP14
P5
P6
P7
P8
PO3
POz
PO4
P9
PO7
PO8
P10
Oz
P11
O1
O2
PO10
P12
PO9
P13
P14
PO11
I1
Iz
I2
PO12
PO13
SO11
SO12
PO14
SIz
SO13
Bz
SO14

A Passive

Head Tap

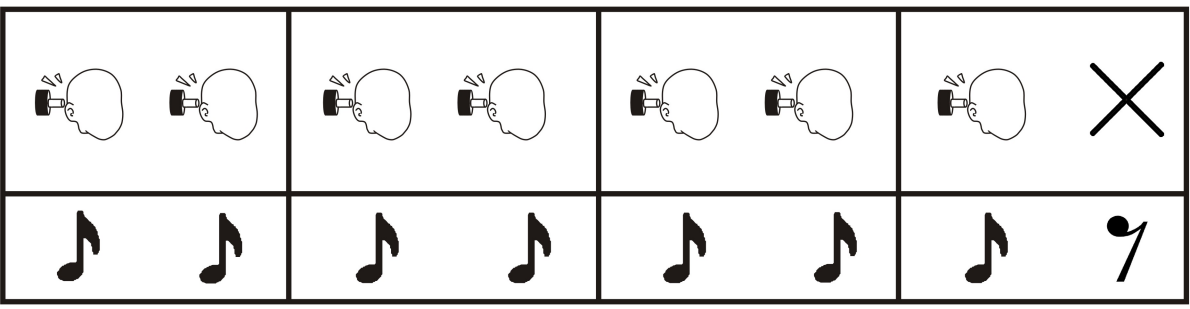


Count

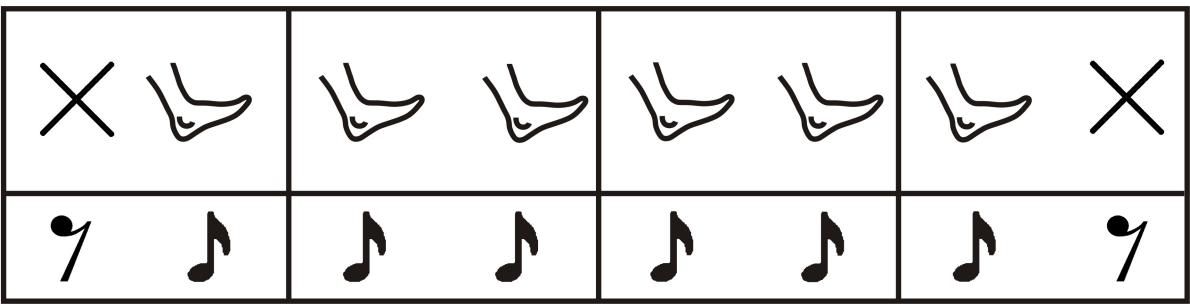


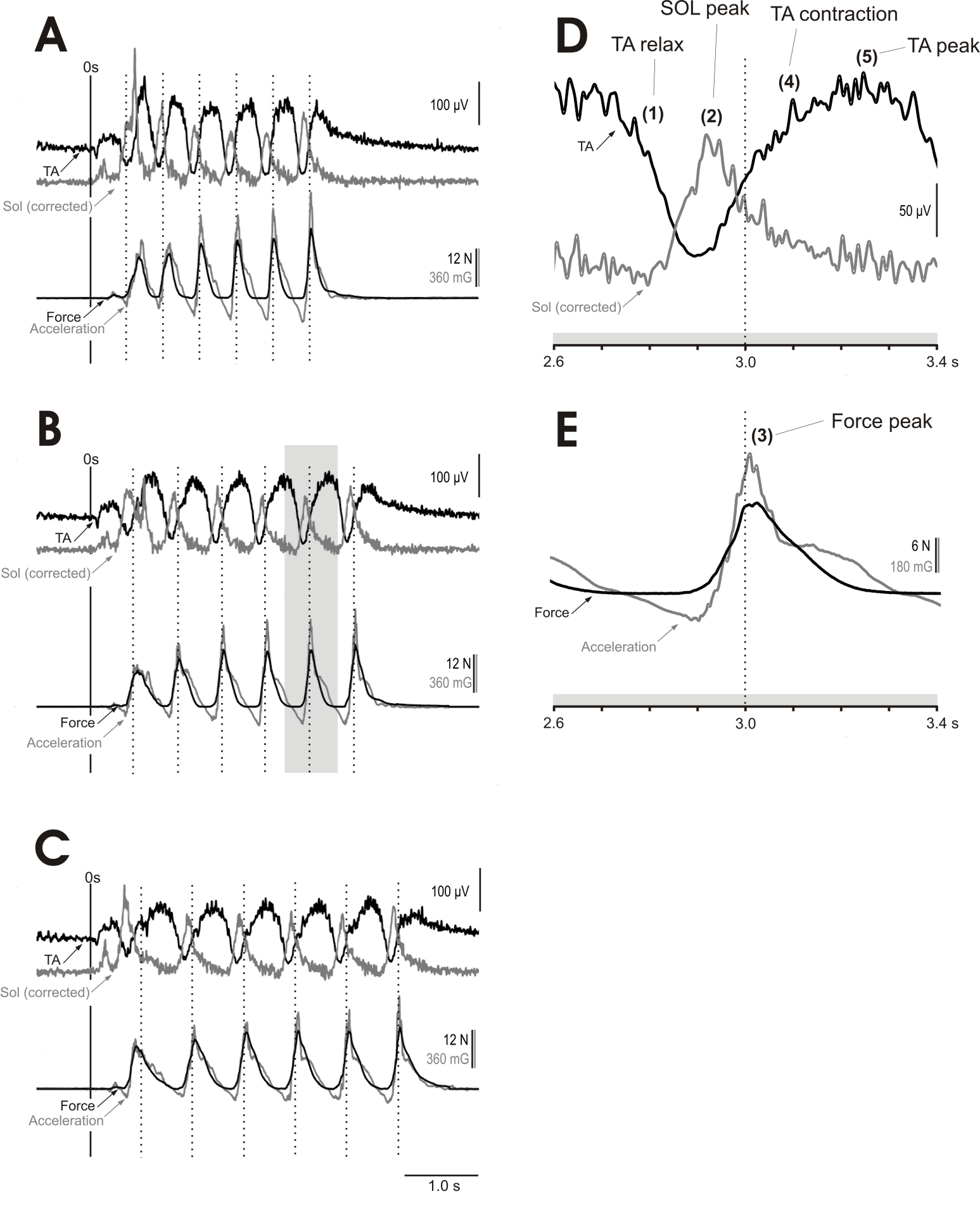
B Active

Head Tap



Foot Tap




A
0s
100 µV
TA
Sol (corrected)
12 N
360 mG
Force
Acceleration
B
0s
100 µV
TA
Sol (corrected)
12 N
360 mG
Force
Acceleration
C
0s
100 µV
TA
Sol (corrected)
12 N
360 mG
Force
Acceleration
1.0 s
D
TA relax
SOL peak
TA contraction
TA peak
(1)
(2)
(4)
(5)
TA
50 µV
Sol (corrected)
2.6
3.0
3.4 s
E
(3)
Force peak
6 N
180 mG
Force
Acceleration
2.6
3.0
3.4 s

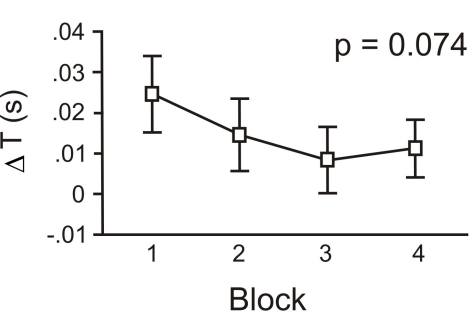
ANOVA effects

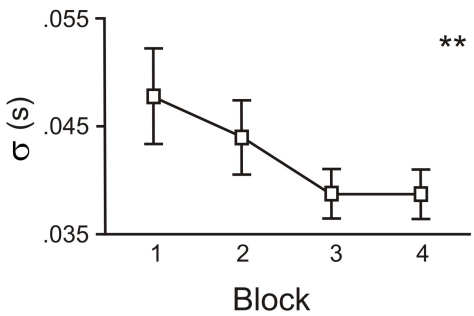
A Asynchrony

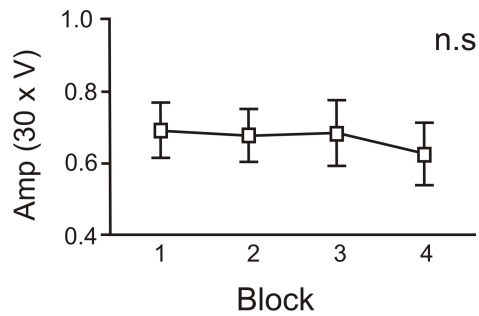
B Variability

C Amplitude

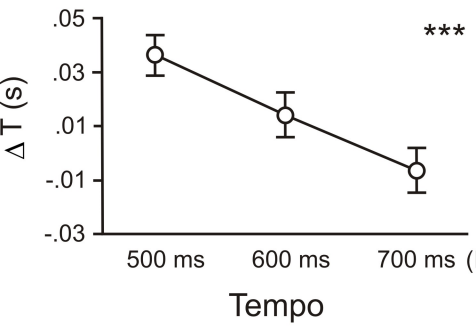
Main effect of block

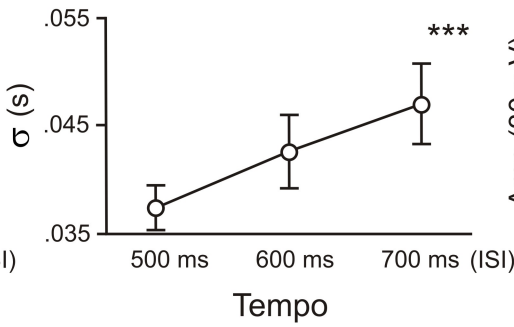


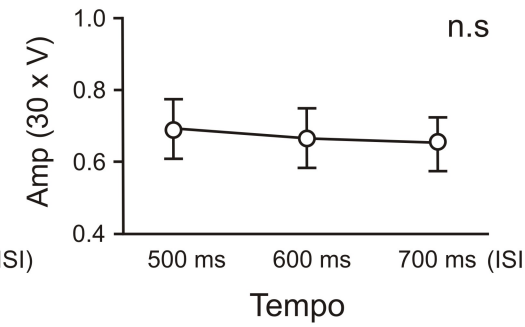




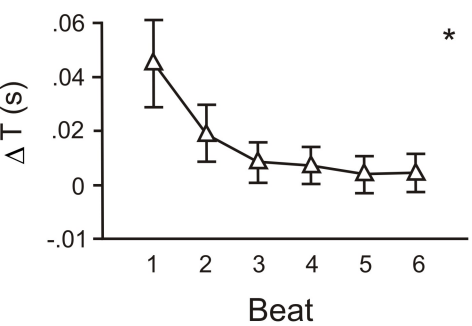
Main effect of tempo

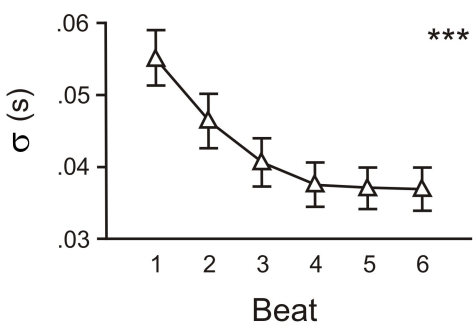


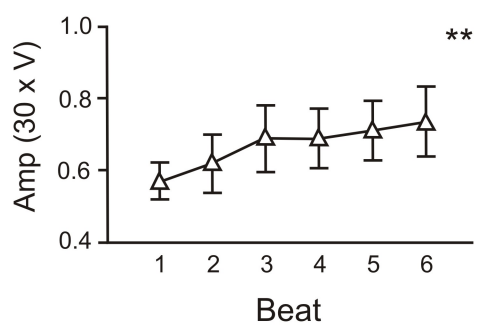




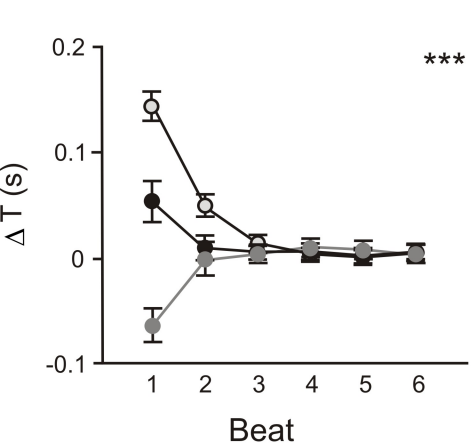
Main effect of beat

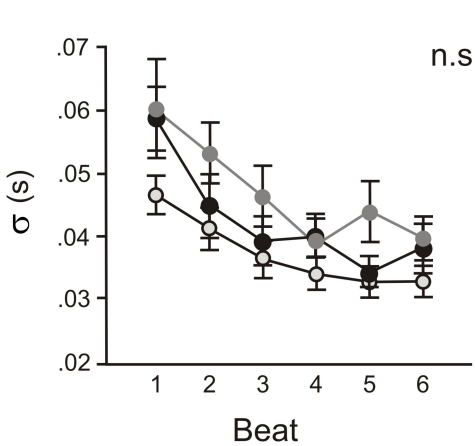


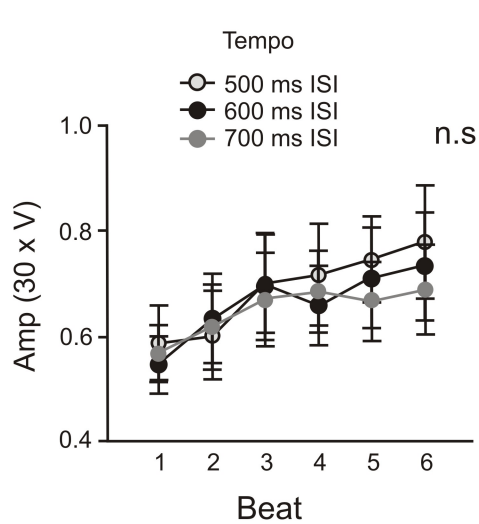




*Beat*tempo interaction*



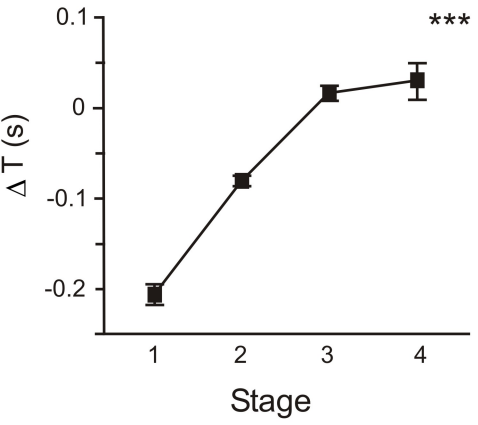




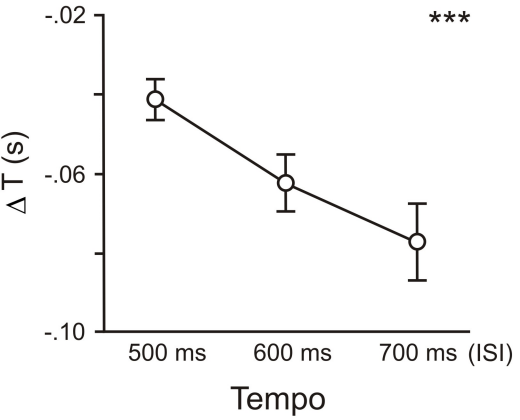
Asynchrony

Variability

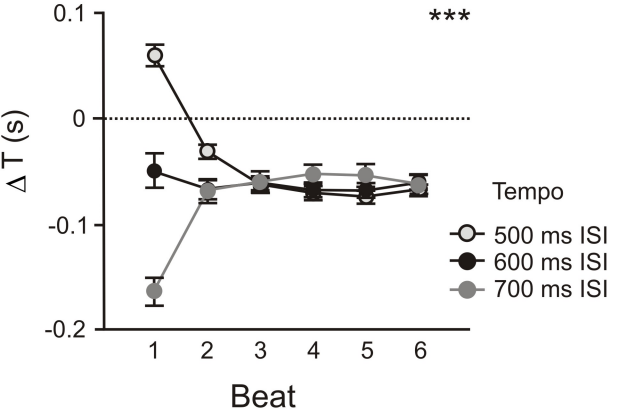
A ***Main effect of stage***



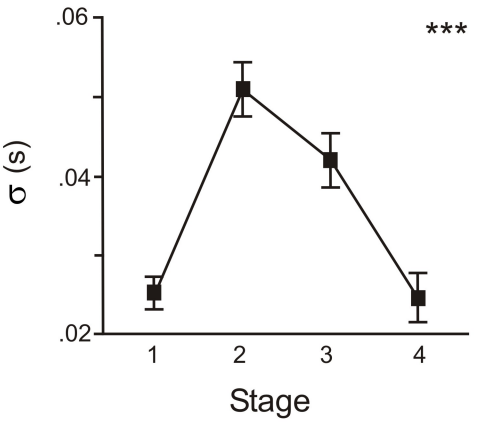
B ***Main effect of tempo***



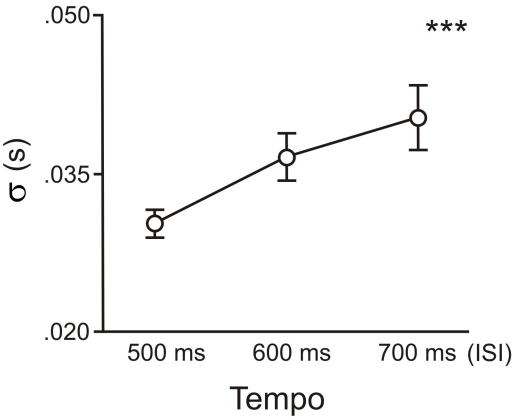
C ***Beat*tempo interaction***



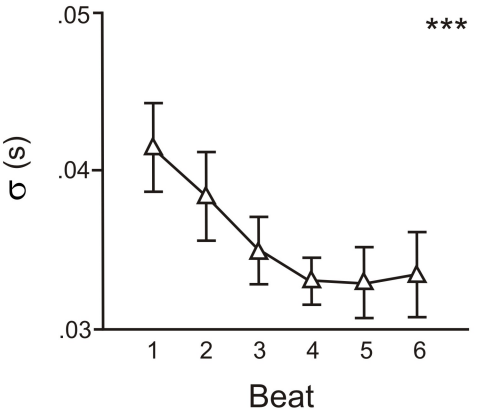
D ***Main effect of stage***



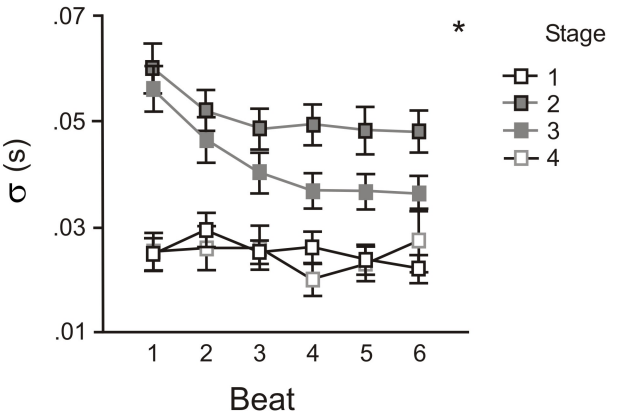
E ***Main effect of tempo***

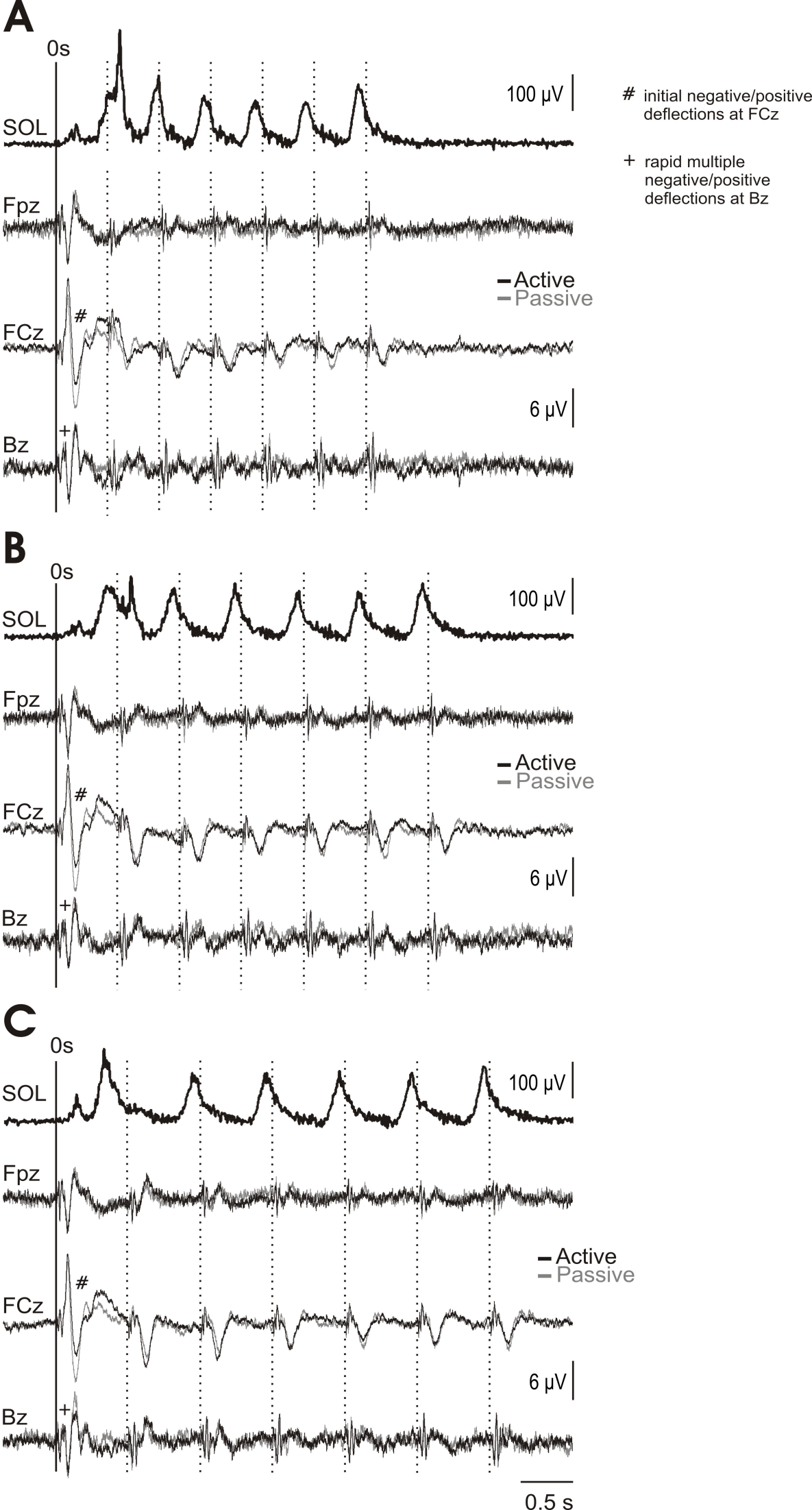


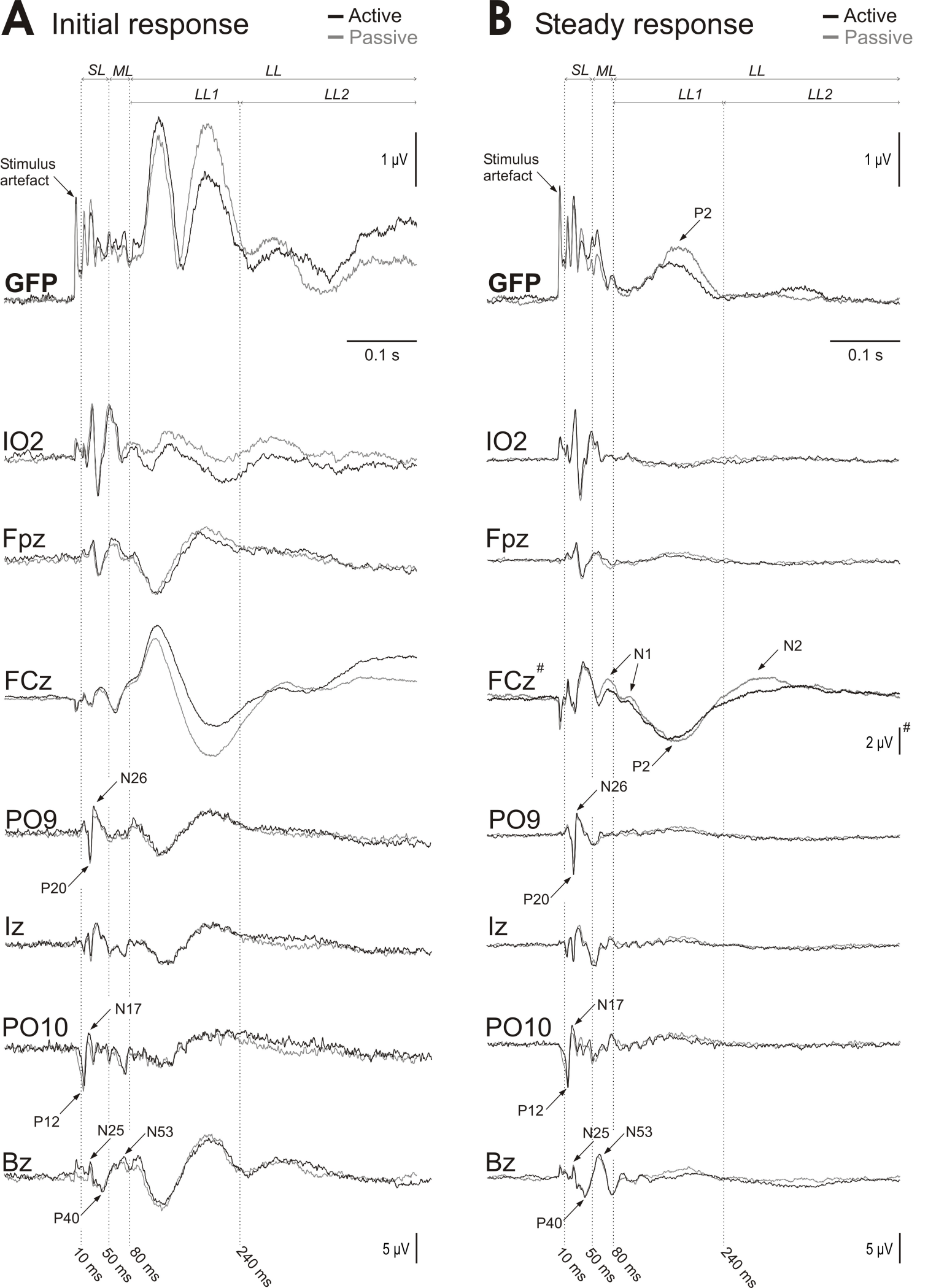
F ***Main effect of beat***

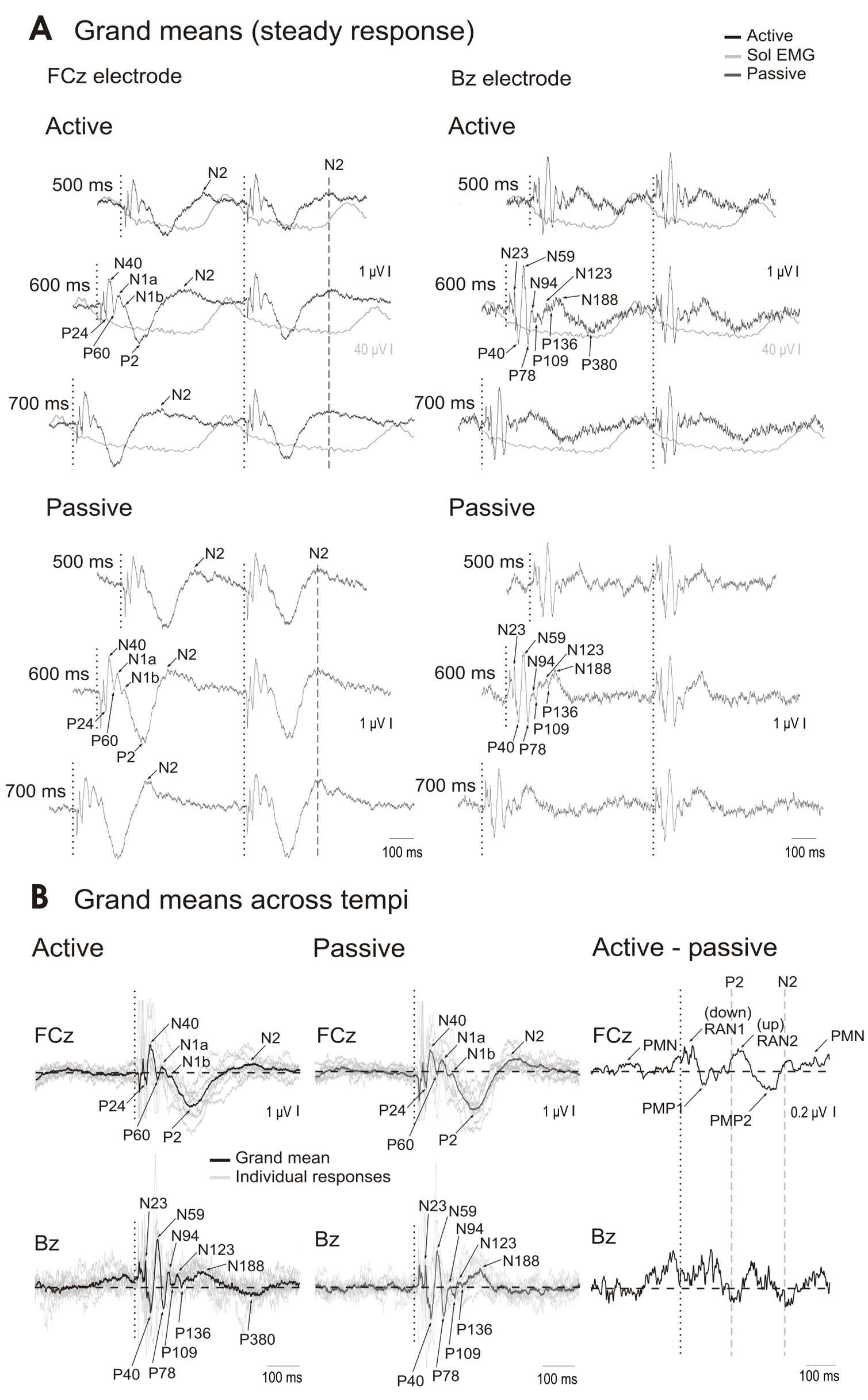


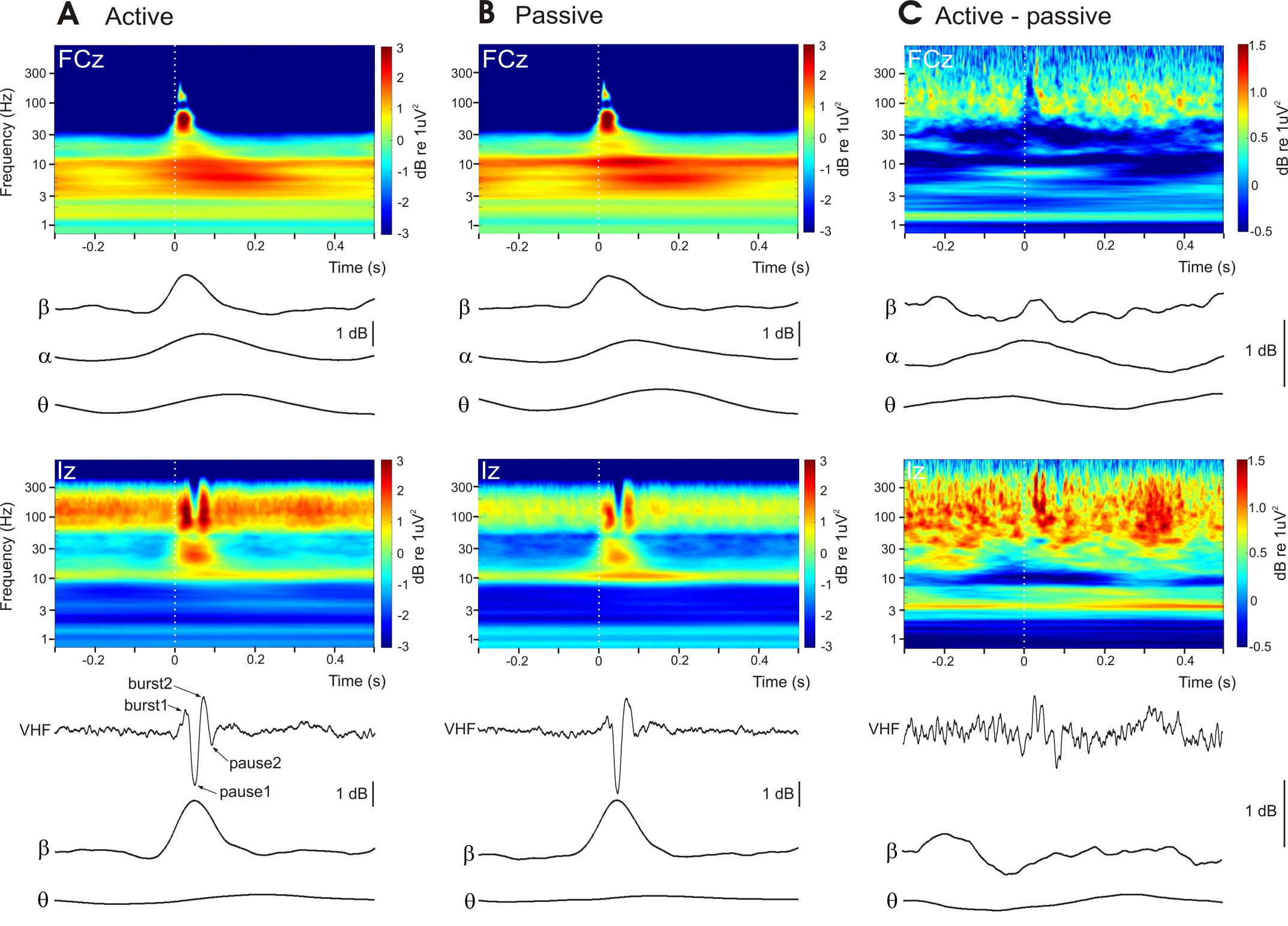
G ***Beat*stage interaction***

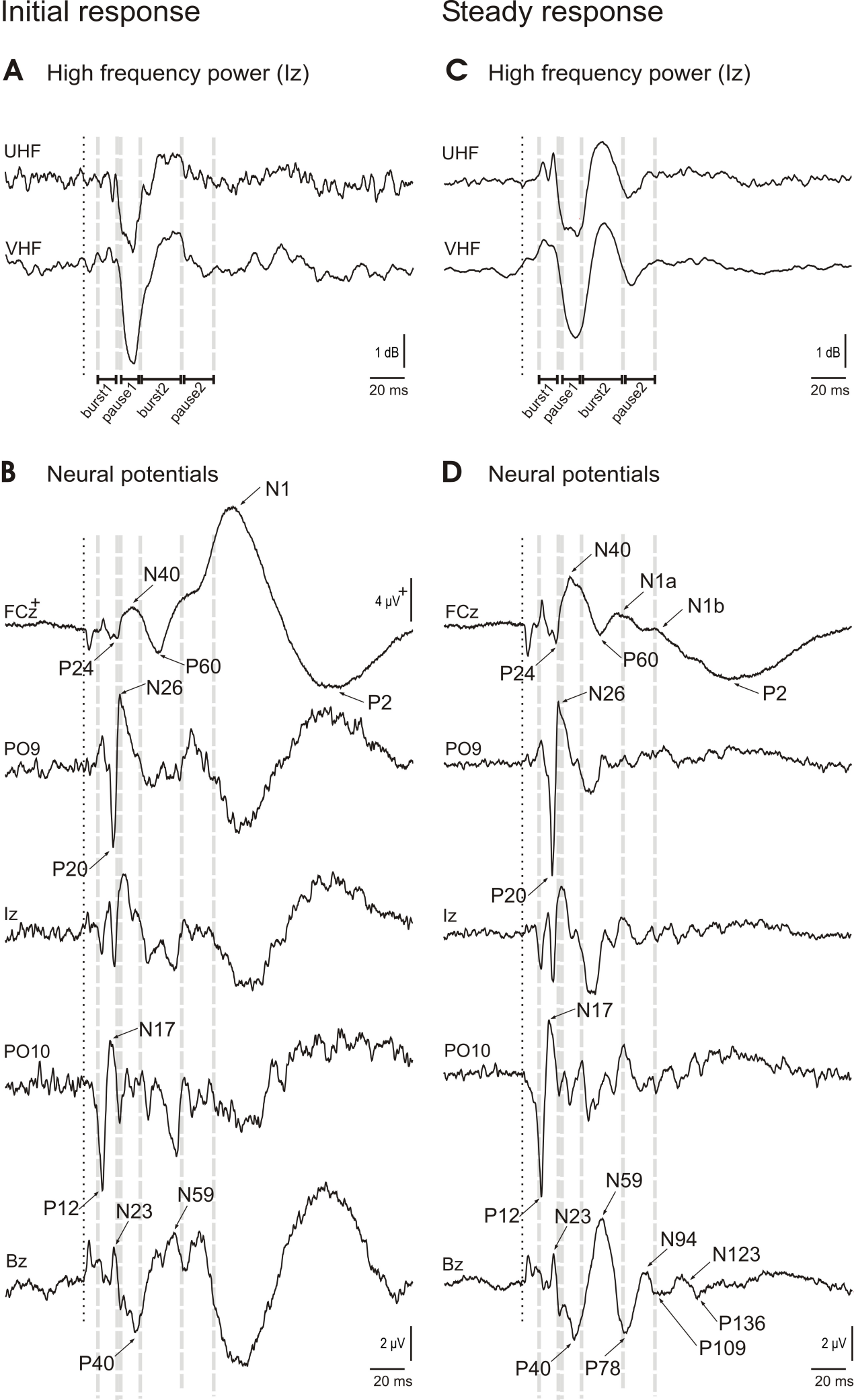


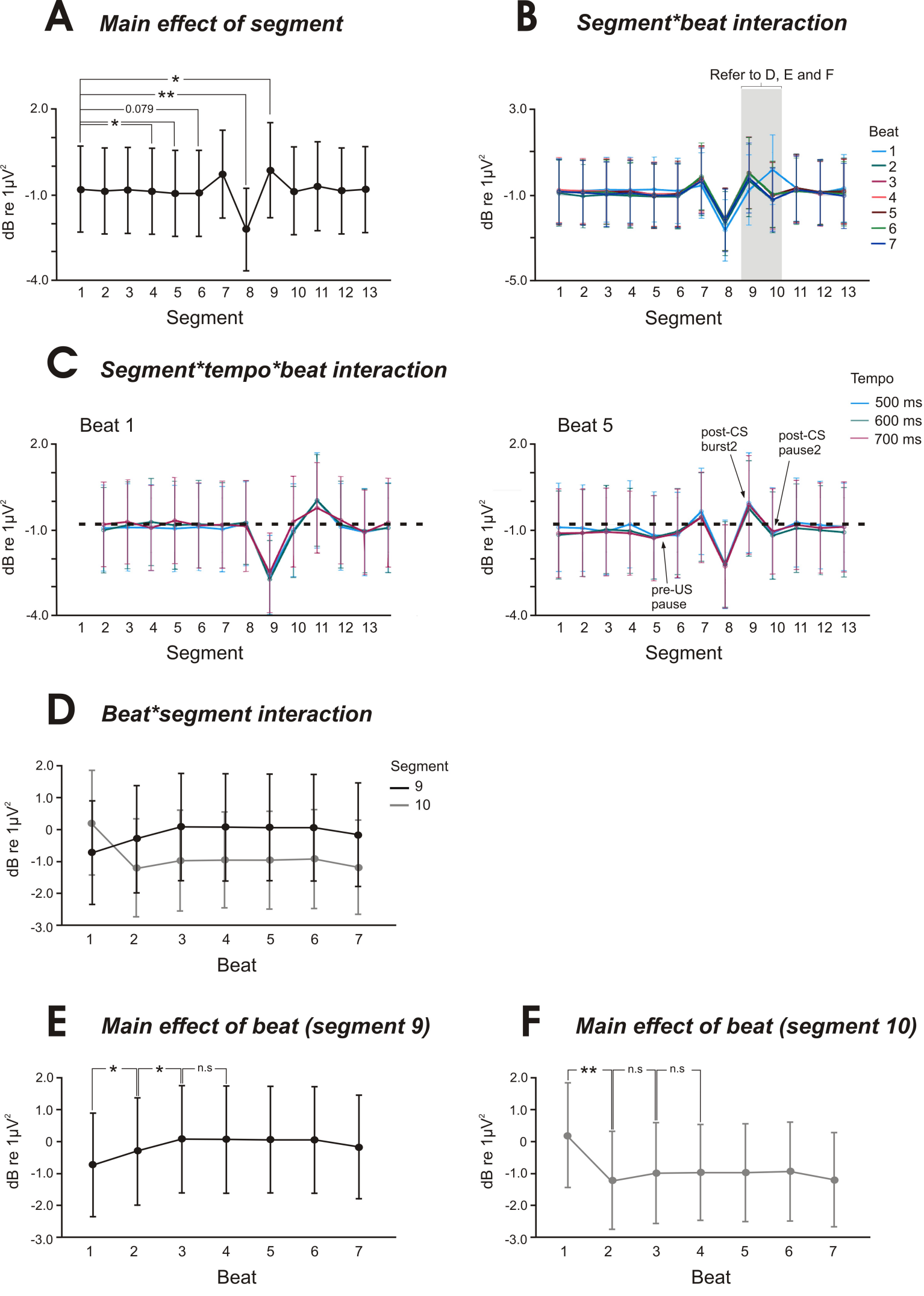

A
0s
SOL
100 μV
Fpz
Active
Passive
FCz
#
6 μV
Bz
+
B
0s
SOL
100 μV
Fpz
Active
Passive
FCz
#
6 μV
Bz
+
C
0s
SOL
100 μV
Fpz
Active
Passive
FCz
#
6 μV
Bz
+
0.5 s
initial negative/positive deflections at FCz
+ rapid multiple negative/positive deflections at Bz

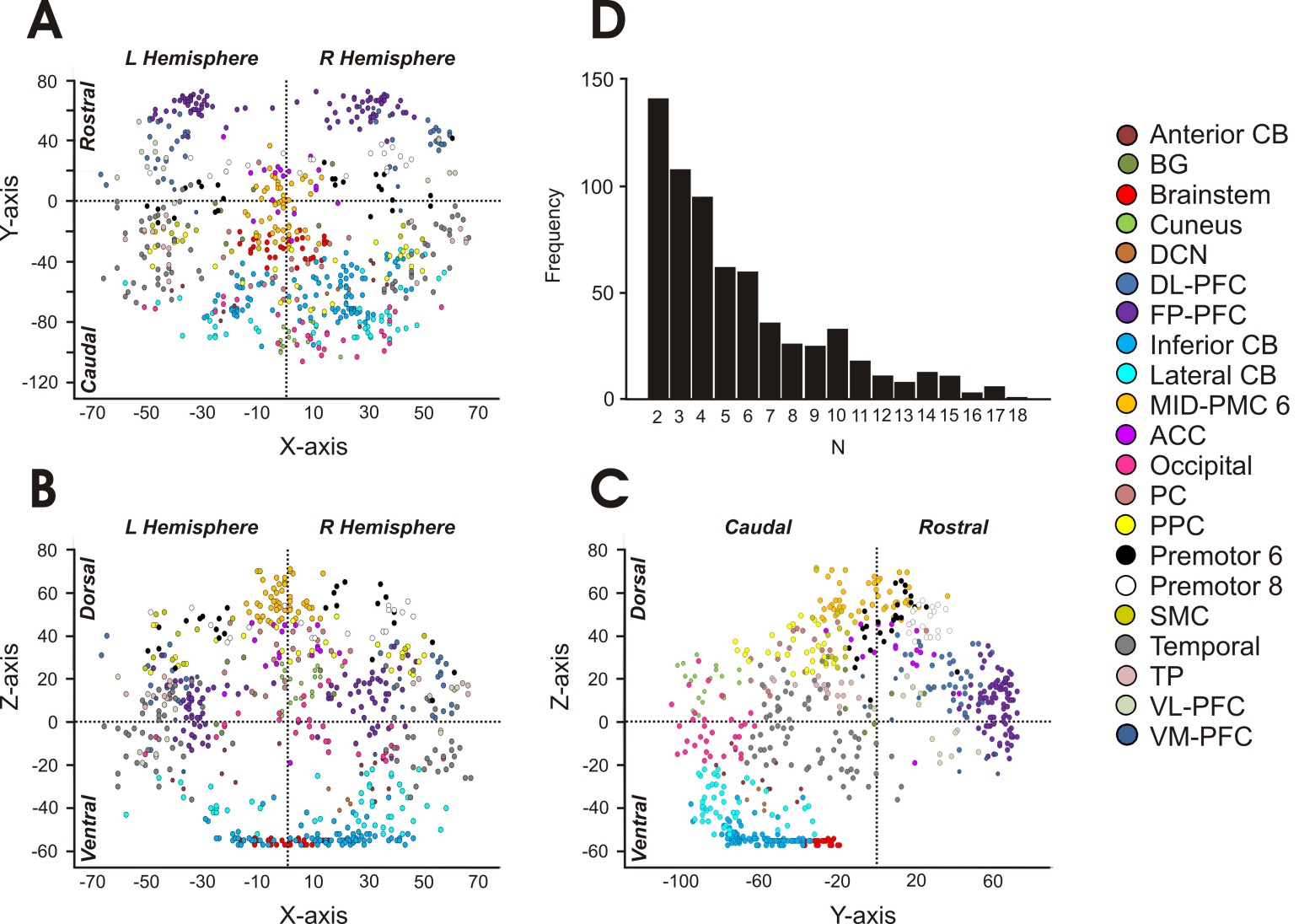

A
Initial response
Active
Passive
SL
ML
LL
LL1
LL2
Stimulus artefact
1 µV
GFP
0.1 s
IO2
Fpz
FCz
N26
PO9
P20
Iz
N17
PO10
P12
N25
N53
Bz
P40
10 ms
50 ms
80 ms
240 ms
5 µV
B
Steady response
Active
Passive
SL
ML
LL
LL1
LL2
Stimulus artefact
1 µV
P2
GFP
0.1 s
IO2
Fpz
N1
N2
FCz#
2 µV
#
P2
N26
PO9
P20
Iz
N17
PO10
P12
N25
N53
Bz
P40
10 ms
50 ms
80 ms
240 ms
5 µV

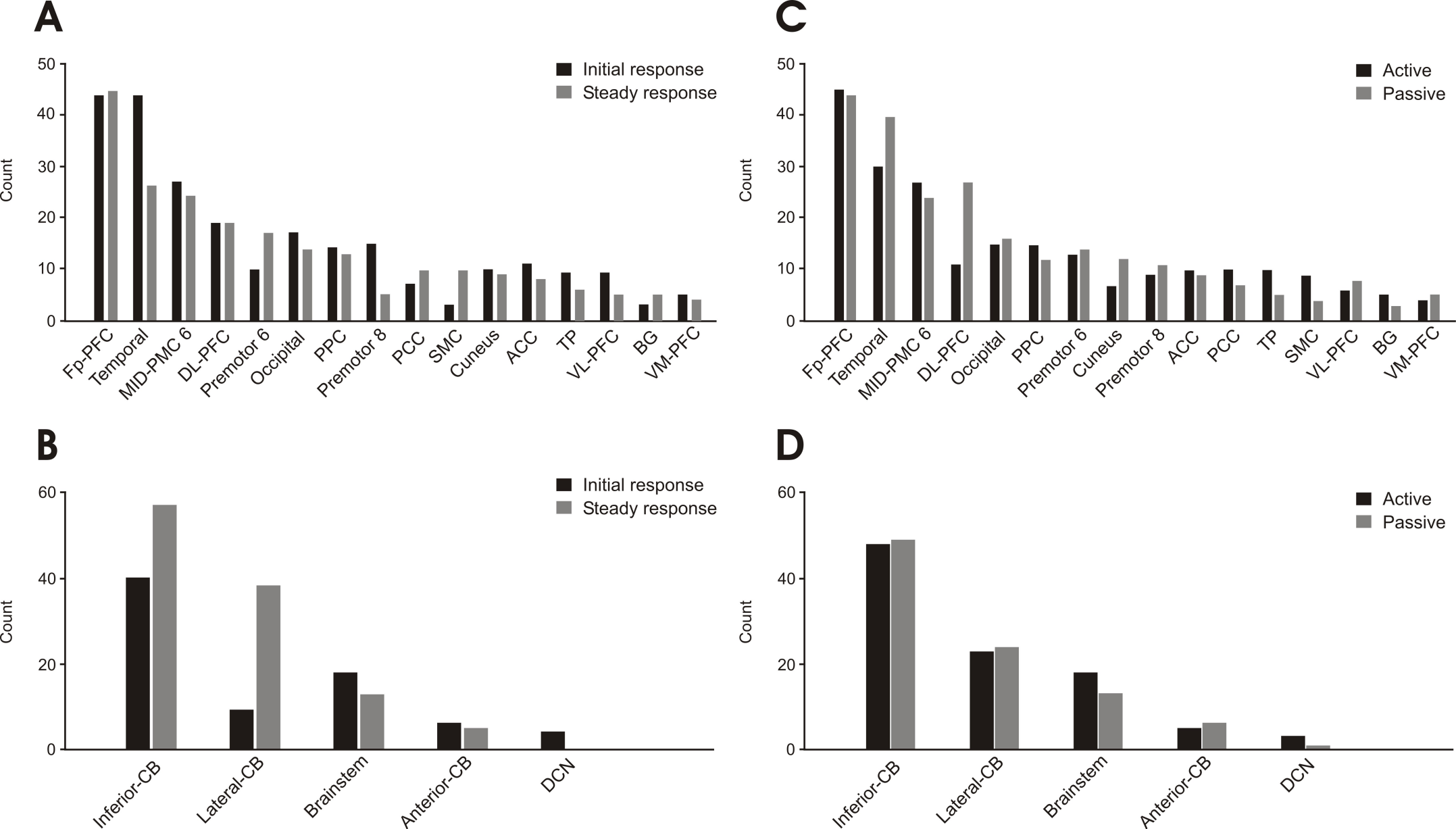

A Grand means (steady response)
Active
Sol EMG
Passive
FCz electrode
Bz electrode
Active
Active
500 ms
600 ms
700 ms
N2
N40
N1a
N1b
P24
P60
P2
N23
N59
N94
N123
N188
P136
P109
P380
P40
P78
1 µV
40 µV
Passive
Passive
100 ms
B Grand means across tempi
Active
Passive
Active - passive
FCz
Bz
Grand mean
Individual responses
P2
N2
(down)
RAN1
(up)
RAN2
PMN
PMP1
PMP2
0.2 µV

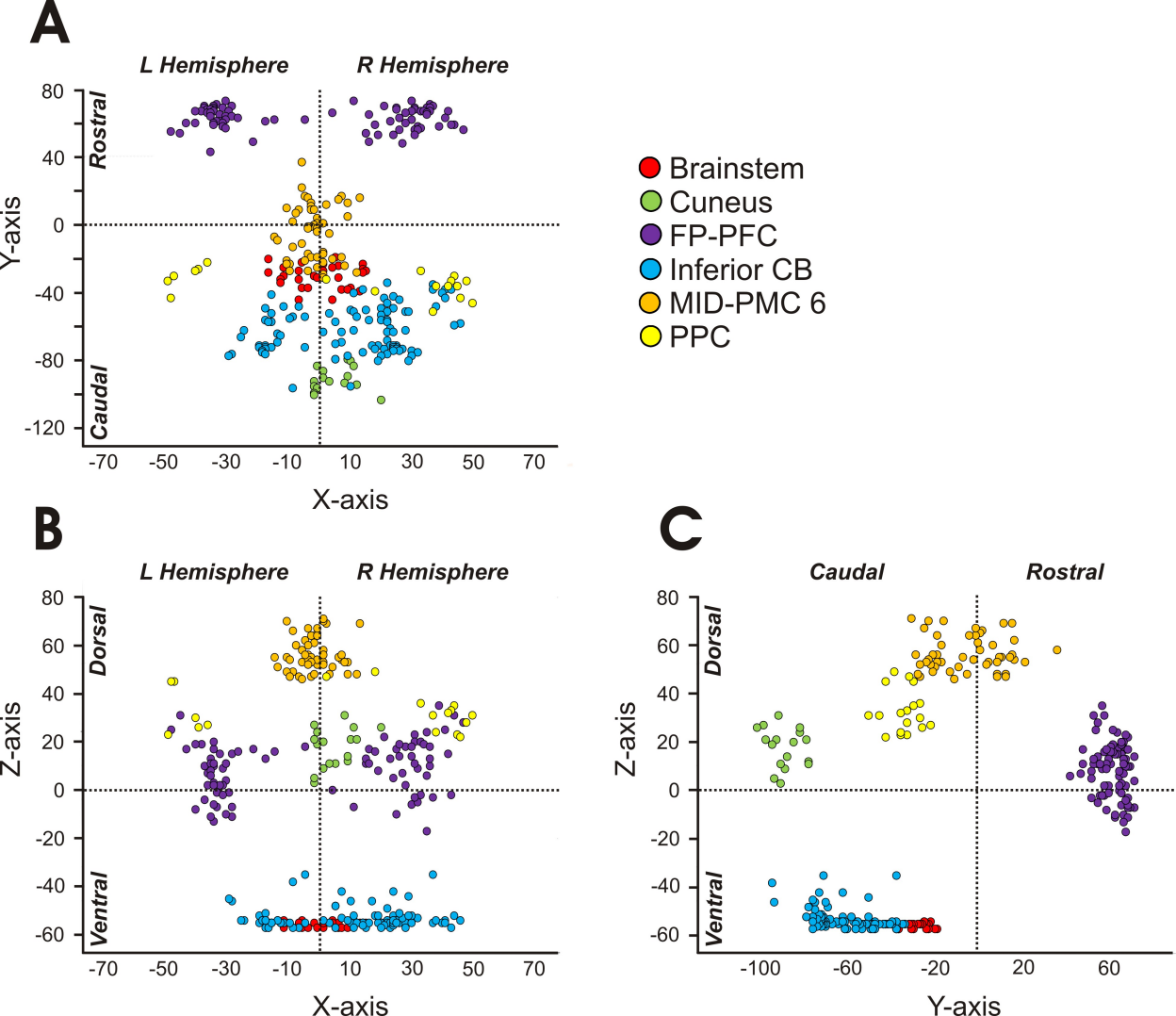

A Active
B Passive
C Active - passive
FCz
Iz
Frequency (Hz)
300
100
30
10
3
1
-0.2
0
0.2
0.4
Time (s)
dB re 1uV²
3
2
1
0
-1
-2
-3
1.5
1.0
0.5
-0.5
β
α
θ
1 dB
VHF
burst2
burst1
pause2
pause1

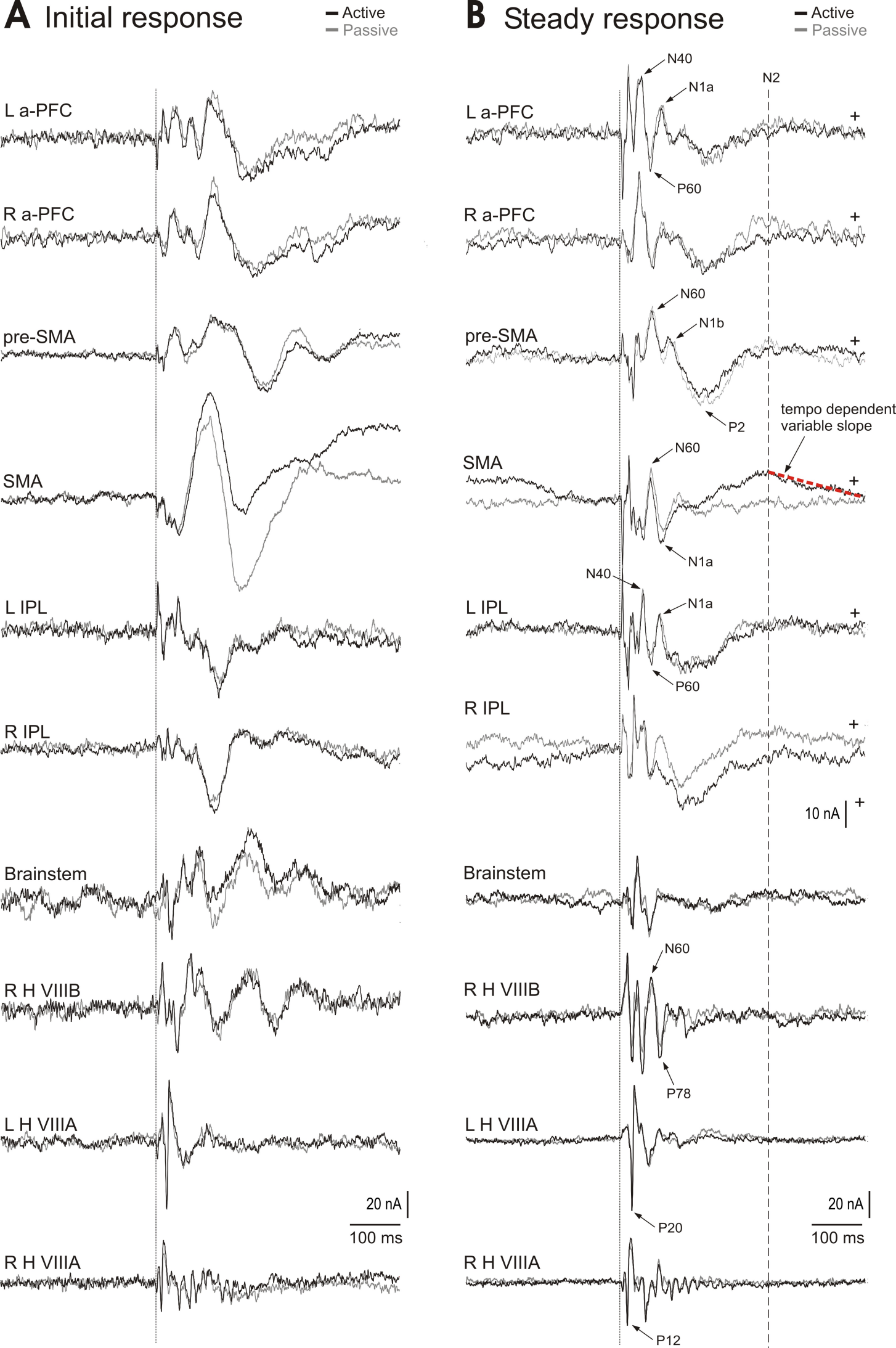

Initial response
Steady response
A
High frequency power (Iz)
UHF
VHF
1 dB
20 ms
burst1
pause1
burst2
pause2
C
High frequency power (Iz)
UHF
VHF
1 dB
20 ms
burst1
pause1
burst2
pause2
B
Neural potentials
N1
N40
FCz
4 μV
P24
P60
P2
N26
PO9
P20
Iz
N17
PO10
P12
N23
N59
Bz
P40
2 μV
20 ms
D
Neural potentials
N40
N1a
N1b
FCz
P24
P60
P2
N26
PO9
P20
Iz
N17
PO10
P12
N23
N59
N94
N123
Bz
P136
P109
P40
P78
2 μV
20 ms

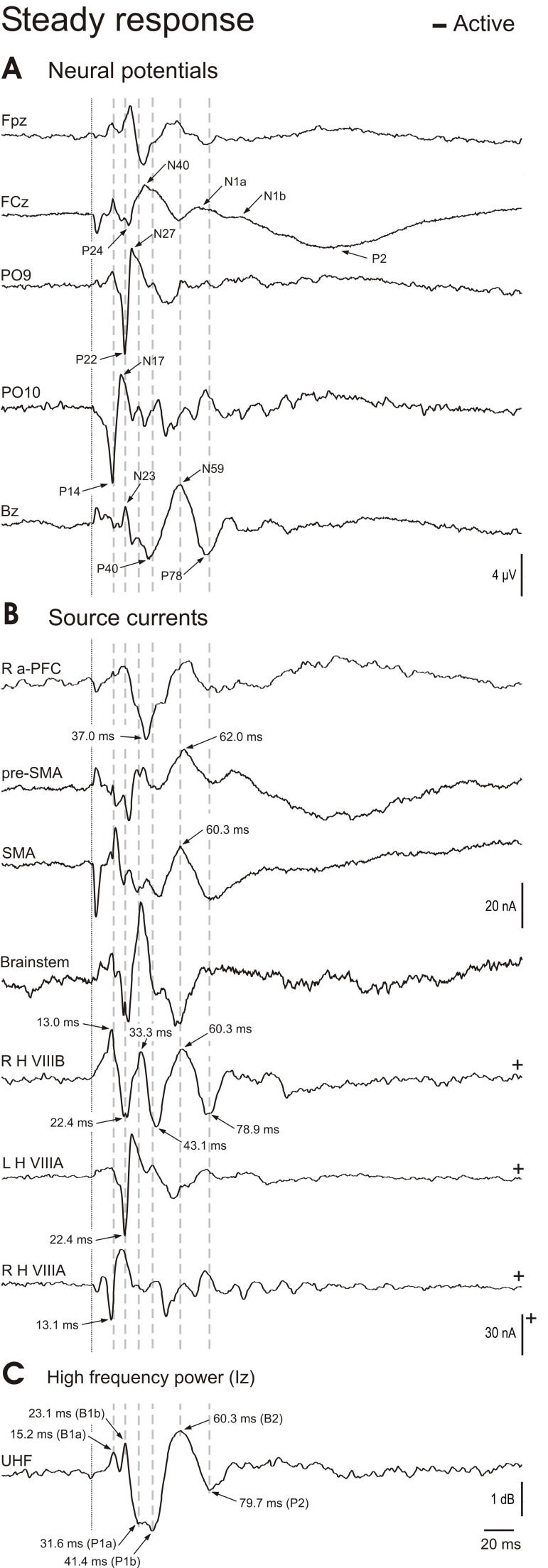

A
Main effect of segment
*
**
0.079
*
2.0
-1.0
-4.0
dB re 1μV²
1 2 3 4 5 6 7 8 9 10 11 12 13
Segment
B
Segment*beat interaction
Refer to D, E and F
3.0
-1.0
-5.0
dB re 1μV²
Beat
1
2
3
4
5
6
7
1 2 3 4 5 6 7 8 9 10 11 12 13
Segment
C
Segment*tempo*beat interaction
Tempo
500 ms
600 ms
700 ms
Beat 1
2.0
-1.0
-4.0
dB re 1μV²
1 2 3 4 5 6 7 8 9 10 11 12 13
Segment
Beat 5
post-CS burst2
post-CS pause2
pre-US pause
2.0
-1.0
-4.0
dB re 1μV²
1 2 3 4 5 6 7 8 9 10 11 12 13
Segment
D
Beat*segment interaction
Segment
9
10
2.0
1.0
0
-1.0
-2.0
-3.0
dB re 1μV²
1 2 3 4 5 6 7
Beat
E
Main effect of beat (segment 9)
*
*
n.s
2.0
1.0
0
-1.0
-2.0
-3.0
dB re 1μV²
1 2 3 4 5 6 7
Beat
F
Main effect of beat (segment 10)
**
n.s
n.s
2.0
1.0
0
-1.0
-2.0
-3.0
dB re 1μV²
1 2 3 4 5 6 7
Beat

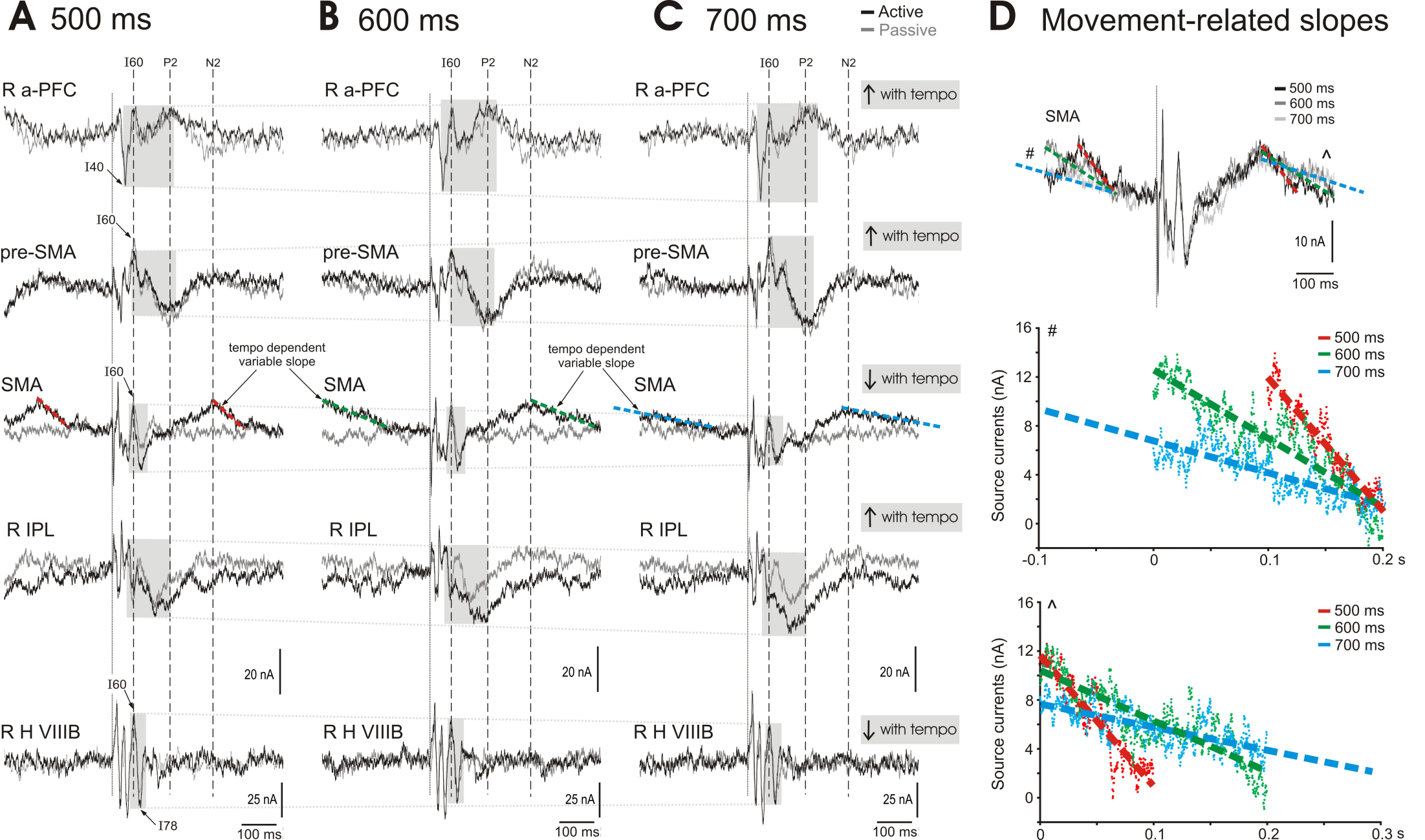

A
L Hemisphere
R Hemisphere
Rostral
Caudal
Y-axis
X-axis
B
L Hemisphere
R Hemisphere
Dorsal
Ventral
Z-axis
X-axis
C
Caudal
Rostral
Dorsal
Ventral
Z-axis
Y-axis
D
Frequency
N
Anterior CB
BG
Brainstem
Cuneus
DCN
DL-PFC
FP-PFC
Inferior CB
Lateral CB
MID-PMC 6
ACC
Occipital
PC
PPC
Premotor 6
Premotor 8
SMC
Temporal
TP
VL-PFC
VM-PFC

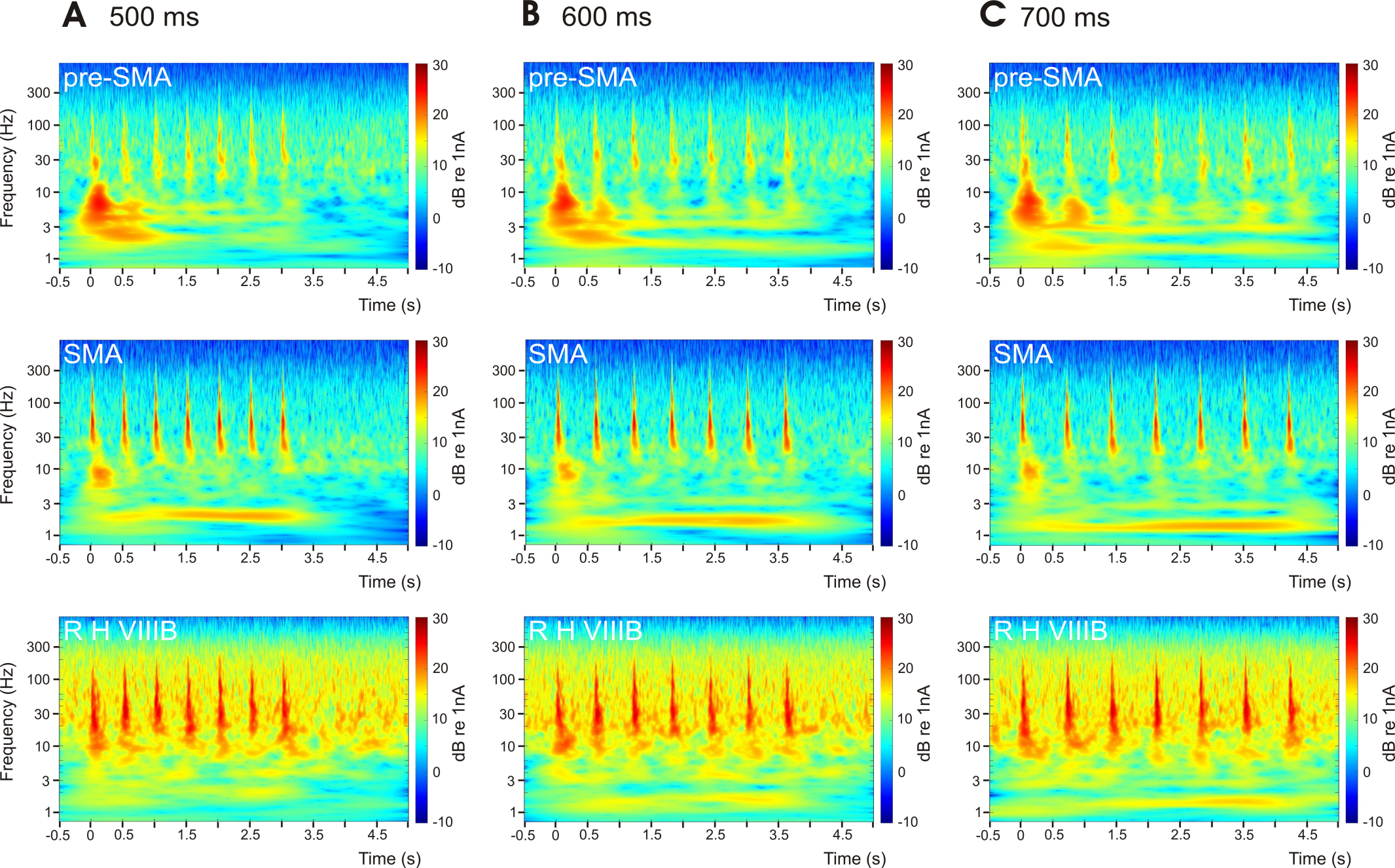

A
Count
Initial response
Steady response
Fp-PFC
Temporal
MID-PMC 6
DL-PFC
Premotor 6
Occipital
PPC
Premotor 8
PCC
SMC
Cuneus
ACC
TP
VL-PFC
BG
VM-PFC
C
Count
Active
Passive
Fp-PFC
Temporal
MID-PMC 6
DL-PFC
Occipital
PPC
Premotor 6
Cuneus
Premotor 8
ACC
PCC
TP
SMC
VL-PFC
BG
VM-PFC
B
Count
Initial response
Steady response
Inferior-CB
Lateral-CB
Brainstem
Anterior-CB
DCN
D
Count
Active
Passive
Inferior-CB
Lateral-CB
Brainstem
Anterior-CB
DCN


A
L Hemisphere
R Hemisphere
Rostral
Caudal
Y-axis
X-axis
80
40
0
-40
-80
-120
-70
-50
-30
-10
10
30
50
70
Brainstem
Cuneus
FP-PFC
Inferior CB
MID-PMC 6
PPC
B
L Hemisphere
R Hemisphere
Dorsal
Ventral
Z-axis
X-axis
80
60
40
20
0
-20
-40
-60
C
Caudal
Rostral
Dorsal
Ventral
Z-axis
Y-axis
-100
-60
-20
20
60


A Initial response
Active
Passive
L a-PFC
R a-PFC
pre-SMA
SMA
L IPL
R IPL
Brainstem
R H VIIIB
L H VIIIA
R H VIIIA
20 nA
100 ms
B Steady response
Active
Passive
N40
N1a
N2
P60
N60
N1b
P2
tempo dependent
variable slope
10 nA
P78
P20
P12


Steady response
Active
A
Neural potentials
Fpz
FCz
PO9
PO10
Bz
N40
N1a
N1b
P24
N27
P2
P22
N17
P14
N23
N59
P40
P78
4 µV
B
Source currents
R a-PFC
pre-SMA
SMA
Brainstem
R H VIIIB
L H VIIIA
R H VIIIA
37.0 ms
62.0 ms
60.3 ms
20 nA
13.0 ms
33.3 ms
60.3 ms
22.4 ms
78.9 ms
43.1 ms
22.4 ms
13.1 ms
30 nA
C
High frequency power (Iz)
23.1 ms (B1b)
15.2 ms (B1a)
60.3 ms (B2)
UHF
79.7 ms (P2)
1 dB
31.6 ms (P1a)
41.4 ms (P1b)
20 ms


A 500 ms
B 600 ms
C 700 ms
Active
Passive
D Movement-related slopes
I60
P2
N2
I40
I78
R a-PFC
pre-SMA
SMA
R IPL
R H VIIIB
tempo dependent variable slope
with tempo
20 nA
25 nA
100 ms
10 nA
500 ms
600 ms
700 ms
Source currents (nA)
0.2 s
0.3 s


A 500 ms
B 600 ms
C 700 ms
pre-SMA
SMA
R H VIIIB
Frequency (Hz)
300
100
30
10
3
1
-0.5
0
0.5
1.5
2.5
3.5
4.5
Time (s)
dB re 1nA
30
20
10
0
-10

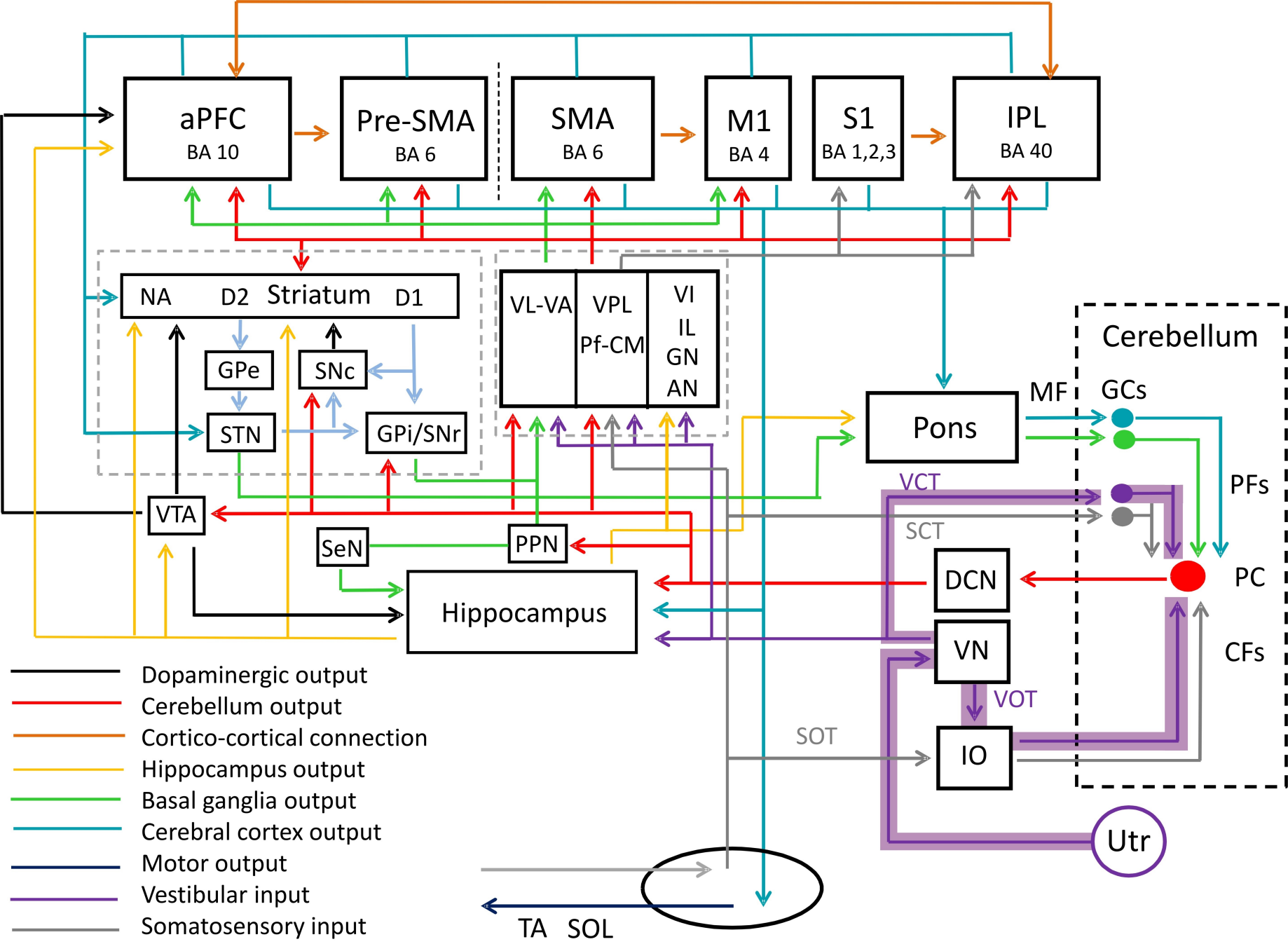

aPFC
BA 10
Pre-SMA
BA 6
SMA
BA 6
M1
BA 4
S1
BA 1,2,3
IPL
BA 40
NA
D2 Striatum D1
GPe
SNc
STN
GPi/SNr
VTA
SeN
PPN
Hippocampus
VL-VA
VPL
Pf-CM
VI
IL
GN
AN
Pons
MF
Cerebellum
GCs
PFs
PC
CFs
VCT
SCT
DCN
VN
VOT
IO
SOT
Utr
TA
SOL
Dopaminergic output
Cerebellum output
Cortico-cortical connection
Hippocampus output
Basal ganglia output
Cerebral cortex output
Motor output
Vestibular input
Somatosensory input

TABLE 1: Latencies and amplitudes of potentials at Fcz.

Wave	Latency (ms)	SE	Amplitude (μV)	SE
P24	24.2	0.5	1.65	0.64
N40	39.1	1.1	3.14	0.54
P60	57.6	0.9	1.05	0.57
N1a	73.9	1.2	1.62	0.31
N1b	104.9	1.7	0.02	0.50
P2	165.7	4.2	4.06	0.38
N2	315.2	6.4	1.83	0.25

TABLE 2: Latencies and amplitudes of potentials at Bz.

Wave	Latency (ms)	SE	Amplitude (μV)	SE
N24	23.2	0.4	2.8	0.7
P40	40.1	1.0	4.1	0.9
N60	59.2	1.0	5.6	2.1
P78	77.8	0.8	3.4	1.7
N94	94.4	1.2	1.8	0.5
P110	109.8	0.9	1.8	0.7
N120	122.9	0.9	1.7	0.5
P135	136.1	0.7	1.2	0.4
N190	187.8	2.9	2.5	0.4
P370	373.0	4.7	2.4	0.3

TABLE 3: ANOVA outcomes for high-frequency power at Iz.

		Passive		**Active**		**Combo**	
Effects	**df**	***F***	***p***	***F***	***p***	***F***	***p***
ACTIVITY	1,9					3.3	= .10
TEMPO	2,18	1.2	ns	1.5	ns	2.4	ns
BAND (BA)	2,18	29.3	< .001	40.2	< .001	35.0	< .001
BEAT (BE)	6,54	4.7	< .05	1.0	ns	2.1	ns
SEGMENT (SEG)	12,108	5.3	< .05	4.7	< .05	5.2	< .05
BA*BE	12,108	3.4	< .05	0.72	ns	2.2	ns
BA*SEG	24,216	9.1	<.001	8.9	< .005	9.7	= .001
BE*SEG	72,648	3.4	<.05	4.1	< .005	4.8	< .01

TABLE 4: ANOVA outcomes for high-frequency power at 5 by 4 grid.

		uGamm		VHF		UHF	
Effects	**df**	***F***	***p***	***F***	***p***	***F***	***p***
X	4,36	13.4	< .001	1.5	ns	2.4	ns
Y	3,27	1.0	ns	40.2	< .001	35.0	< .001
BEAT (BE)	6,54	0.7	ns	1.0	ns	2.1	ns
SEGMENT (SEG)	12,108	6.6	< .01	4.7	< .05	5.2	< .05
X*SEG	48,432	5.3	= .005	0.72	ns	2.2	ns
Y*SEG	36,324	1.0	ns	8.9	< .005	9.7	= .001
X*Y*SEG	144,1296	2.0	ns	4.1	< .005	4.8	< .01
BE* SEG	72,648	4.4	< .05				

TABLE 5: Clusters from source analysis of SL/ML potentials, passive condition, steady response.

ZONE	N	X	Y	Z	Location	Gyrus/Area	BA/SA
CEREBRAL	7	30	67	-6	Frontal	SFG	10
CORTEX	3	4	66	0		MeFG/SFG	10
	16	-32	69	2		SFG/MiFG	10
	4	-48	39	-16		IFG /MiFG	47/11
	7	55	49	21		MiFG	46/45
	2	-40	40	10		MiFG/IFG	46/10
	7	-51	23	13		IFG/PrCG	45/46
	3	40	22	37		MiFG/ PrCG	9/8
	7	9	13	48		SFG/MeFG/CG	6/32/8/24
	4	-3	9	53		SFG/MeFG	6
	3	19	-1	32	Limbic	ACG	24
	3	3	-8	45	Frontal/Limb	ACG/ MeFG/PCL	24/6/31
	4	11	-32	38	Parietal	PCG/Precun	31/7
	3	-20	-47	-10	Temporal	PHG/ FG	19/37/36
	3	39	-55	-12		FG	37
	14	1	-90	9	Occipital	Cuneus/LG	18/17
SUB-CORTEX	3	2	-14	-55	Brainstem		
	4	14	-23	-55			
	2	-24	-6	-5	Basal Ganglia	Putamen	
	2	31	-39	-31	Cerebellum	Anterior	H V
	2	27	-83	-20			H VI
	2	41	-85	-29		Lateral	Cr I
	5	38	-81	-44			Cr II
	3	-27	-74	-42			
	10	26	-74	-51		Posterior	H VIIB/ H VIIIA
	3	-18	-72	-54			H VIIIA
	2	-16	-57	-55			H VIIIB
	14	22	-51	-55			
	4	12	-54	-55			H VIIIB/IX
NON-CEPHALIC	3	17	77	-25	Ocular		
	2	-35	51	-37			
	6	5	71	-42			
	6	-1	58	-54			
	4	25	60	-48			
	6	13	21	-54			
	6	65	26	-19	Artefact		
	8	70	-5	-11			
	5	73	-29	-5			
	2	34	-23	-54	Neck		

Abbreviations: Anterior cingulate gyrus (ACG), Brodmann area (BA), fusiform gyrus (FG), inferior frontal gyrus (IGF), lingual gyrus (LG), medial frontal gyrus (MeFG), middle frontal gyrus (MiFG), paracentral lobule (PCL), para-hippocampal gyrus (PHG), posterior cingulate gyrus (PCG), pre-central gyrus (PrCG), Schmahmann atlas (SA), superior frontal gyrus (SFG). **Definitions:** N is the cluster weight, i.e. dipoles per cluster from 15 runs; X, Y, Z are Talairach and Tournoux coordinates (Talairach and Tournoux 1988); cerebellar nomenclature is from the Schmahmann atlas (Schmahmann et al. 1999).

TABLE 6: clusters of clusters (Six epochs, four conditions)

	W	X	Y	Z	Side	Sub-Zone	Gyrus/Area	BA/SA
CEREBRUM								
Frontal	**48**	**29**	**62**	**10**	**Right**	**Fp-PFC**	**MiFG/SFG**	**10**
	53	**-34**	**61**	**8**	**Left**	**Fp-PFC**	**MiFG/SFG**	**10**
	9	-48	44	-15	Left	VL-PFC	IFG/MiFG	47/11/10
	23	54	38	15	Right	DL-PFC	MiFG/IFG	46
	13	-50	22	21	Left	DL/VL-PFC	MiFG/IFG	46/45/9/44
	18	39	20	48	Right	lateral PMC	SFG/MiFG	8/6
	12	9	19	32	Midline	Limbic (VM-PFC)	ACG	32/24
	13	-26	19	46	Left	lateral PMC	MiFG/SFG	8/6
	44	**1**	**8**	**55**	**Midline**	**Med PMC (pre-SMA)**	**SFG/MeFG**	**6**
	6	-17	-4	34	Left	Limbic	ACG	24
	29	**-1**	**-26**	**53**	**Midline**	**Med PMC (SMA)**	**MeFG/PCL**	**6/5**
Temporal								
	18	-45	-7	-8	Left	Temporal	Ins/STG	21/13/22/38
	8	58	-15	13	Right	Temporal/Parietal	TTG/STG/PrCG/PoCG	42/41/43/22
	16	56	-22	-20	Right	Temporal	ITG/FG/MTG	20/21
	15	-47	-50	6	Left	Temporal	STG/MTG	39/22
	10	43	-59	-11	Right	Temporal	FG	37
Parietal								
	33	**-45**	**-23**	**25**	**Left**	**Parietal/PPC**	**Ins/PoCG/IPL**	**13/2/40**
	24	**40**	**-36**	**26**	**Right**	**Parietal/PPC**	**Ins/IPL**	**13/40**
	10	-11	-43	33	Midline	Limbic/Parietal/PPC	CG/Precun/SPL	31/7
	12	3	-66	25	Midline	Occipital/Parietal/PPC	Precun/SPL/Cuneus	31/7/23/18
Occipital								
	8	-17	-67	-5	Left	Occipital	LG/FG	18/19
	32	**7**	**-91**	**11**	**Midline**	**Occipital**	**Cuneus**	**18/19**
SUB-CORTEX								
Brainstem	**25**	**-2**	**-28**	**-55**	**Midline**	**Brainstem**		
Cerebellum	**53**	**27**	**-47**	**-51**	**Right**	**Posterior**	**Lob biv, pars cop**	**H VIIIB**
	11	-49	-63	-22	Left	Lateral	Semilun lob, sup	Cr I
	44	**-18**	**-70**	**-50**	**Left**	**Posterior**	**Lob biv, pars parafloc**	**H VIIIA/VIIB**
	49	**22**	**-75**	**-48**	**Right**	**Posterior**	**Lob biv, pars parafloc**	**H VIIIA/VIIB**
	18	35	-86	-22	Right	Lateral	Semilun lob, sup	Cr I

Abbreviations: Anterior cingulate gyrus (ACG), Brodmann area (BA), dorsal-lateral (DL), fusiform gyrus (FG), fronto-polar (Fp), inferior frontal gyrus (IGF), insula (ins), lingual gyrus (LG), medial frontal gyrus (MeFG), middle frontal gyrus (MiFG), paracentral lobule (PCL), para-hippocampal gyrus (PHG), post-central gyrus (PoCG), posterior cingulate gyrus (PCG), pre-frontal cortex (PFC), pre-motor cortex (PMC), pre-central gyrus (PrCG), Schmahmann atlas (SA), superior frontal gyrus (SFG), supplementary motor area (SMA), ventral-medial (VM). **Definitions:** W is the super ordinate cluster weight, i.e. sub-clusters per cluster from 24 combinations; X, Y, Z are Talairach and Tournoux coordinates; cerebellar nomenclature is from the Schmahmann atlas.